

https://dspace.org/

Synthesis and characterization of novel short antimicrobial peptides with wound healing properties

Machumele, Khanani Peggy

2019

University of the Witwatersrand, Johannesburg

https://hdl.handle.net/10539/28758

Machumele, Khanani Peggy. (2019). Synthesis and characterization of novel short antimicrobial peptides with wound healing properties. [Master's dissertation, University of the Witwatersrand, Johannesburg]. https://hdl.handle.net/10539/28758

Downloaded from a DSpace repository. https://dspace.org/

Synthesis and characterization of novel short antimicrobial peptides with wound healing properties

By: Khanani Machumele

Supervised by: Dr Maya Makatini

29 May 2019

A thesis submitted to the Faculty of Science, University of the Witwatersrand, Johannesburg

In fulfilment of the requirements for the Degree of Master of Science

DECLARATION OF ORIGINALITY

I hereby state that the work recorded in this document was conducted by me. This thesis was wholly conducted and written by myself under the supervision of Dr Maya Makatini. I have rightfully credited the sources were used in the thesis. This thesis has not been submitted before for any degree.

_____

Khanani Machumele

Abstract

In recent years, there has been an increasing health crisis due to multidrug-resistant microbes. These pathogens are strains of bacteria that have become resistant to antibiotic drugs.

In the year 2016, the World Health Organisation (WHO) had appealed to the members of states in the USA to create a priority list of other bacteria that are resistant to antibiotics in order to support research and development of effective drugs.

According to literature, antimicrobial peptides have the potential to be potent agents against pathogens that have multidrug-resistant properties. Despite these studies, there are still substantial limitations (toxicity and susceptibility to proteases) that have affected their clinical and commercial development. In this study, the focus was on bacteria that infect wounds. The lack of potent chronic wound treatment has resulted in an enormous financial and physical burden on patients and the health care system. The stress of multi-resistant microbes heighten the challenges plagued on a patient due to untreatable infected wounds. Peptides which are able to kill bacteria and promote the wound healing process would greatly benefit patients. For example, patients with diabetic foot ulcers are prone to chronic wounds because of their condition, which may lead to amputation. Wound healing antimicrobial peptides are able to kill bacteria in the wound and induce the formation of collagen which will result in fewer amputations. The aim of this proposed research is to develop novel wound healing and antimicrobial compounds by derivatizing bioactive peptides into selective and protease-stable peptidomimetics.

Tigerinin RC1 is an antimicrobial peptide with wound healing properties. It was chosen as a starting point for the design of analogues with drug-like properties and it was also conjugated to silver nanoparticle (AgNPs) to improve its bactericidal activity. In this study, 16 Tigerinin RC1 peptide analogues were successfully synthesized using the solid phase peptide synthesis strategy. Peptides were purified using the semi prep-HPLC however, the desired purity of > 90% was only achieved after two or more purification runs. Thus only 4 of the peptide analogues had a purity great than 90% which were KM-PEP-carb, KM-PEP-cyc-amide, KM-PEP-ada and KM-PEP-CT. These peptides were tested for antimicrobial activity and KM-PEP-cyc-amide peptide showed promising results with the minimum inhibitory concentration of 128 µg/ml against *P. aeruginosa*.

Cytotoxicity studies also revealed that conjugation of KM-PEP-carb to AgNPs improved cytotoxicity because when 25 µg/ml of KM-PEP-carb was tested against human T cells the cell viability was -1.48% and when conjugated to AgNPs the cell viability increased to 35.17%.

Acknowledgements

First, I would like to thank God for giving me an opportunity to glorify His name through my work.

I would like to thank the school of Chemistry for giving me a chance to advance and to the National Research Foundation for financially assistance.

I would also like to thank my supervisor Dr Maya Makatini for giving me this project and pouring out her extensive knowledge. I appreciate all of the encouragement that she gave me when I had no hope. Her dedication to her work and determination to promote women in science is inspirational.

My mother and father, Nomalungelo Felicia Machumele and Nkateko Jones Machumele, have been so supportive of my postgraduate studies. They are my pillars of strength when others discourage my pursuit of an academic career. No words can express the amount of gratitude I have because they have made many sacrifices to make me the woman I am today. Thank you for being amazing parents.

Special thanks to my brother, Nkateko Machumele, for always motivating me and pushing me every day. Thank you to my sister, Gauta Maseko for frequently calling me and lifting up my spirit. I also thank Nombulelo Kwayiba, Tsebo Utlwa, Nicole Baloyi, Khensi Baloyi, Irene Machumele, Maggy Machumele, Khongelani Machumele and everyone in my family.

I would like to thank my colleagues: Pious Shuro, Thapelo Mbele, Refilwe Moepya, Ndivhuwo Shumbula Thabo Peme, Tebello Mofokeng, Ntombizanele Ngqinayo, Phathutshedzo Masithi, Mudzuli Maphupha, Sinazo Cobongela, Kamogelo Butsi, Memory Zimuwandeyi, Adelaide Mashweu, Donald Seanego, Edward Chavalala, Fatema Jagot, Nompumelelo Mathebula, Peter Juma and Tianqi Lu

Special thanks my friends: Tshwarela Kolokoto, Mulweli Nethathe, Lindelwa Didiza, Dineo Tiro, Oreneile Tshetlo and Nthabiseng rakatleho khanye. Finally, I would like to thank National Research Foundation (NRF) and South African Medical Research Council (SAMRC) for funding.

Table of Contents

DECLARATION OF ORIGINALITY ii

Abstract iii

Acknowledgements v

List of abbreviations xii

List of tables xv

Chapter 1 1

Introduction and literature review 1

1.1 Chronic wounds 1

1.1.1 The process of wound healing 2

1.1.2 The hemostasis phase 2

1.1.3 The inflammatory phase 3

1.1.4 The proliferation phase 4

1.1.5 Remodelling stage 4

1.2 Common causes of chronic wounds 5

1.2.1 Lack of oxygen in wounds 5

1.2.2 Infection in wounds 7

1.2.3 Role of nutrition 8

1.3 Diabetic foot ulcers 9

1.4 Biofilms in chronic wounds 10

1.5 Global impact 11

1.5.1 Impact in SA 12

1.5.2 High costs of wound management 12
1.6 Current conventional treatment 13
1.7 Different novel approaches for treatment of chronic wounds 14
1.7.1 Apligraf 14
1.7.2 Trafermin 15
1.7.3 Murepavadin 16
1.8 Introduction to Antimicrobial peptides 17
1.8.1 What are Antimicrobial peptides? 17
1.8.2 Mode of action of antimicrobial peptides 19
1.8.3 Benefits of antimicrobial peptides 21
1.8.4 Turning antimicrobial peptides into drugs 21
1.9 Tigerinin RC1 24
1.10 Aim and Objectives 25
1.11 Hypothesis and question 26
Chapter 2 27
Synthesis and characterization of Tigerinin RC 1 and its derivative peptides 27
2.1 Introduction 27
2.2 The KM-PEP-carb peptide 29
2.2.1 Design and synthesis of KM-PEP-carb 29
2.2.2 Purification of KM-PEP-carb peptide 30
2.2.3 Biological testing of KM-PEP-carb peptide 31
2.3. KM-PEP-cyc-amide peptide 33
2.3.1 Design and synthesis of KM-PEP-cyc-amide peptide 33
2.3.2 Purification of KM-PEP-cyc-amide peptide 34
2.3.3 Biological testing of KM-PEP-cyc-amide peptide 36

2.4 KM-PEP-ada peptide 36
2.4.1 Design and synthesis of KM-PEP-ada peptide 36
2.4.2 Purification of KM-PEP-ada peptide 37
2.4.3 Biological testing of KM-PEP-ada peptide 38
2.5 KM-PEP-cyc-ada peptide 39
2.5.1 Design and synthesis of KM-PEP-cyc-ada peptide 39
2.5.2 Purification of KM-PEP-cyc-ada peptide 39
2.6 KM-PEP-pal peptide 41
2.6.1 Design and synthesis of KM-PEP-pal peptide 41
2.6.2 Purification of KM-PEP-pal peptide 41
2.7 KM-PEP-cyc-pal 43
2.7.1 Design and synthesis of KM-PEP-cyc-pal peptide 43
2.7.2 Purification of KM-PEP-cyc-pal peptide 43
2.8 KM-PEP-DAA 44
2.8.1 Design and synthesis of KM-PEP-DAA peptide 44
2.8.2 Purification of KM-PEP-DAA peptide 46
2.9 KM-PEP-Nmethyl peptide 47
2.9.1 Design and synthesis of KM-PEP-*N*-methyl peptide 47
2.9 KM-PEP-toid peptide 50
2.9.1 Design and synthesis of KM-PEP-toid peptide 50
2.10 Conclusion 53
Chapter 3 55
Synthesis and characterization of Cationic and RGD Tigerinin RC1 peptide derivatives 55
3.1 The cationic peptide sequences 56
3.1.1 Design of the KM-CT peptide analogues 56

3.1.2 Synthesis of the KM-CT peptide and analogues 57
3.1.3 Results and discussion 57
3.2 The RGD integrin homing peptide sequence 60
3.2.1 Design of the KM-RGD peptide 60
3.2.2 Synthesis of KM-RGD peptide 61
3.2.3 Results and discussion 62
3.3 Conclusion 65
Chapter 4 66
Silver nanoparticles and peptides 66
4.1. Introduction 66
4.1.1 Surface Plasmon Resonance (SPR) 68
4.2. Results and Discussion 70
4.2.1 Colour change due to the dielectric environment 70
4.2.2 UV-Vis spectroscopy of AgNPs and the conjugates 71
4.2.3Transmission electron microscopy (TEM) 75
4.2.4 Size distribution of silver nanoparticles 78
4.2.5 Cytotoxicity tests 80
4.2.6 Antibacterial activity 83
4.3 Conclusion 84
Chapter 5 85
Summary and conclusion 85
Chapter 6 87
Experimental procedures 87
6.1 Reagents and chemicals 87
6.1.1 Reagents for peptides 87

6.1.2 Reagents for AgNP-PEP 87
6.2 Instrumentation 88
Instrumentation used for peptides and amino acids 88
6.2.1 Ultra High Pressure Liquid Chromatography (UHPLC) 88
6.2.2 Preparative High Pressure Liquid Chromatography (PREP-HPLC) 88
6.2.3 Peptide automated synthesis 88
6.2.4 Ultraviolet–visible spectroscopy 88
6.2.5 Mass spectroscopic analysis 89
6.2.6 Nuclear magnetic resonance spectroscopy (NMR) 89
Instrumentation used for silver nanoparticle and its conjugates 89
6.2.7 Transmission electron microscopy (TEM) 89
6.2.8 Ultraviolet–visible spectroscopy 90
6.3 Biological screening 90
6.3.1 Cytotoxicity 90
6.3.2 Antimicrobial tests 90
6.4 General procedures 91
6.4.1 General procedure for the swelling, activation and coupling of the first amino acid to 2-chlorotitryl resin 91
6.4.2 General procedure for the swelling, activation and coupling of the first amino acid to rink amide resin 91
6.4.3 General procedure for analysing the substitution of the first amino acid 92
6.4.4 General procedure for the synthesis of peptides 92
6.4.6 General procedure for the synthesis of peptides containing adamantane and palmitic acid on the N-terminal 94
6.4.8 General procedure for the cyclization of the peptides 96
6.4.9 General procedure for the cleavage of the peptides from the resin 98

6.4.10 General procedure for the purification of the peptides 98
6.4.11 General procedure for the synthesis of the peptoids 101
6.4.12 General procedure for the cleavage of the peptoids 102
6.4.13 General procedure for the synthesis of the *N*-methylated Fmoc leucine 102
6.4.14 General procedure for the synthesis of the *N*-methylated Fmoc isoleucine 105
6.4.15 General procedure for the synthesis of the *N*-methylated Fmoc alanine 107
6.4.16 General procedure for the synthesis of the *N*-methylated Fmoc valine 109
6.4.17 General procedure for the synthesis of the silver nanoparticles (AgNPs) 111
6.4.18 General procedure for the synthesis of the silver nanoparticles (AgNPs) conjugated to KM-PEP-carb peptide 111
References 113
Appendix 123

List of abbreviations

AA: Amino Acid

Ada: Adamantane carboxylic acid

Ag: Silver

AgNP: Silver nanoparticles

$AlCl_3$: Aluminium chloride

AMPs: Antimicrobial Peptides

Boc: *tert*-butyloxycarbonyl

$CDCl_3$: Deuterated chloroform

$(CD_3)_2SO_2$: Deuterated Dimethylsulfoxide

DCM: Dichloromethane

DIC: 1, 3-Diisopropylcarbodiimide

DIPEA: *N*,*N*-diisopropylethylamine

DMF: *N*,*N*-dimethylformamide

DMSO: Dimethylsulfoxide

d: Doublet

EDT: 1,2-Ethanedithiol

EtOAc: Ethyl acetate

Fmoc: 9-Fluorenylmethoxycarbonyl

FWHM: Full width at half maxima

HATU: Hexafluorophosphate Azabenzotriazole Tetramethyl Uronium

HBTU: O-Benzotriazole-*N*,*N*,*N*,*N*-tetramethyl-uronium hexafluorophosphate

HOBt: *N*-hydroxybenzotriazole

Hz: Hertz

UHPLC: Ultra High Performance Liquid Chromatography

Prep-HPLC: Preparative High Performance Liquid Chromatography

ppm: Parts per million

HRMS: High resolution mass spectroscopy

mg: Milligram

MIC: Minimum Inhibitory Concentration

Min: Minute

ml: Milliliter

mM: Millimolar

MS: Mass spectrometry

m.p. : Melting point

m: Multiplet

m/z : Mass charge

nm: Nanometres

NMR: Nuclear Magnetic Resonance

SPPS: Solid phase peptide synthesis

s: Singlet

SPR: Surface plasmon resonance

t :Triplet

TEM: Transmission electron microscopy

TFA: Trifluoroacetic acid

TIS: Triisopropyl silane

TIC: Total ion chromatograms

μg: Microgram

μL: Microliter

TLC: Thin Layer Chromatography

UV-VIS: Ultraviolet-visible spectroscopy

List of tables

Table 2. 1 Cytotoxicity study on KM-PEP-carb 32
Table 2. 2 *N*-methylated Fmoc amino acids with respective yields 49
Table 2. 3 Detailed summary of the masses found on the UHPLC-MS and respective yields of the KM-PEP peptide analogues 52

Table 3. 1 Detailed summary of the masses found on the UHPLC-MS and respective retention times of the cationic peptides 59
Table 3. 2 Detailed summary of the masses found on the UHPLC-MS and respective yields of the RGD peptides 65

Table 4. 1 SPR band according to the UV-visible spectra for silver nanoparticles 72
Table 4. 2 Average size and standard deviation for AgNPs 80
Table 4. 3 The amount of AgNP and KM-PEP-carb added in each fraction when preparing the samples. 82
Table 4. 4 Cytotoxicity test of silver nanoparticles conjugated to KM-PEP-carb evaluated on MT4 cell. 83
Table 4. 5 Minimum inhibitory concentration (µg/ml) for conjugates against different organisms 84

Table 6. 1 Summary of peptides synthesized in chapter 2 99
Table 6. 2 Summary of peptides synthesized in chapter 3 100
Table 6. 3 Summary of AgNPs and KM-PEP-carb volume used for each sample and the particle sizes 112

Chapter 1

Introduction and literature review

A number of researchers have reported wound healing biological agents and antimicrobial peptides.[1] Despite these studies, there are still substantial limitations (toxicity and susceptibility to proteases) that have affected their clinical and commercial development.[2] The lack of potent chronic wound treatment has resulted in an enormous financial and physical burden on patients and the health care system. The worldwide crisis of multi-resistant microbes amplifies the challenges afflicting a patient by causing infected wounds not to be treatable or disinfected efficiently.[3] The aim of this proposed research is to develop novel wound healing and antimicrobial compounds by derivatizing bioactive peptides into selective and protease-stable peptidomimetics.

1.1 Chronic wounds

After an injury has occurred, the wound goes through a cascade of a physiological events which partly overlaps in time. The wound healing process is delicate and can be prone to interruptions. When one or more of these stages is inhibited or prolonged the wound becomes a chronic wound.[4]

A chronic wound is defined as a wound that cannot heal in a regular set of stages and in an expected amount of time.[2] This is due to the lack of oxygen, blood supply and nutrients which are essential in all of the stages of the wound healing process. Gjodsbol *et al.* investigated the bacterial profile of chronic leg ulcers and found Staphylococcus aureus (in 93.5% of the investigated ulcers), *Enterococcus faecalis* (71.7%), *Pseudomonas aeruginosa* (52.2%), *coagulase-negative staphylococci* (45.7%), *Pro-teusspecies* (41.3%), and anaerobic bacteria (39.1%). It is crucial to analyse the bacterial profile of a chronic wound because they can prolong the healing process and treatment can be decisively chosen for a specific patient.

1.1.1 The process of wound healing

The proper treatment of chronic wounds is highly dependent on understanding the function of the skin and fundamental processes that occur in the natural healing process. The skin is a large layered organ that covers the body consisting of the epidermis layer and the dermis layer. Some of the functions of the skin are to protect the body by having an anatomical barrier from external micro-organisms and to be able to sense cold, warmth, pressure and pain. [5]

There are three main stages to wound healing which are the hemostasis phase, inflammatory phase, proliferation phase and the remodelling phase.

1.1.2 The hemostasis phase

In the hemostasis phase, the early events are identified by the vascular and cellular response to the injury which initiates healing response.[6] First the blood vessels on the surface of the wound will shrink and the bruised area will begin to clot due to the platelets fusing together to prevent the wounded area from bleeding further. [7]

An insoluble protein called fibrin is formed during clotting and forms a fibrous mesh to stop the bleeding. This process will be followed closely by the vasodilation (widening) of the capillaries illustrated in blue and red in **Figure 1.1**. This allows a rush of oxygenated blood through the capillaries to the injured area to provide the wound with the necessary healing agent such as platelets, white blood cells (ready to attack and kill invading bacteria), nutrients and vitamins which are crucial for cell repair and regrowth. Platelets are found in large quantities in the blood and are responsible for releasing cytokines and growth factors which initiate recruitment of neutrophils, fibroblasts and macrophages.[8]

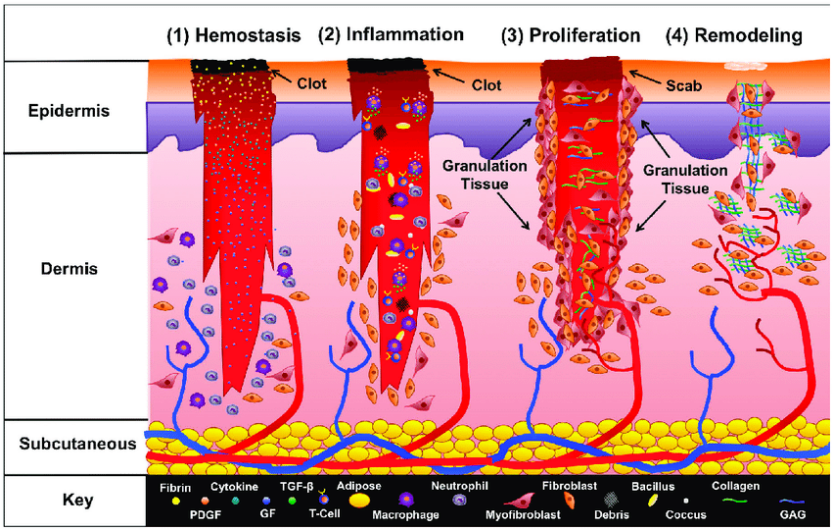


Figure 1. 1 This is an illustration of how the different cells repair the wound in the wound healing process and the cascade of events that occur in each phase. It is divided into these four overlapping phases: Haemostasis, Inflammatory, Proliferative, and Maturation.[9]

1.1.3 The inflammatory phase

In the inflammatory phase, the body will begin by cleaning the wound by eliminating foreign material and bacteria. Leukocytes such as neutrophils and macrophages are white blood cells which are the initial defence mechanism against bacteria and infection.[10] These cells are produced in bone marrow and have the ability to squeeze through small holes of blood vessels and this process is called diapedesis.[11] This process allows the macrophages and neutrophil to easily travel to areas which are infected.

Macrophages are the oldest moderators in the innate system and neutrophils are the most abundant type of white blood cells and are terminally differentiated cells.[11] The difference between macrophages and neutrophils is that macrophages live longer and are larger in size which means that they engulf and ingest more pathogens than neutrophils. Macrophages are recruited by T-cells present in the wound site.[13] The elimination of bacteria in the inflammatory stage is crucial because if the wound is still infected then the wound healing process will be prolonged and may become chronic.

This stage lasts 2-5 days immediately after the injury and is characterized by the redness, heat and swelling of the damaged area.[13] The activation of macrophages leads to the release of

transformation growth factor-beta (TGF-β) and platelet-derived growth factors (PDGF) from platelets, which are instrumental to the initiation of the 3rd phase (proliferation). [15,16]

1.1.4 The proliferation phase

The proliferation phase begins with the mitotic activity of the epidermal cells on the surface of the wound which migrate across the wound surface. Cells in connective tissue which produce collagen and other fibres are called fibroblasts.[17] Fibroblasts multiply rapidly in the deeper parts of the wound and begin to synthesize some collagen which is deposited and cross-linked by enzymes like lysyl oxidase.[18,19]

The function of the collagen is to make a support structure for further migration of cells and proliferation. The extracellular matrix formed by collagen and glycosaminoglycans stabilizes the construct and mechanical integrity of the tissue.[20] New connective tissue and blood vessels i.e. granulation tissue, begin to grow from the base of the wound and fills up the wound by growing on the collagen support scaffold matrix which consists of capillary loops as seen in **Figure 1.1**.

Proliferation lasts for 24-72 hours leading to the fibroblastic stage where type 3 collagen is produced by fibroblast in very large quantities. Type 3 collagen is produced by young fibroblast.[21,22] The collagen fills the defect left by the open wound and collagen fibres that are randomly laid down are cross-linked to continuously reduce the wound size which lasts 15-20 days.[23] The wound then enters the remodelling phase.

1.1.5 Remodelling stage

During the maturation/remodelling stage the wound contracts and scar formation initiates. Myofibroblast produces alpha-smooth muscle actin (α-SMA), which allows collagen to pull the edges of the wound together.[23] The excess cells which were involved in the repairing of the wound are eliminated by apoptosis or cell death. The randomly laid type 3 collagen which formed in the proliferation phase causes the wound to appear thick. In the final stage of the healing phase it is remodelled into an organized matrix of type 1 collagen (mature collagen which is the end product of healed tissue by repair) which aligns the collagen along tension lines and water is reabsorbed so that the collagen fibres can lie more closely together.[25,26]

Cellular waste and impaired extracellular matrix fibre are eliminated by an enzyme called matrix metalloproteinase (MMPs) produced by fibroblasts, macrophages and endothelial cells. If there are disruptions in the remodelling where excess collagen is deposited then keloid scars may form. The wound will only achieve 80% of its original tensile strength even after the wound is completely healed.[27]

1.2 Common causes of chronic wounds

The most common chronic wounds include pressure ulcers, venous leg ulcers and diabetic foot ulcers.[28] Factors that influence chronic wounds include local factors (oxygenation, infection and venous sufficiency) and systemic factors (nutrition, obesity and weak immune system). The insufficient blood supply causes the veins to be reduced in size and also limits the amount of nutrients and growth factors to reach the wound.[29] This causes irreversible nerve damage which leads to chronic wounds. This implies that if an injury occurs they might not feel the pain due to nerve damage and the wound will fail to adequately heal due to the lack of blood supply.[30] The standard wound care is not sufficient to heal a chronic wound and an advanced treatment is needed. [31]

1.2.1 Lack of oxygen in wounds

The amount of oxygen available to the wound is imperative and it is known that wounds that bleed at a greater quantity heal better than wounds that bleed less.[32] Oxygen plays a role in numerous physiological processes which explains these physiological phenomena. [32]

One of the functions that oxygen plays a part in is the production of energy for cells. This metabolic reaction is called cellular respiration and converts biochemical energy from nutrients into Adenosine triphosphate (ATP) which provides energy for cells.[34] This is very significant because during the wound healing process there are many cells such as macrophages, neutrophils and epithelial cells which need energy in order to carry out their task.[35]

Oxygen can also prevent infection of the wound and oxygen treatment such as Hyperbaric oxygen therapy which is a well-established treatment where the patient is placed in a Hyperbaric chamber for severe infections is very efficient.[36] Oxygen also plays a role in the activation of angiogenesis.

Hypoxia is sensed by cells which trigger the angiogenetic factors.[37] The microvascular network is largely governed by hypoxia-inducible transcription factors-1α and -2α.[38] Even though hypoxia induces angiogenetic factors, high levels of oxygen is needed in the proliferation and remodelling/maturation stage of the wound as seen in **Figure 1.2.**

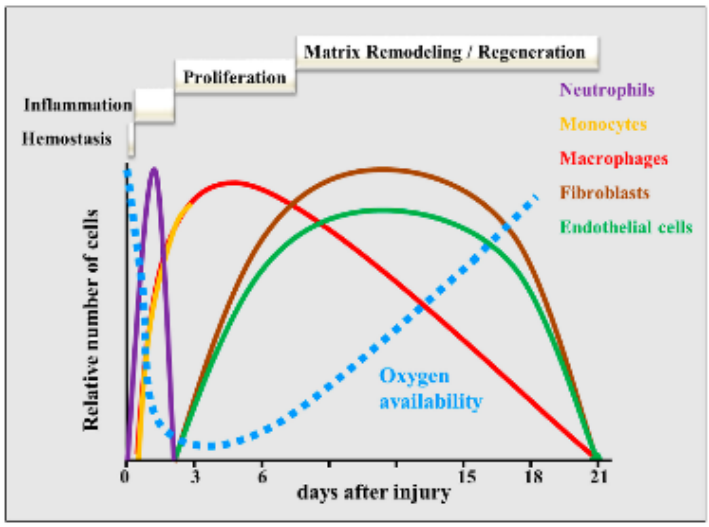


Figure 1. 2 Oxygen is a crucial component of wound healing. This graph illustrates how the level of oxygen affects the presence of macrophages, neutrophils, fibroblast, endothelial cells and monocytes. At certain stages of the normal wound healing, the wound either requires conditions of hypoxia or normal levels of oxygen[39]

Oxygen also enhances the production of fibroblast and endothelial cells and also causes the wound to contract.[40] The partial pressure of oxygen in the tissues is strongly related to the production, formation and development of collagen.[41]

Smokers have lower levels of oxygen in their tissue because the carbon dioxide in the cigarette smoke reduces the oxygen content in blood. The tissue perfusion reduces by more than 30% for more than 45 minutes in specific areas of the body of smokers after one cigarette. In those particular areas of the body, the production of collagen is elevated 1.8 times higher in non-smokers compared to smokers (more than 20 cigarettes per day).[43] Superoxide is a reactive oxygen species which is produced by enzyme NADPH oxidase to kill invading micro-organisms.[44] In **Figure 1.3**, we see how Hydrogen peroxide is produced from the superoxide which is required by other enzymes to kill pathogens.

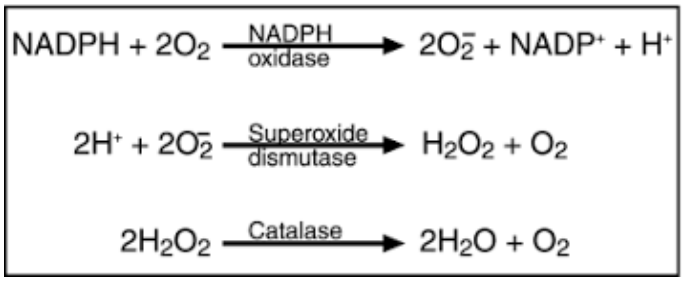


Figure 1. 3 Production $2O_2^-$ reactive molecule and membrane potential changes initiated by electron transfer via the $2O_2^-$-generated by NADPH oxidase. Both $2O_2^-$ and ion movements contribute to the killing of some microorganisms [45]

1.2.2 Infection in wounds

It is very common for a wound to get infected even for healthy patients.[46] When a wound is formed, the micro-organisms which are normally found on the outer surface of the skin have access to the underlying skin tissue.[47] The skin is the largest organ in the body and its primary function is protection, sensation and regulation.[48] Most micro-organisms found on the skin are not harmful when they are on the external layer of the skin but when the outer skin barrier is broken, the bacteria are able to contaminate, colonize or invade the host (the patient).[49] Good hygiene practice is crucial in order to avoid infection because it helps keep pathogens outside the body and increases the ability of your immune response to adequately fight infections and facilitate the wound healing process. [50]

When there is an infection in the wound, the healing process will be inhibited which is why it is important to prevent and/or treat any infection appropriately.[51] In order to determine the type of infection, the condition of the wound and the replication rate of the micro-organisms will help identify the type of infection and the severity of the infection.[52] When a non-replicating organism is present in the wound then the infection is classified as a contamination.[53] The presence of a replicating organism that does not damage tissue in a wound is classified as colonization.[54,55] If the organism is replicating in the wound and causing a tissue response then it is a local infection/colonization.[55] When the infection is severe, the organism would replicate in the wound and cause significant injury to the host. This would be classified as an invasive infection.[57,58]

1.2.3 Role of nutrition

Nutrition plays a crucial role in the maintenance, growth, reproduction and well-being of a patient.[59] Many diseases and ailments are associated with the deficiency of vitamins and other essential nutrients in the body.[60] These nutrients are also very important for a wound to be able to heal thoroughly.[61] They are transported to the wound by the blood and are required for the production of new cells. Patients with malnutrition often need to supplement with special nutrients after trauma or surgery.[62]

Fats and carbohydrates are the main source of energy for the healing of wounds.[63] Cellular ATP is fuelled mainly by glucose and is responsible for providing energy for angiogenesis and the process of introducing new cells into the wounded area.[64] When glucose is used as a source of energy it prevents the depletion of other amino acids and protein substrates. [65]

Proteins are another important nutrient needed for wounds.[67] If there are enough proteins in the body, the formation of capillaries, fibroblast proliferation and synthesis of collagen will be sufficient for the healing process.[67] Deficiency of proteins can result in impaired formation of cells and tissue in the wound and also weaken the immune system which consequently lowers the leukocyte phagocytosis.[69] Collagen is mostly made up of proteins which primarily consist of amino acids such as proline, hydroxyproline and glycine.[69] In order for the body to synthesize collagen, the hydroxylation of lysine, proline needs to take place in the presence of co-factors such as ferrous iron, zinc and copper needs to take place.[71]

During periods of maximum growth, grievous stress and injury, there is a high metabolic demand for arginine.[72] This semi-essential amino acid affects the modulation of the immune system, healing process and hormone secretion. It is also a precursor of proline which implies that sufficient arginine levels are needed to aid with collagen deposition, angiogenesis and wound contraction.[73] Some studies have shown that arginine supplementation is an effective adjuvant therapy in wound care and treatment.[74]

Glutamine is another amino acid which plays a key role in wound healing. It is the most abundant amino acid in plasma and is a vital source of metabolic energy for rapid proliferation of cells such as fibroblasts, lymphocytes, epithelial cells and macrophages.[75] Oral glutamine supplements have

been used by patients who have severe burns, critical illness/trauma and surgical wounds.[76] It is known to improve wound break strength, increase the quantity of mature collagen and reduce infections.[77]

There are several vitamins that play a vital role in the healing process of wounds. Vitamin C also known as L-ascorbic acid is a powerful antioxidant and has anti-inflammatory properties. A deficiency in vitamin C may lead to impairment of the repaired tissue.[78] A lack of vitamin C has been shown to negatively affect the synthesis of collagen and fibroblasts. It also decreases the immune response and angiogenesis which makes the wound increasingly more susceptible to wound infection.[79] Vitamin A and E are other nutrients that have antioxidant properties and play a similar role as vitamin C. Vitamin E is known for reducing the amount of scarring in chronic wounds.[80]

The overall quality of health and nutritional state of the human body is quintessential because it benefits both chronic and acute wounds. Supplements for chronic pressure ulcer containing arginine, vitamin A, vitamin E, vitamin C, and zinc have been shown to improve the overall healing of ulcers.[81] In summary, fatty acids, proteins, vitamins, carbohydrates, arginine, glutamine and zinc contribute to the quality of the healing tissue and the restoration of the wound.

1.3 Diabetic foot ulcers

According to the Health 24 organization, diabetic foot ulcers are one of the biggest problems in South Africa currently. There are three and a half million people living with diabetes (6% of the population) and five million living with prediabetes which is due to high levels of glucose in the blood. Among the three and a half million patients with diabetes, an estimated 15% of them will develop diabetic foot ulcers and 14-24% of them will require amputation. A diabetic foot ulcer is a complication that occurs due to the peripheral nerve dysfunction linked with diabetic neuropathy which causes weakness, numbness and pain due to nerve damage.[82] The peripheral nervous system in the body is the system that sends information from the brain and spinal cord, which is the central nervous system, to the rest of the body. Common causes of foot ulcers in people with diabetes are:

- Loss of feeling
- Poor blood flow

- High blood pressure
- Direct injury

Diabetic foot ulcers have a high risk of infection because they can easily become chronic and the infection can move from the wound to the bone.[83] There are antibiotics available that can treat bone infection however if the infection is critical or too much bone is infected then the bone might need to be amputated to promote better healing and provide a better functioning.[84] Diabetic foot ulcers can be effectively managed and treated if carefully taken care of which can significantly reduce the severity of the complication. According to Harold Brem and Marjana Tomic-Canic from Weill Medical College of Cornell University, New York, 50-70% of all lower limb amputations are due to diabetic foot ulcers and every 30 seconds one leg is being amputated due to diabetic foot ulcers worldwide.[85] It is the leading cause of hospitalization among patients with diabetes and the numbers of people with diabetes are increasing exponentially.[86] This is very alarming because many people in South Africa and the world are affected by this disease but there is very little to no awareness or education about diabetes and its potential complications.[87,88]

1.4 Biofilms in chronic wounds

A biofilm is a layer of bacteria that forms in the wound bed caused by a diverse collection of small micro-organisms that float in fresh or salt water.[89] Patients with a diabetic foot ulcer can be more susceptible to biofilms because of the lack of macrophages and neutrophils in the wounded area to eliminated bacteria.[90] Although they are microscopic, they can present themselves as a shiny layer in the wound depending on how mature the biofilm is.[91]

The formation of the biofilm begins with a free-floating micro-organism that latches onto the surface of the wound. Then the first colonist bacterium secretes a thick slimy layer, which is the production of the extracellular polymeric substance, to protect the bacteria and help it to bind more permanently to the wound.[92] If the attachment of the micro-organism is immediately removed then the biofilm will not form but if the bacteria attaches for a few hours then the biofilm will form as seen in **Figure 1.4**. Detecting a biofilm in the initial stages is difficult because the process happens at a microscopic level which makes it difficult to detect. This layer is impenetrable by conventional antiseptics and antibiotics because it becomes increasingly resistant within a day of formation and

occurs in 90% of all chronic wounds. The biofilms are fully matured after a few days and spit out bacteria in order to spread to other areas.[93]

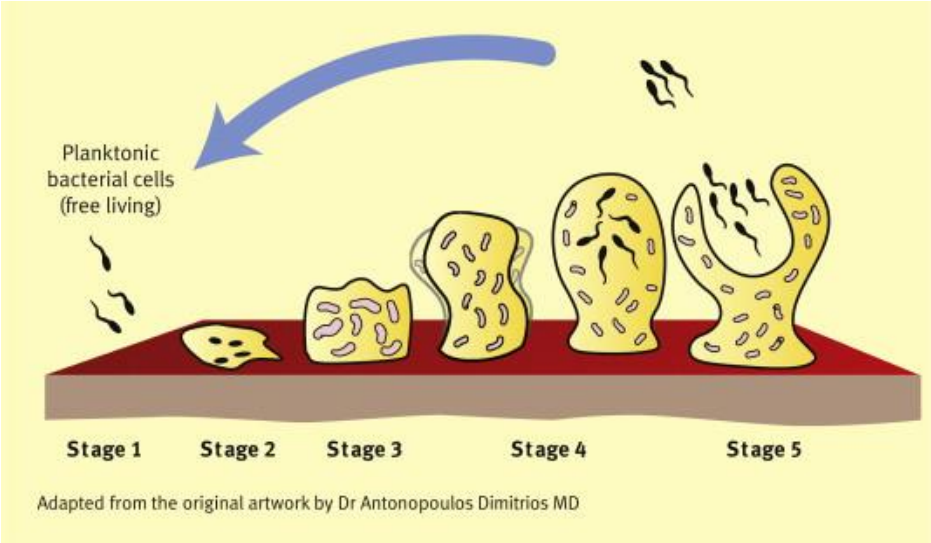


Figure 1. 4 Diagram showing the formation of a biofilm occurring in 5 stages[93]

A chronic inflammatory response is induced by a biofilm which prolongs the wound healing process. Resistant bacteria grow in the biofilm because the community of micro-organisms exchange information rendering antibiotics and antiseptics ineffective.[94] There are potentially two ways to combat biofilms, firstly by prevention and using aggressive antibiotics and antiseptics or by treatment and physically removing the biofilm by debriding the wound.[95] This is the reason why there is a great need in developing an antimicrobial treatment that kills multi-drug resistant bacteria which may be able to reduce the occurrence of biofilms.

1.5 Global impact

Studies conducted by the World Health Organization have shown that there is a great increase in the prevalence of diabetes. In 1980, it was reported that there were 108 million people living with diabetes and that number had increased to 422 million by 2014. This increase disproportionally affects countries with middle to low income such as South Africa.

1.5.1 Impact in SA

Most of the resources and research has been directed towards illnesses such as HIV, TB and malaria in Africa which has led to the insufficient awareness of diabetes and its complications.[88,96] Diabetes is a silent killer, many cases go undiagnosed because the initial symptoms are very subtle. According to Chantal van Rooyen, the founder of NuFit, in the year 2010 the prevalence of diabetes in South Africa was 4.5% which means that it increased by 155% over the past 7 years. This is alarming because 25% of people living with diabetes will develop a diabetic chronic wound and if the wound is not treated properly, it may lead to amputation of the foot. [96]

Besides the physical burden that chronic wounds bring, there are psychological effects that need to be put into consideration which will negatively affect the patient. The major after-effect of having a chronic wound is depression.[97] This is due to potential job loss as a result of not being able to walk. It also causes a reduced quality of life because of the inability to do chores and other activities.[98] Interactions with people will also be difficult since the wound can produce an unpleasant odour and visible drainage.[99] This can likely be embarrassing, causing a person to be withdrawn and isolated. Living with a chronic wound can affect many aspects of a person's life which is why it is important to have proper therapeutic agents to treat the wound as well as a good support system.

1.5.2 High costs of wound management

The cost of wound care treatment for each wound is alarming and according to the Unspiked investigation team, a media operation based in Cape Town, there is no credible recorded data on the amount of money spent for managing chronic wounds in the health care system but, more than R250 million was claimed from medical insurance providers in the year 2016.[99]

Some patients are victims of ‘snake oil’ suppliers as well as reckless surgeons who are too quick with their scalpel which causes the costs to be even higher. More than half of the South African population is living in poverty which means many patients may not afford to adequately treat chronic wounds which can lead to amputation and sometimes death. One controversial treatment that has recently gained popularity is Negative wound pressure therapy (NWPT)[100]. Despite the

evidence that it improved healing, the treatment was found to be flawed and had exorbitant fees as seen in **Figure 1.5**.

NWPT	CONVENTIONAL DRESSINGS
R1,500 – R3,000 per dressing change	R100 – R250 per dressing change
If infected: R2,000 – R3,500 per dressing change	If infected: R250 – R650 per dressing change
Additional costs: Theatre costs R 20,000 Wound Contact layers R200 – R600	Additional costs: Complications depending on aetiology Compression bandaging R 250 – R500 per dressing change

Figure 1. 5 A comparison of the costs of conventional wound care treatment and dressing versus Negative wound pressure therapy (NWPT).[100]

1.6 Current conventional treatment

Topical disinfectants are the most common type of treatment found commercially for wound care.[101] These products have antimicrobial properties and can be divided into two categories. Firstly we have antiseptic products which have antimicrobial properties against a wide range of microbes.[102] The main disadvantage of antiseptic products is that they are often toxic to the host tissue which means it damages cells such as fibroblasts which plays a vital role in the proliferation phase.[103] They are also known to slow down the replication of microbes rather than killing them off. The second classes of antimicrobial agent are antibiotics. These are often chemicals that can be produced synthetically or by microorganisms that inhibit or kill other microorganisms in a dilute solution.[104] Antibiotics can be administered orally or can be applied directly on the affected area. Antibiotics are non-toxic in most cases but they are only potent against a small spectrum of bacteria and can cause some bacteria to become drug resistant.[105] The use of antimicrobial agents on chronic wounds can become effective for infected chronic wound but the treatment for the uninfected chronic wound is still more challenging.

The wound care products which are currently available include[106]:

- dressings containing silver or silver sulfadiazine cream
- polyhexamethylene biguanide (PHMB) gel or solutions
- iodine (either povidone or cadexomer)
- medical grade honey in ointment or gel form

All of these products can promote a clean and infection-free wound but cannot assist in other wound healing processes such as the proliferation of fibroblasts or collagen formation.

1.7 Different novel approaches for treatment of chronic wounds

1.7.1 Apligraf

In the past couple of years, a vast number of biotechnological advances have been made in pursuit of finding a substitute for skin and tissue. Apligraf is a new approach for chronic wound care that accelerates wound closure.[107] This unique treatment involves creating a living bilayer from healthy human cells of the skin and placing them directly on the wound. The idea is to assist the wound healing process by incorporating collagen directly on the wound to enhance cell maturation and cellular matrix.[108]

Apligraf is different to skin graft because in skin grafts, a piece of skin is transplanted from a more healthy part of the body to the wounded area or a different individual can donate a piece of skin to the patient.[109,110] Apligraf, on the other hand, integrates allogeneic cultured cells from humans.[111] The bilayer contains an epidermis which is the outer layer that contains living keratinocytes and a dermis layer which is the inner layer that contains fibroblast and collagen. [95]

Most ulcers are caused by a lack of biological substances which are inhibited by poor blood circulation to the wounded area. Many physiological processes on the healing process are hindered

due to lack of nutrients which inhibits cell proliferation and the recruitment of growth factor.[112] Apligraf is able to supply the wound with more fibroblast and collagen to promote the healing process and also protects the wound from mechanical damage as well as bacteria. Unfortunately, this treatment is very expensive and costs approximately €4656 in the first year.[113] Another disadvantage is that the patient needs to wrap the wound with a dressing to keep it in place and another dressing which will be changed every week.[114]

1.7.2 Trafermin

Trafermin is a synthetic thrombin peptide-based compound which is used as a spray for ulcers and has gained popularity in Japan in recent years. Trafermin is a human clone lambdaHFL1 reduced precursor which is a recombinant form of basic fibroblast growth factor (bFGF).[115] It strongly binds to fibroblast growth factor receptor 2 and fibroblast growth factor receptor 8 which makes it a potent agonist.[116] This product's main function is to enhance the migration of monocytes, neutrophils, macrophages, fibroblasts and also assists in the production of granulation tissue.[117]

There are several other developments in the wound treatment industry which aim at enhancing the cells involved in the proliferation phase of the healing process. Patients with non- healing wounds usually have illnesses that inhibit angiogenesis hence there is a great need for therapeutic agents that stimulate the production of growth factors and new cells.

1.7.3 Murepavadin

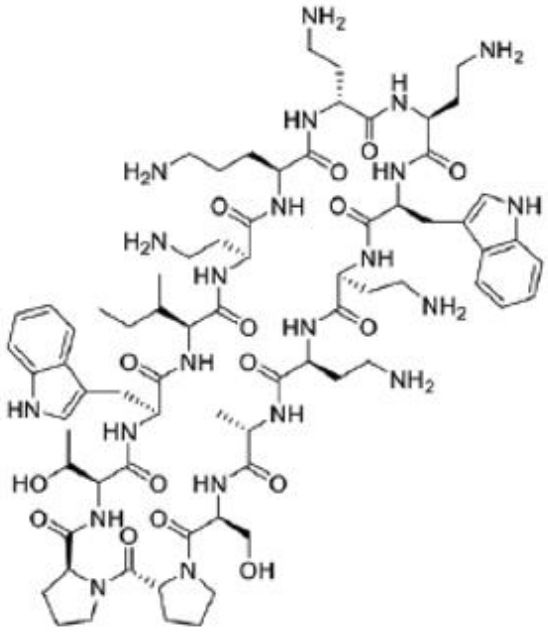


Figure 1. 4 Murepavadin which is also known as POL7080 is an antimicrobial peptidomimetic based on the cationic peptide called protegin 1[118]

Polyphor is a biopharmaceutical company which is based in Allshwil, Switzerland which has developed a cyclopeptide which can be considered to be the first of a novel class of antibiotics. [119] According to Polyphor, murepavadin targets the most dangerous multi-drug resistant microbe called *P.aeruginosa* and is highly selective to all known *P.aeruginosa* strains. *P.aeruginosa* is the second leading cause of Hospital-acquired pneumonia and is estimated to cause 200,000 deaths in Sub-Saharan Africa.[120] Murepavadin was tested against 1500 strains of *P.aeruginosa* and is highly active *in vivo* with an $MIC_{90} \leq 0.25$ µg/ml. It has 14 amino acids as illustrated in **Figure 1.6** and is administered intravenously. The peptide targets the lipopolysaccharide transport protein (LptD) of the bacterium. This protein is essential for lipopolysaccharide biogenesis.

This peptide is currently undergoing phase III trials and if successful, will help develop more antimicrobial peptides as a new generation of antibiotics.

1.8 Introduction to Antimicrobial peptides

1.8.1 What are Antimicrobial peptides?

Antimicrobial peptides and proteins (AMPs) are a diverse class of naturally occurring molecules that are produced as the first line of defence by all multicellular organisms.[121] Recent studies have shown that antimicrobial peptides have the potential to be potent agents against pathogens which have multidrug-resistant properties. They are crucial components of the innate immunity and permit humans to resist infection by microbes. These peptides can have a broad activity and directly kill bacteria, yeasts, fungi, viruses and even cancerous cells.[122]

Antimicrobial peptides are normally cationic and have an overall charge that typically ranges from +2 to +9. These peptides are relatively short with approximately 10 to 50 amino acids.[123] A considerable portion of the peptide is hydrophobic and all of these properties contribute to the different types of resulting peptide folds. The peptide fold allows the peptide to have amphiphilic structures which have hydrophobic regions and cationic regions in the peptide as shown in **Figure 1.7**.[124]

Four types of peptide structural folding[125]:

1. β-sheet peptides: which are stabilized by two or more disulfide bridges and have pleated sheets.
2. α-helical peptides: which are stabilized by two or more disulfide bridges and have coiled structure.
3. Extended structures: are polypeptides rich in glycine, proline, tryptophan, histidine and arginine.
4. Loop peptides: peptides with one disulfide bridge.

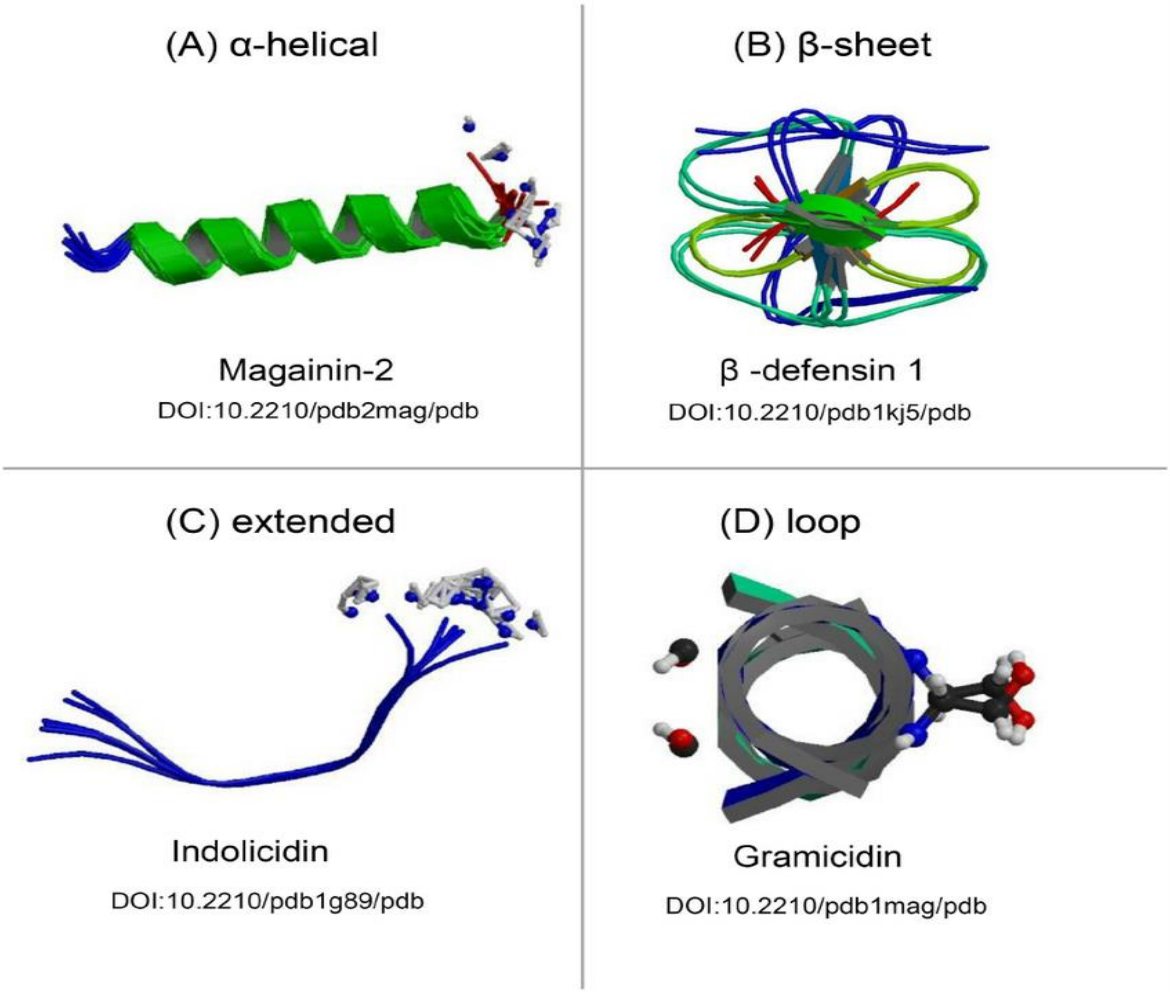


Figure 1. 5 The different structures that antimicrobial peptides can adopt [126]

AMPs are released by humans, animals and insects as antibiotics to protect against potential pathogenic microbes, but microbes also produce AMPs to defend their environmental niche.[127] In higher eukaryotic organisms, AMPs can also be referred to as 'host defense peptides', spotlighting their additional immunomodulatory activities.[128] These activities vary and are specific to the type of AMP and include a diverse set of cytokine and growth factor-like effects that are relevant to normal immune homeostasis. In some instances, the inappropriate expression of AMPs can also induce autoimmune diseases, thus further highlighting the importance of understanding these molecules and their complex activities.[129]

These peptides are crucial in numerous roles as seen in **Figure 1.8** and can provide templates for two classes of drugs, direct-acting antimicrobial peptides and immune modulation peptides. Antimicrobial peptides are able to induce a T-cell regulatory immune response and also destroy

pathogens directly by making contact with the target organism by electrostatic attraction.[130] The peptide has a positive charge and most bacterial surfaces are anionic which causes disruption in the bacterial membrane.

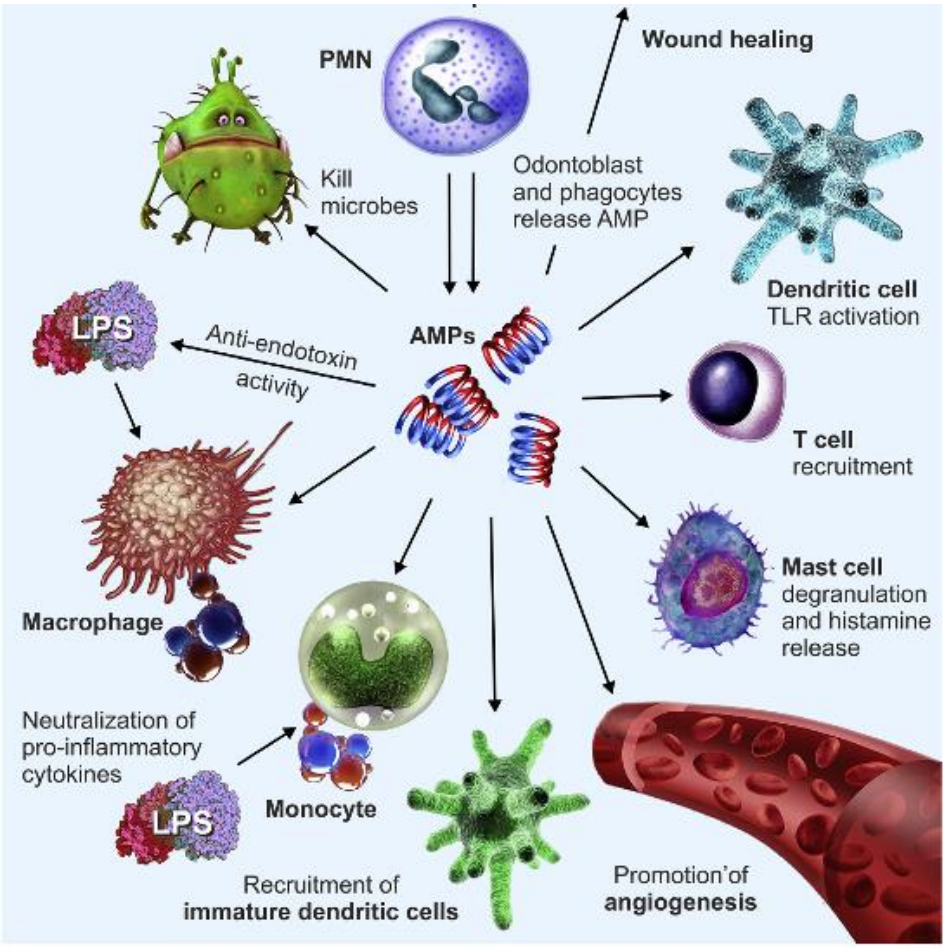


Figure 1. 6 An illustration of the roles that AMPs play in cell proliferation and migration, immune modulation, wound healing, angiogenesis and the release of cytokines[131]

1.8.2 Mode of action of antimicrobial peptides

There are several models that describe the mechanism of the antimicrobial peptides against the bacterial membrane. The interaction between the peptide and the bacterial membrane differ because bacteria have different lipid structures and pore stability and peptides have different charges and hydrophobicity distribution, which is why there is such a variety of mechanisms as seen in **Figure 1.9.** Most antimicrobial peptides share some similar features such as having cationic

and hydrophobic regions. These properties assist in predicting the mechanism by which the peptides can disintegrate the membrane of the bacteria, but each peptide may interact differently with the membrane due to the specific properties of the peptide and the membrane.[132]

The most notable models are the barrel-pore, carpet-like and toroidal pore. The barrel-pore mechanism involves the binding of a monomer to the membrane. The monomer then assembles with other peptide monomer and inserts into the membrane. The peptide monomers then recruit more monomers which cause the pore size to increase.[133] The carpet like model is the most common mechanism for antimicrobial peptides. In this mechanism, the peptides bind on the membrane and cover it like a carpet. The peptides then re-orientate themselves so that the hydrophobic region of the peptide faces the lipid area and the hydrophilic parts faces towards the phospholipid areas. This causes disruption of the curvature of the membrane resulting in the disintegration of the bacterial membrane.[134] The toroidal pore is similar to the barrel-pore model but the peptide always associates with the lipid layer which means that when it inserts itself it causes the lipid monolayer, represented in blue in **Figure 1.9**, to bend and the curvature disrupts the membrane causing it to disintegrate.[135]

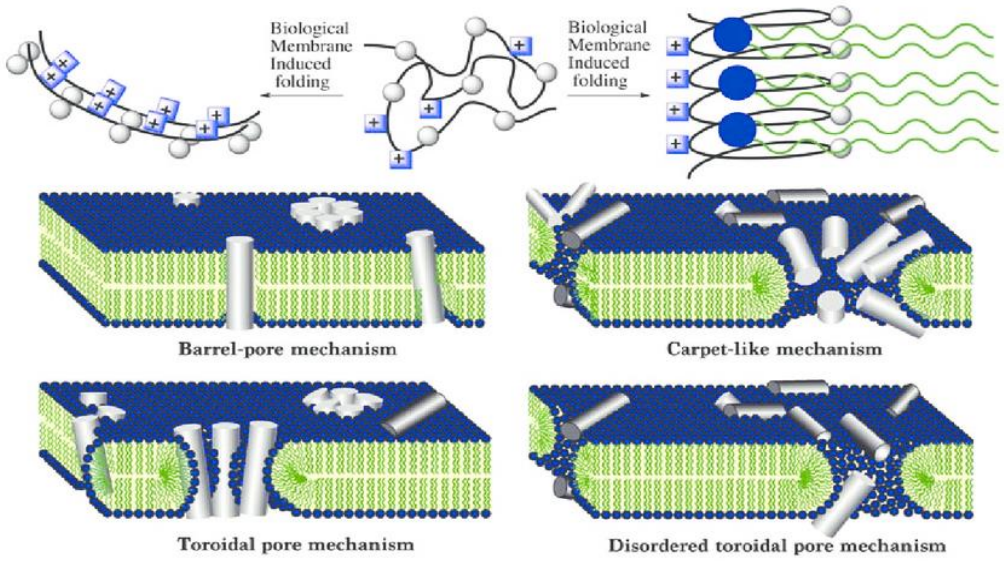


Figure 1. 7 The different types of interaction between the AMP and the target membrane[136]

1.8.3 Benefits of antimicrobial peptides

There is a great interest in these biological compounds because of the multitude of immunomodulatory roles they play which include cell recruitment, enhancement of cell maturation and increase in the formation of the new blood vessel (angiogenesis). Another advantage is that they are very synergic. In a study conducted by Ulvatne *et al*., several synthetic antimicrobial peptides were combined with clinically used antibiotic to observe synergetic interaction.[137] The study showed that all of the peptides synthesized in the study have a synergetic interaction with erythromycin when tested against *E. coli*. Synergy was also observed with rifampicin and two peptides against *E. coli*.[105]

Many AMPs are effective against multi-drug resistant (MDR) bacteria and possess a low propensity for developing resistance.[137] The bacteria achieve resistance to antibiotics by several routes including inhibition of the drug-target interaction, modification of the drug-binding site in target proteins, and efflux of the drug from target cells.[138] Microorganisms can also alter their genetic patterns in response to environmental changes using their own complex systems called sensor-transducer response systems. Bacteria struggle to modify their gene expression in the presence of AMPs.[139] The low propensity for developing resistance is due to their distinguished mode of action. Most AMPs, with their amphipathic nature, directly act on the membrane of the pathogen.

1.8.4 Turning antimicrobial peptides into drugs

The increasing occurrence of multidrug-resistant pathogens has created an urgent need for suitable alternatives to current antibiotics. Antimicrobial peptides (AMPs), which act as defensive weapons against microbes, have received great attention over the years because of the broad-spectrum activities, unique action mechanisms and rare antibiotic-resistant variants.[140] There are numerous FDA approved antimicrobial peptides in the market and even more are sold commercially, but not many of them can substitute conventional antibiotics. Even though most peptides are not US FDA approved other countries have approved many peptides for commercial use. In **Table 1.1** are a few of the peptides that Rawalpindi Development Authority (RDA) approved. Despite the desirable characteristics of peptides, they have shown limitations in pharmaceutical development due to

toxicity, stability and manufacturing costs. Because of these drawbacks, only a few AMPs have been tested in Phase III clinical trials and even fewer AMPs have been approved by the US FDA.[141] The clinical development of antimicrobial peptides has mostly been restricted to topical applications for diabetic foot ulcers, oral candidiasis and skin disease.

Table 1. 1 A short list of RDA approved peptides for therapeutic treatment[118]

Company name	Generic name	Trade name	Year of RDA approval
Johnson & Johnson	Nesiritide	Natrecor, Noratak	2001
Lily	Teriparatide	Forteo	2002
Trimeris	Enfuvirtide	Fuzeon	2003
Praecis	Abarelix	Plenaxis	2003
Elan	Ziconotide	Prialt	2004
Amylin	Pramlintide	Symlin	2005
Amylin	Exenatide	Byetta	2005
Ipsen	Lanreotide	Somatuline, Angiopeptin	2007
Amgen	Romiplostim	Nplate	2008
Ferring	Degarelix	Firmagon	2008
Sanofi	Aflibercept	Zaltrap	2011
Forest Laboratories	Linaclotide	Constella	2012
DiscoveryLabs	Sinapultide	Surfaxin	2012

Synthetic antimicrobial peptides have a short half-life because they are easily broken down by proteases in the body. These obstacles could be overcome by well-known methods such as changing physicochemical characteristics of the peptide, introducing non-natural amino acids, acetylation or amidation, as well as modern techniques such as molecular targeted AMPs and liposomal formulations.[142,143]

Membrane permeability, selectivity and enzyme stability are the challenges faced by peptide-based molecules targeting various ailments. We, therefore, have selected the following modifications to improve our wound healing peptides:

1. To improve membrane permeability we will utilise fatty acids and cage moieties such as palmitic acid and adamantane.

- Palmitic acid (Fatty acid) has been reported to be a good mitochondrial permeability transition promoter and various cosmetics companies have designed anti-ageing creams with peptides coupled to palmitic acids.[144]
- Adamantane (Cage) derivatives enhance the biological activity, membrane permeability and retard biodegradation when incorporated into biologically active molecules according to reported studies. [145]

2. Improving selectivity and enzyme stability will be achieved through peptoids, and incorporation of *N*-methylated and D-amino acids:

- Peptoids are polymeric compounds composed of *N*-substituted glycine (NSG) residues. They are particularly flexible due to the lack of hydrogen bonding as well as the tertiary nature of the amide bonds that permit them to isomerize between trans and cis conformations far more freely than secondary amides in peptides.[146] They have been reported to possess increased enzymatic stability.[147]
- *N*-methylated peptide amide bonds have been proven to exhibit higher resistance to proteolysis and thus results in improved bioavailability and enhanced duration of action of the peptide.[148]
- D-amino acids have been reported to induce an exceptional specificity of the immune response hence many researchers are applying them in the design of vaccines.[149]

Thus, the current challenge in this field is to develop therapeutic AMPs at a reasonable cost as well as to overcome the limitations.

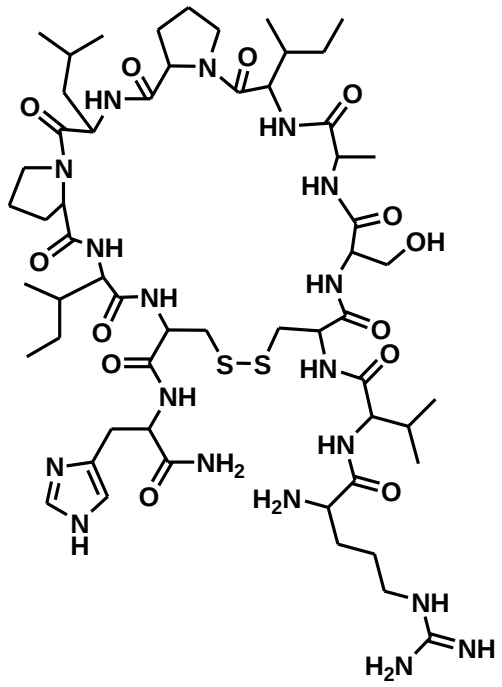


Figure 1. 8 ChemDraw sketch of the original Tigerinin RC 1 peptide with the amide ending and disulfide bridg

1.9 Tigerinin RC1

Antimicrobial peptides that are derived from amphibians are mostly classified into two categories, linear α-helical peptides without cysteine and peptides with C terminal loop via a disulfide bond. There is a wide variety of amphibian antimicrobial peptides and each has a different antimicrobial spectrum.

Tigerinin RC1 is a peptide secreted from the Indian frog Rana tigerina. This peptide has the ability to cause damage to the bacterial membrane in the formation of pores or membrane disintegration. The formation of the pores is caused when the cationic region of the peptide binds to the anionic membrane of the bacteria. The cation region is able to penetrate the membrane while the hydrophilic part of the peptide remains outside the membrane. This causes disruption in the bacterial membrane and pore formation occurs. This is the manner in which most antimicrobial peptides destroy microbes.

This peptide is one of the smallest non-helical cationic antimicrobial peptides from amphibians. Tigerinin RC1 is made up of 12 amino acids (Arg–Val–Cys–Ser–Ala–Ile–Pro–Leu–Pro–Ile–Cys–

His–$CONH_2$) as seen in **Figure 1.10**. This dodecapeptide has a disulfide bridge and is the most active member of the family of peptides derived from amphibians.[122] This disulfide bridge which forms a loop gives the β-turn conformation and contributes to the resistance against proteolysis. Another advantage that Tigerinin RC1 has over other antimicrobial peptides is that it induces transforming growth factors for wound healing and promotes collagen formation during the wound healing process as illustrated in **Figure 1.8**. Research has shown that it exerts significant effects on the induction of macrophage recruitment to the wound site and promotion of keratinocytes which lead to re-epithelialisation and granulation tissue formation. Additionally, this peptide promotes the proliferation and remodelling phase. These peptides have the ideal properties of a wound healing agent and can address some of the challenges which we face with conventional antimicrobial treatments.

1.10 Aim and Objectives

Main Aim: To design and synthesize a library of novel, bioavailable, non-cytotoxic wound healing and antimicrobial peptides and peptidomimetics derived from Tigerinin RC1. The focus will be on making these peptides and peptidomimetics less toxic and more bioavailable.

To achieve these aims the following strategies or objectives were used:

- Cyclization of the peptides to improve metabolic stability and binding affinity/specificity to their molecular targets
- Addition of palmitic acid to the peptide sequences to improve membrane permeability
- Addition of adamantane carboxylic acid to the peptide to increase biological activity
- The incorporation of D- amino acids to induce specificity and increase stability
- Incorporation of peptoids which are highly flexible to improve metabolic stability
- The incorporation of *N*-methylated amino acids to improve resistance to proteolysis

1.11 Hypothesis and question

Antimicrobial peptides derived from Tigerinin RC1 can eliminate bacteria and induce growth factors to speed up the wound healing process. The main questions to test this hypothesis are as follows:

- Can the cationic properties of Tigerinin RC1 increase the binding and wound healing properties?
- Is there a correlation between structure and activity?

Chapter 2

Synthesis and characterization of Tigerinin RC 1 and its derivative peptides

2.1 Introduction

Tigerinin RC1 (Arg–Val–Cys–Ser–Ala–Ile–Pro–Leu–Pro–Ile–Cys–His-COOH) peptide, was chosen as a starting point for the design of antimicrobial peptides. Researchers have proven that this peptide has strong antimicrobial properties and is active against a wide variety of gram-negative bacteria.[1]Tigerinin RC1 belongs to a family of peptides that is characterized by a disulfide-bridged cationic nonapeptide ring, highlighted in blue in **Figure 2.1**, and adopt a β-turn conformation.[150] These peptides have the potential to be powerful new generation antibiotics however several improvements need to be made in order to achieve this.

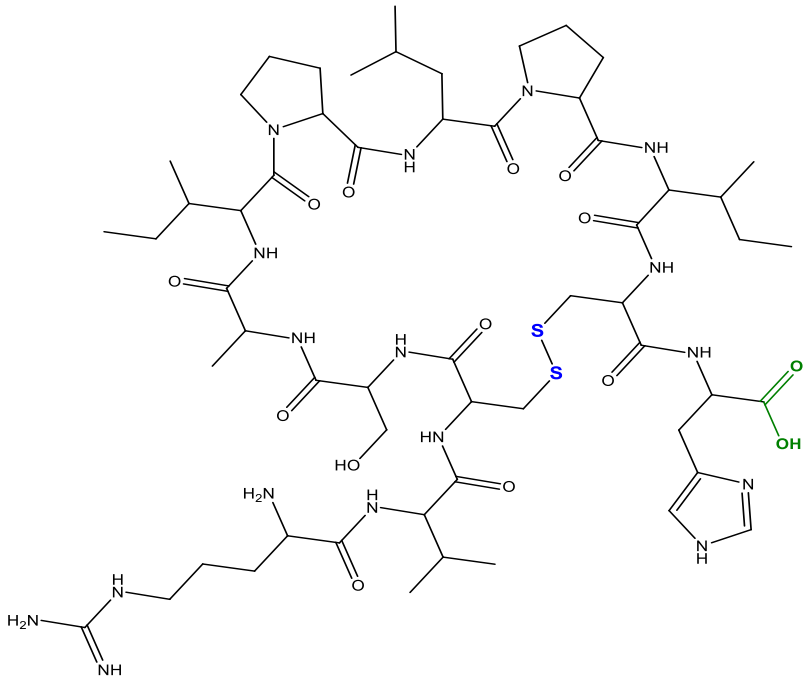


Figure 2. 1 The molecular representation of the Tigerinin RC1 peptide

In this chapter, several peptides based on the Tigerinin RC1 sequence were synthesized and characterized. The properties of the peptides were slightly varied in an attempt to improve the biological properties of the original peptide and to evaluate the crucial moieties of the peptide that contribute towards its antimicrobial properties. One of the properties that was evaluated was the effect of the C-terminal ending. This was achieved by amidation of the C-terminal. This may affect the solubility of the peptide as well as the susceptibility to attack by proteases which may not recognise the amidated C-terminal. The linear version of the peptide was also assessed to better understand the significance or effect of the peptide structure on the membrane pore formation. Several species of bacteria have been identified to have membrane permeability barriers to many antibiotics. In order to overcome this challenge, fatty acids were incorporated into the peptide. According to literature, fatty acids are able to penetrate cell membranes. These compounds are carboxylic acids and are widely used in cosmetic product and personal care products as surfactants and opacifying agents. Fatty acids usually contain long aliphatic chains although they can be branched or caged. Unnatural amino acids were also integrated into the peptide sequence in order to make the peptide less susceptible to enzymes, which break up peptides in the body. As discussed in Section 1.8.4, these modifications were a venture to turn our wound healing antimicrobials into drug-like molecules.

The peptides were synthesised using a similar methodology or synthetic route. Slight changes were made to accommodate difficult coupling reactions in each peptide such as changing coupling time and the choice of couple reagents. Due to the changes in each peptide sequence, the solubility and polarity of the peptides were affected which changed the retention time of the peptides in the High-Performance Liquid Chromatography (HPLC) as well as the solvent used to dissolve the peptides for purification.

In this chapter, Tigerinin RC1 peptide analogues that contained all 12 amino acids were synthesized although the C-terminal and N-terminal endings were varied and the overall structure cyclized. We anticipate that the potency of the peptide will be amplified along with the distinct parts of the peptide molecule that contribute towards its antimicrobial properties.

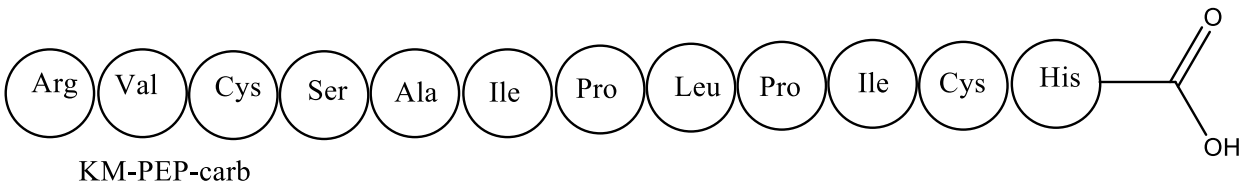
2.2 The KM-PEP-carb peptide

2.2.1 Design and synthesis of KM-PEP-carb

In this section, the linear version of Tigerinin RC1 (KM-PEP-carb) was investigated. This peptide assisted in evaluating the importance of the structure on the antimicrobial activity of the peptide. Previous studies have shown that naturally occurring antimicrobial peptides may occur as linear or cyclized however there is evidence that the structure of the peptide affects the activity. Considering the known structure-activity correlation, it can be postulated that Tigerinin RC1 will lose its activity due to the lack of **s-s** bond even though some linear cationic peptides have also been proven to have antimicrobial activity. In this section, this claim was investigated. According to *et al*. the minimal peptide concentration needed for the complete inhibition of cell growth in liquid medium for Tigerinin RC1 against *P*. *aeruginosa* ATCC27853 is 10 µg/ml. This shows that it has strong antimicrobial properties. Since the KM-PEP-carb peptide (**Figure 2.2**) is precisely the same as the Tigerinin RC1 peptide with the exception of the disulfide bond between the cysteine amino acids, the effect of the structure on the antimicrobial activity was explored.

Basic solid phase peptide synthesis (SPPS) with Fmoc chemistry was used for the synthesis of the KM-PEP-carb. The synthesis was carried out using a peptide synthesizer in a reaction vessel with a frit at the bottom. The resin chosen for this peptide was an activated 2-chlorotrityl resin (1.15 mmol/g, 292 mg) to produce the COOH C-terminal. The first amino acid which was coupled was histidine (2 M) coupled using *N*, *N* diisopropylethylamine (DIPEA) (1 ml) and dry DCM. The following amino acids that were coupled were activated with HBTU (1.9 M) in DMF which was at a slightly lower concentration to the amino acids in order to avoid the nucleophilic coupling reagent from attacking other possible electrophilic molecules in the reaction mixture which can cause side products. The full sequence of the peptide chain was confirmed using mass spectroscopy however incomplete peptides, as well as peptide masses with one amino acid missing, were also detected. F-moc protected amino acids with large side chain protecting groups such as arginine (2,2,4,6,7-pentamethyldihydrobenzofuran-5-sulfonyl), histidine (tert-butyloxycarbonyl) and cysteine (trityl) are known to give challenges due to steric hindrance. The combination of the protecting group on the side chain, the amino acid as well as the F-moc on the amine group led to the low efficiency of the coupling reaction. Since the peptide contained two cysteines, arginine

and histidine, challenges in the synthesis of the peptide were expected. The HPLC-MS also revealed that some amino acids did not completely couple such as proline, valine, isoleucine and/or leucine. Other possible problems that could have occurred include aggregation which is caused by hydrogen bonding, where secondary structures form, as well as enantiomerization whereby the carboxyl group activation enhances the acidity of the H atom on the α-carbon.



KM-PEP-carb

Figure 2. 2 The linear peptide sequence of KM-PEP-carb

Even though these amino acids are known to give challenges, each peptide behaved significantly different during synthesis because we believe they adopt different structural conformations, which causes them to have different properties. Consequently, since KM-PEP-carb was the first peptide synthesized the coupling reaction time was 20 minutes for all amino acids. The full peptide sequence which was attached on the resin was cleaved off the resin using a cleavage mixture described in section 6.4.9 and the peptide was dissolved in 100% HPLC grade DMSO.

2.2.2 Purification of KM-PEP-carb peptide

Several attempts were made during method development to obtain the run time and solvent gradient system that can purify the peptides. The gradient elution method employing water and acetonitrile in 15 minutes was used, buffer A, 0.1% formic acid in H_2O; buffer B, 0.1% formic acid in CH_3CN and the column temperature was set to 20 °C. Acetonitrile was allowed to increase from 5% to 95% in 15 minutes with a 15 ml/min flow rate and this method gave the best separation.

When the run time was extended to 20 minutes with the intention of increasing the amount of time the peptide interacts with the stationary phase the elution time of the compound of interest did not have a significant change. An isocratic system of 45% acetonitrile in water from 5 minutes to 10 minutes was also investigated and the compound of interest co-eluted with the impurities. **Figure 2.3** below displays the UHPLC-MS of the peptide with the retention time of 8.54 minutes. The

calculated mass for KM-PEP-carb was 1307.68 m/z and the mass found was $[M+H]^+$ 1308.68. The purity was also determined using the UHPLC-MS which yielded a value of 98%. After purification, the peptide was dried on the rotary-evaporator resulting in a mass of 14.7 mg and a yield of 3.5%.

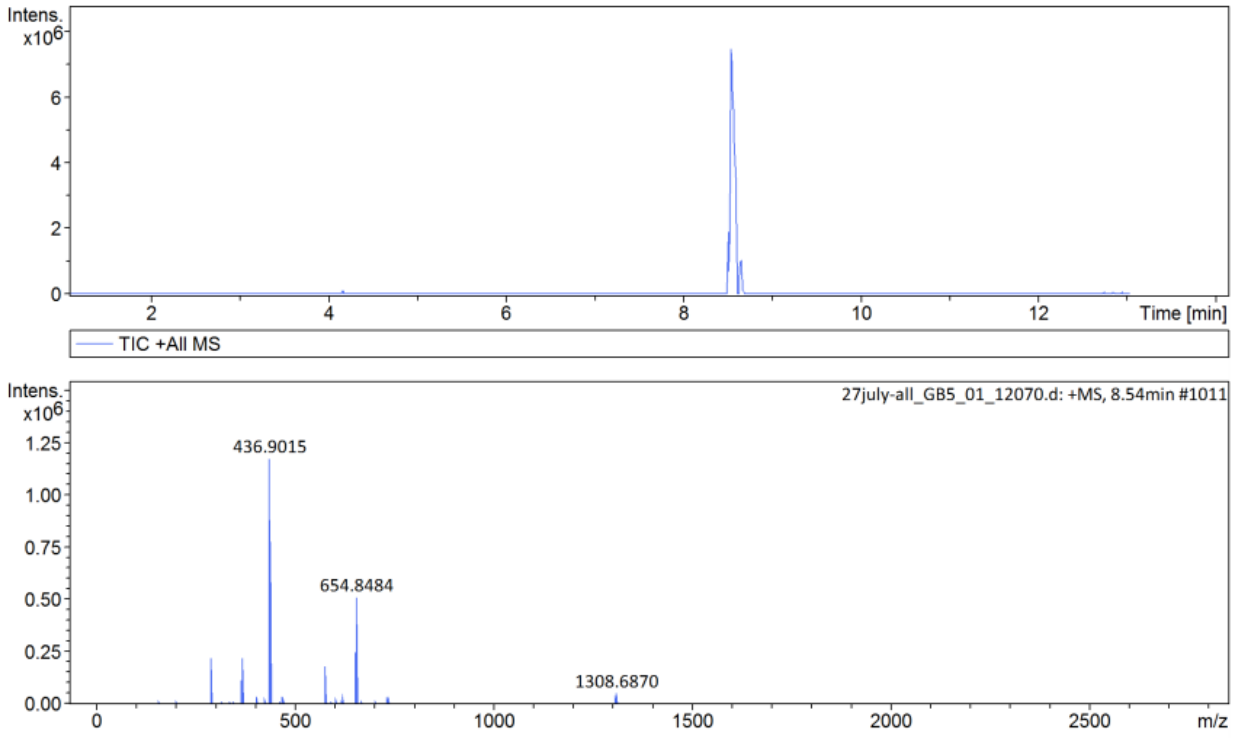


Figure 2. 3 UHPLC TIC chromatogram of purified KM-PEP-carb peptide with the retention time of 8.54 minutes

2.2.3 Biological testing of KM-PEP-carb peptide

A cytotoxicity study was done on KM-PEP-carb to determine the concentration that would have the most adverse effect on human cells. The study was conducted on the HIV growth support human T cell-line, Human T cell leukaemia (MT-4). The biological source of MT-4 cells is human lymph which is a fluid that runs through vessels and nodes in the lymphatic system. The cytotoxicity study was outsourced to Mintek- Advanced Material Division and further information is in the appendix. The peptide was weighed out to 0.6 mg and was further diluted with concentration ranging from 100 µg/ml to 1.56 µg/ml.In **Table 2.1** the various concentrations of

KM-PEP-carb and the results show that the toxic effect increases as the concentration increases. This showed that at 100 µg/ml the peptide had a Toxicity % of 52.05. This implied that the peptide could be considered as toxic however the level of toxicity may be relatively low considering that MT-4 cells are rather sensitive. In order to lower the cytotoxicity, several changes will have to be employed on the peptide.

Table 2. 1 Cytotoxicity study on KM-PEP-carb

Concentration(µg/ml)	KM-PEP-carb (Toxicity %)
100	52.05
50	44.34
25	43.24
12.5	42.49
6.25	43.26
3.125	31.96
1.56	26.88

The peptide was then evaluated for antibacterial activity in order to determine the minimum inhibitory concentration (µg/ml) against *E.coli*, *P. aeruginosa*, *S.aureus* and *B.subtilis*. The peptide was found to be inactive against all of the bacteria at 256 µg/ml. A high concentration of the peptide would have been needed to inhibit the growth of the bacteria. However, a study conducted by Y. Song *et al.* showed that the cyclic Tigerinin RC1 with an amide ending was active against

P. aeruginosa (MIC ≤ 10 μg/ml). [150] This suggests that the activity of the peptide has been significantly affected by the structural changes and that the disulfide bond is a key moiety for antimicrobial activity.

2.3. KM-PEP-cyc-amide peptide

2.3.1 Design and synthesis of KM-PEP-cyc-amide peptide

Recent evidence shows that cyclic peptides have better biological activity compared to their linear counterparts due to the conformational rigidity. The rigidity of the peptide strengthens the binding efficacy to the target site. This is due to the decrease in entropy in terms of the Gibbs free energy. Consequently, the binding energy of antimicrobial peptides towards the target site increases.

The KM-PEP-cyc-amide analogue and Tigerinin RC1 are both cyclic peptides and have identical amino acids but the C terminal is converted into an amide rather than the carboxylic ending for KM-PEP-cyc-amide (**Figure 2.4**). The choice of peptide endings often depends on the intended function of the peptide and the nature of the binding site.

One of the benefits of having an amide ending on the C-terminal is that it avoids the abnormal inception of a charged group on the peptide ending. Another advantage of having an unnatural C-terminal is that the peptide may behave like and/or be recognized as if it were a part of the whole protein. The peptide may be more resistant to the degradation resulting from the actions of a peptidase that cause the cleavage of the ending of the peptide bond. According to Y. Song *et al.* the amidation of the C-terminal of Tigerinin RC1 resulted in stronger antimicrobial activity than the non-amidated dervative.[150]

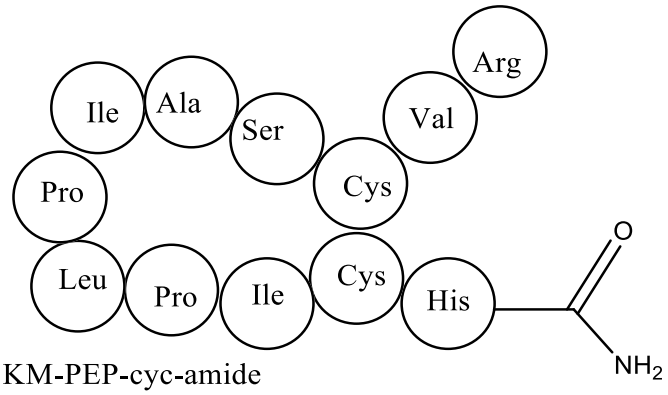


Figure 2. 4 The peptide sequence of KM-PEP-cyc-amide

Manual solid phase peptide synthesis (SPPS) and Fmoc chemistry was used for the synthesis of the KM-PEP-cyc-amide. The synthesis was carried out using a peptide synthesizer in a long-necked reaction vessel with a frit at the bottom. The resin used for this peptide was a rink amide resin (0.4 mmol, 291 mg) to produce the $CONH_2$ C-terminal. The first amino acid which was coupled was histidine (2 M) using *N, N* diisopropylethylamine (DIPEA) (1 M) in DMF. The following amino acids that were coupled were activated with HBTU (1.9 M) in DMF. Double coupling was used for proline, cysteine, isoleucine and leucine to enhance the coupling efficiency and increase the peptide yield. Double couple is when the coupling reaction is repeated without removing the Fmoc protecting group to enable efficient coupling. The full sequence of the peptide chain was confirmed using mass spectroscopy and some of the other peptide fragments which formed in the previous peptide were not present in the KM-PEP-cyc-amide peptide spectra, which indicated that double coupling the amino acids increased the coupling efficiency although some impurities were present.

Once the full peptide sequence was confirmed it was cyclized using iodine then cleaved off the resin the resin using a cleavage mixture described in section 6.4.9 and the peptide was dissolved in 100% HPLC grade DMSO.

2.3.2 Purification of KM-PEP-cyc-amide peptide

The 5-95% water/acetonitrile gradient 15-minute method with 15 ml/min flow rate method (as reported above) was used on prep-HPLC because KM-PEP-cyc-amide and KM-PEP-carb are both basic and both had a charge of +2 which means that they could behave similarly. The elution of

KM-PEP-cyc-amide was earlier than KM-PEP-carb. It's evident that the cyclic structure of KM-PEP-cyc-amide caused the peptide to interact differently with the C18 column which resulted in an earlier retention time compared to KM-PEP-carb. A possible reason for the early elution of the peptide may be due to the change in structure which may have decreased or caused less binding with the column.

Demonstrated in **Figure 2.5** is the UHPLC-MS showing the retention time at 6.63 minutes for the peptide. The calculated mass for KM-PEP-cyc-amide was 1304.68 m/z and the mass found was $[M+H]^+$ 1305.69 m/z. The purity was also evaluated using the UHPLC-MS which was found to be 99%. Once purification was complete, the peptide was dried using the rotary-evaporator resulting in a mass of 3.9 mg and a yield of 2.5%.

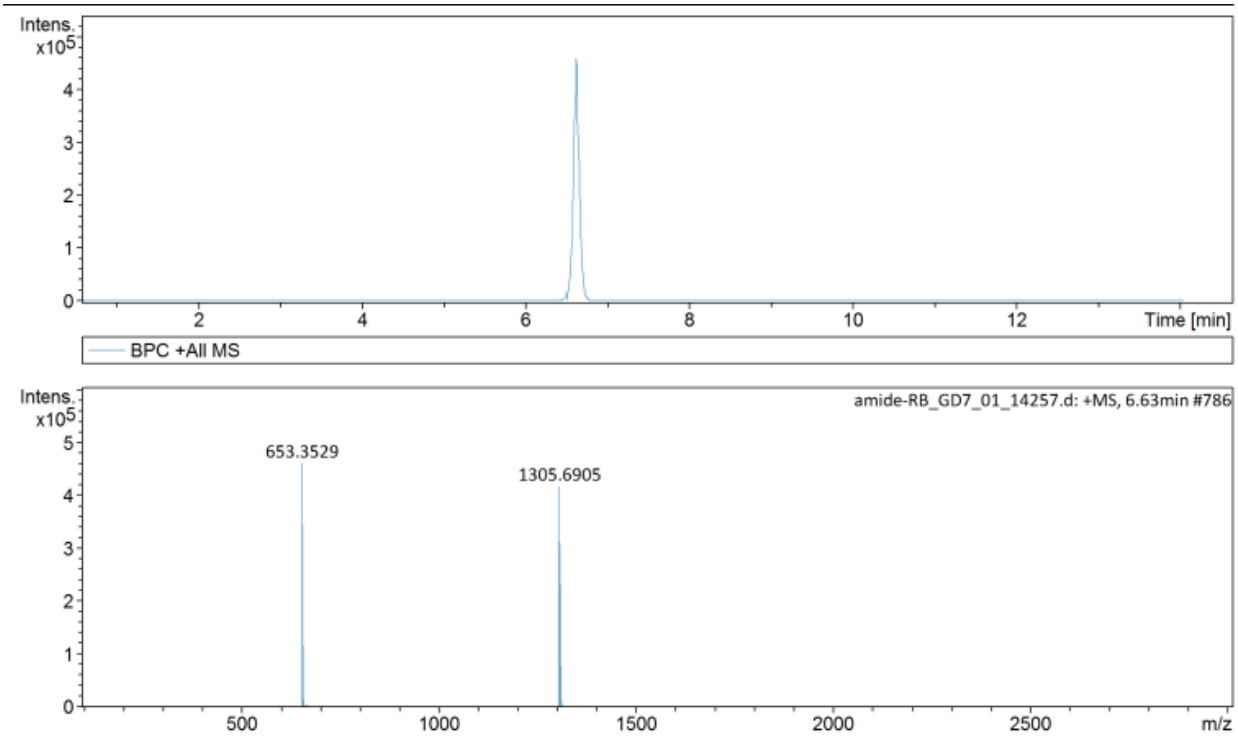


Figure 2. 5 UHPLC TIC chromatogram of purified KM-PEP-cyc-amide peptide with the retention time of 6.63 minutes

2.3.3 Biological testing of KM-PEP-cyc-amide peptide

All antimicrobial testing were outsources to the University of Kwa-Zulu Natal the Pharmaceutical Science Department. The minimum inhibitory concentration (µg/ml) tests were conducted against *E.coli, P. aeruginosa, S.aureus and B.subtilis*. The peptide was found to be active against *P. aeruginosa* at an MIC of 128 µg/ml.

P*seudomonas aeruginosa* is one of the most important bacteria to test against because it causes most gram-negative infections. This mostly affects patients with a compromised immune system. Patients who have been hospitalized longer than a week are more susceptible to contracting an infection and *P. aeruginosa* is the most common pathogen isolated. *P. aeruginosa* is a frequent cause of nosocomial infections and its infections are complicated and can be life-threatening. The antimicrobial activity of KM-PEP-cyc-amide against this pathogen can provide a foundation for developing peptides with enhanced antimicrobial activity. These findings highlight the prospective applicability of KM-PEP-cyc-amide and other analogues as new generation antibiotics.

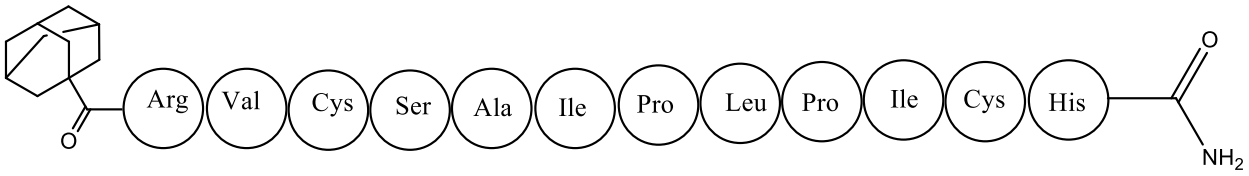
In order to determine whether the amidation enhanced the activity of the peptide, the original Tigerinin RC1 will need to be tested under the same conditions as KM-pep-cyc-amide. Nevertheless, KM-PEP-cyc-amide has antimicrobial activity against *P. aeruginosa*.

2.4 KM-PEP-ada peptide

2.4.1 Design and synthesis of KM-PEP-ada peptide

The transport of small medicinal compounds and other therapeutic peptides using the adamantane based delivery system has been widely utilized over the years because it's known to enhance the biological activity of compounds. This rigid structure consists of four cyclohexane rings merged in chair conformation that can readily cross through the blood-brain-barrier because it is a rigid lipid-soluble molecule. The blood-brain barrier (BBB) is a semi-permeable membrane and is the toughest membrane in the human body. It is known that incorporating adamantane into compounds enhances its biological activity and in this study, it was incorporated into the linear peptide to see whether it will increase the antimicrobial properties. Incorporating this fatty acid into the peptide should cause the antimicrobial activity to be higher than the activity for KM-PEP-carb in section

2.2. This hypothesis is based on the fact that KM-PEP-carb is precisely the same as KM-PEP-ada although the KM-PEP-ada peptide (**Figure 2.6**) has an adamantane group attached to the N-terminus of the peptide. In order to investigate this claim, the KM-PEP-ada peptide was synthesized.



KM-PEP-Ada

Figure 2. 6 The peptide sequence of KM-PEP-Ada

The synthesis of this peptide followed the same method as described in section 2.3.2 but adamantane carboxylic acid was coupled after the 12th amino acid. The full peptide sequence was confirmed by UHPLC, and then it was cleaved off the resin using a cleavage mixture described in section 6.4.9. The peptide was dissolved in 100% HPLC grade DMSO.

2.4.2 Purification of KM-PEP-ada peptide

A gradient elution method employing water and acetonitrile in 15 minutes was used, buffer A, 0.1% formic acid in H_2O; buffer B, 0.1% formic acid in CH_3CN and the column temperature was set to 20 °C (as reported above).

The KM-PEP-ada peptide had a lipid group attached which made the overall peptide to be slightly more hydrophobic causing the retention time to shift to 7.34 minutes as demonstrated in **Figure 2.7** using standard conditions for elution. This is relatively non-polar compared to KM-PEP-cyc carb without the lipid group with at a retention time of 6.63 minutes. The calculated mass for KM-PEP-ada was 1468.80 m/*z* and the mass found was $[M+H]^+$ 1469.81 m/*z*. The purity was examined using the UHPLC-MS which yielded a value of 98%. After purification, the peptide was dried using the rotary-evaporator resulting in the mass of 4.7 mg and a yield of 3.0%.

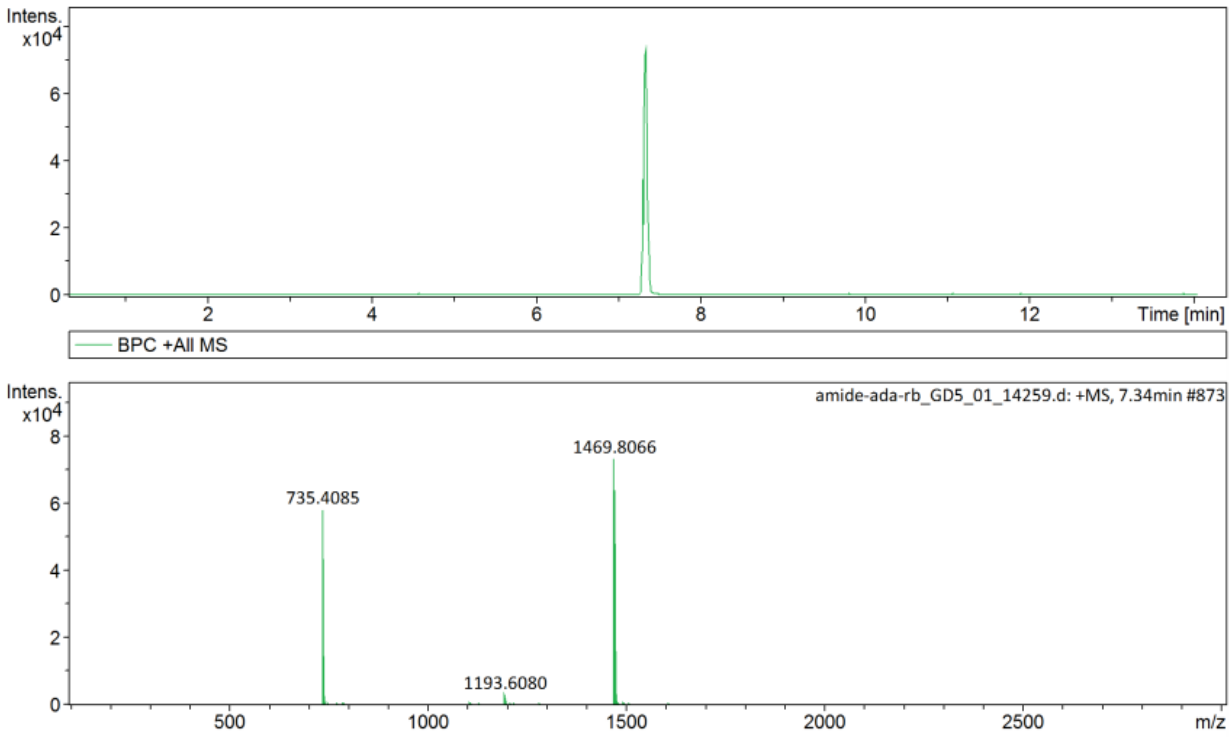


Figure 2. 7 UHPLC TIC chromatogram of purified KM-PEP-ada peptide with the retention time of 7.34minutes

2.4.3 Biological testing of KM-PEP-ada peptide

This peptide was then assessed for antibacterial activity against *E.coli, P. aeruginosa, S.aureus* and *B.subtilis*. The minimum inhibitory concentration (MIC) assay was conducted however the amount of purified peptide that was available for evaluation was too low thus, the maximum concentration used was 256 µg/ml which was not strong enough to inhibit the bacterial growth and higher concentrations could not be prepared. When comparing antibacterial activity of the KM-PEP-cyc-amide and KM-PEP-ada, the KM-PEP-cyc-amide is more active than KM-PEP-ada. Therefore, incorporation of adamantane could have caused structural changes that interfered with KM-PEP-ada interaction with the membrane.

2.5 KM-PEP-cyc-ada peptide

2.5.1 Design and synthesis of KM-PEP-cyc-ada peptide

The benefits of incorporating adamantane into the peptide were discussed in section 2.4.1 yet in this case, the peptide is also cyclized. Since the original Tigerinin RC1 peptide is a cyclized peptide, it can be postulated that the KM-PEP-cyc-ada peptide (**Figure 2.8**) may have antimicrobial properties if not enhanced by incorporating adamantane.

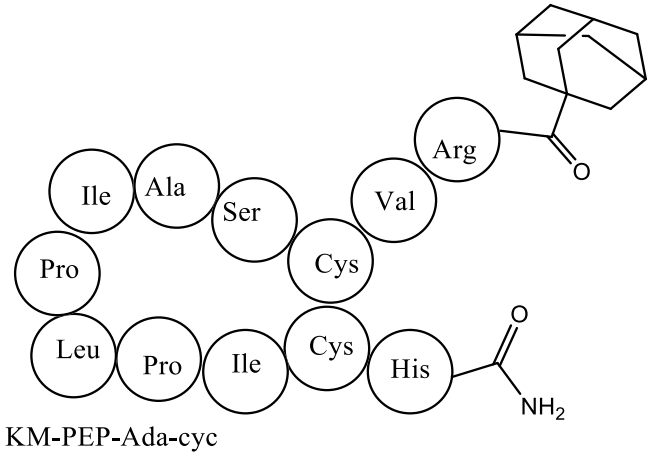


Figure 2. 8 The peptide sequence of KM-PEP-Ada-cyc

The synthesis of this peptide followed the same method as described in section 2.4.1 and the full peptide sequence was confirmed on the UHPLC–MS then it was cleaved off the resin using a cleavage mixture as described in section 6.4.9 and the peptide was dissolved in 100% HPLC grade DMSO Once the peptide was dissolved, oxidative folding may have occurred because the peptide cyclized in the absence of iodine. Oxidative protein folding is a natural process that results in the construction of S-S bonds between cysteine residues in proteins.[169] Thus if the peptide structural folding brought the two cysteine side chains into close proximity the disulfide bridge can spontaneously form.[170]

2.5.2 Purification of KM-PEP-cyc-ada peptide

The purification of the cyclized peptide was done by using 5-95% water/acetonitrile gradient method. The gradient elution method employing water and acetonitrile in 15 minutes was used,

buffer A, 0.1% formic acid in H_2O; buffer B, 0.1% formic acid in CH_3CN and the column temperature was set to 20 °C (as reported above). Displayed in **Figure 2.9** is the chromatogram showing peptide retention time of 10.60 minutes on the UHPLC-MS. The calculated mass for KM-PEP-ada was 1466.80 m/z and the mass found was $[M+2H]^{2+}$ 734.40. The analysis of purity was determined using the UHPLC-MS which yielded in a value of 92%. Further biological tests will be done to determine the antimicrobial activity of KM-PEP-cyc-ada.

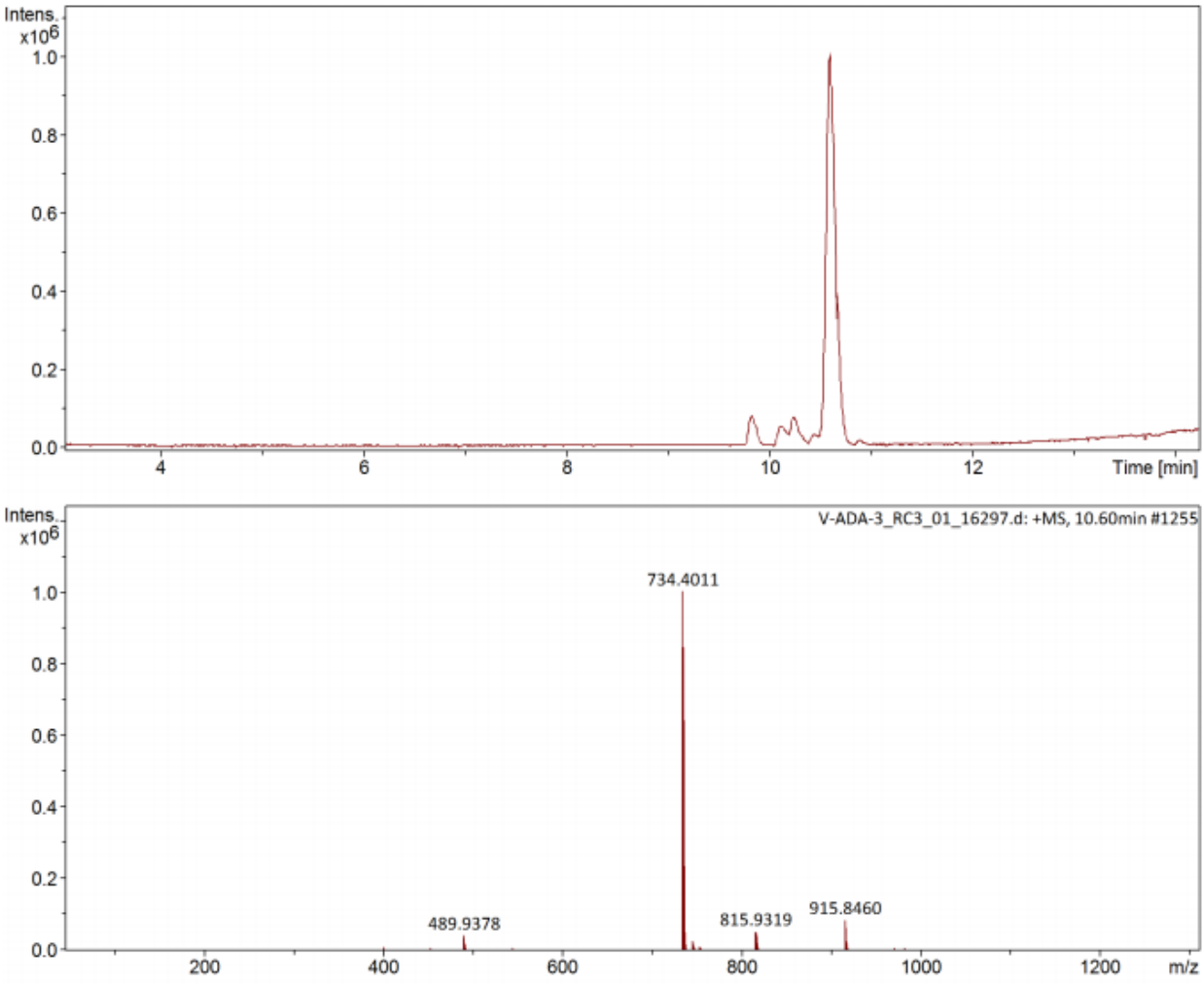


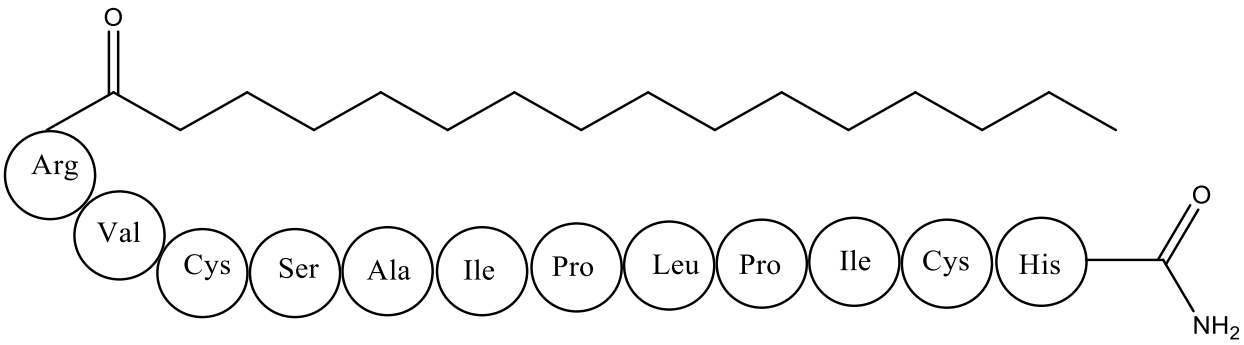
Figure 2. 9 UHPLC TIC chromatogram of purified KM-PEP-cyc-ada peptide with the retention time of 10.60 minutes

2.6 KM-PEP-pal peptide

2.6.1 Design and synthesis of KM-PEP-pal peptide

The peptide KM-PEP-pal is a lipopeptide which is a molecule containing a linear lipid linked to a peptide as seen in **Figure 2.10**. The lipid group used for making the lipopeptide was palmitic acid. Lipopeptides are known to have antimicrobial and antifungal properties. Furthermore, studies have demonstrated that a lipophilic tail can compensate for the hydrophobic and amphipathic structure of the peptide. Palmitic acid is also known to enhance the permeability of the compound.

The synthesis of this peptide followed the same method as described in section 2.4.1 however, palmitic acid was coupled to the 12th amino acid. The full peptide sequence was confirmed by UHPLC. It was then cleaved off the resin using a cleavage mixture described in section 6.4.9 and the peptide was dissolved in 100% HPLC grade DMSO.



KM-PEP-Pal

Figure 2. 10 The peptide sequence of KM-PEP-Pal

2.6.2 Purification of KM-PEP-pal peptide

The peptide was purified using 5-95% water/acetonitrile gradient 15-minute with a flow rate of 15ml/min. The KM-PEP-pal peptide had a linear lipid group attached which made the overall peptide to be slightly more hydrophobic causing the retention time to shift to 10.18 minutes as seen in **Figure 2.11**. This was relatively non-polar compared to KM-PEP-cyc-amide which, without the lipid group, had a retention time of 6.63 minutes. The calculated mass for KM-PEP-

pal was 1544.93 m/z and the mass found was $[M+2H]^{2+}$ 773.5997 m/z. The mass from the UHPLC confirmed that the linear peptide was synthesised. This peptide did not cyclise on its own in the absence of iodine which could be caused by the structural folding of the peptide which does not bring the sulphur groups into close proximity. The purity of this peptide was below 90% which means further purification was needed. This peptide will also be analysed for antimicrobial activity in the future.

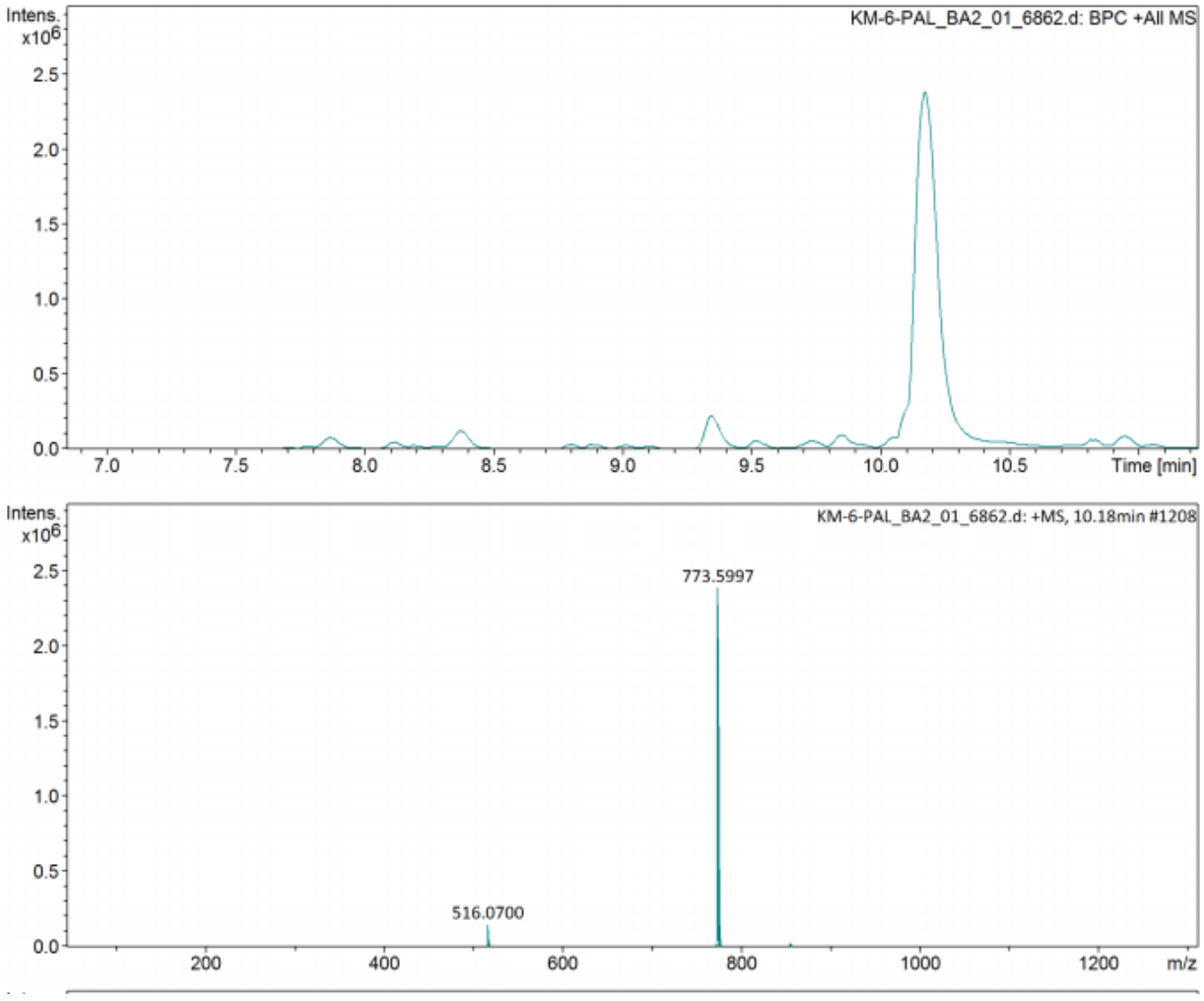


Figure 2. 11 UHPLC TIC chromatogram of purified KM-PEP-pal peptide with the retention time of 10.18 minutes

2.7 KM-PEP-cyc-pal

2.7.1 Design and synthesis of KM-PEP-cyc-pal peptide

This peptide is the cyclized version of KM-PEP-pal. In section 2.6.1 the benefit of integrating palmitic acid was discussed however, KM-PEP-cyc-pal (**Figure 2.12**) may exhibit better activity than its linear counterpart due to its rigid structure.

The peptide KM-PEP-cyc-pal was synthesized using the same method as described in section 2.6.1 and the full peptide sequence was confirmed by UHPLC. The peptide was cleaved off the resin using a cleavage mixture described in section 6.4.9 and the peptide was dissolved in 100% HPLC grade DMSO. The mass spectral molecular ion peak obtained correlated to the cyclised peptide which means the peptide cyclised in the absence of iodine.as in section 2.5.1.

.

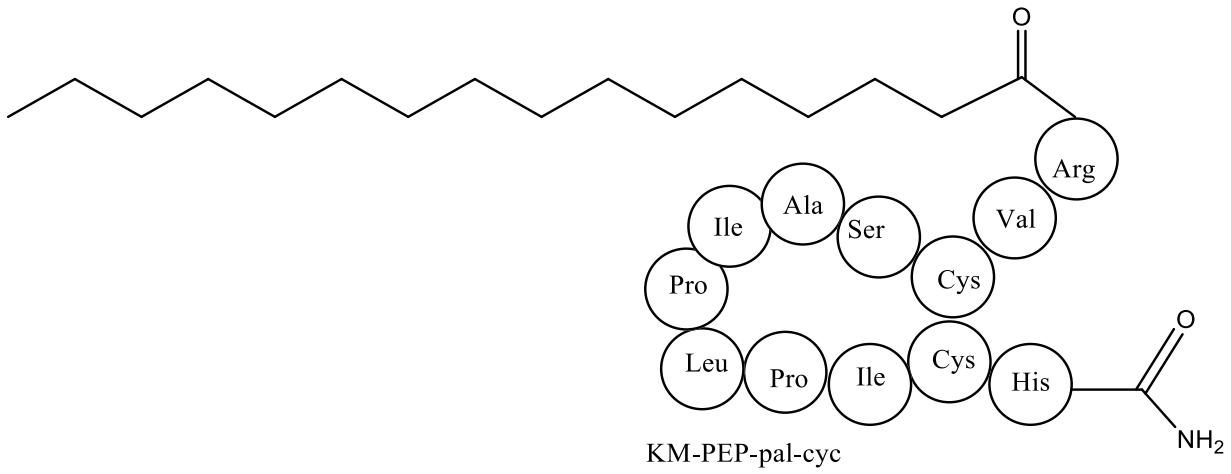


Figure 2. 12 The peptide sequence of KM-PEP-Pal-cyc

2.7.2 Purification of KM-PEP-cyc-pal peptide

The purification of the KM-PEP-pal peptide was the same as for KM-PEP-carb. The KM-PEP-pal peptide had a linear lipid group attached which made the overall peptide to be slightly more hydrophobic resulting in a retention time of 10.75 minutes. The peptide was purified using prep-HPLC however, other impurities co-eluted with the peptide hence further purification is needed.

The calculated mass for KM-PEP-cyc-pal was 1542.91 m/*z* and the mass found was $[M+2H]^{2+}$ 772.46 m/*z* as seen in **Figure 2.13**. This peptide will be assessed for antimicrobial activity in the future.

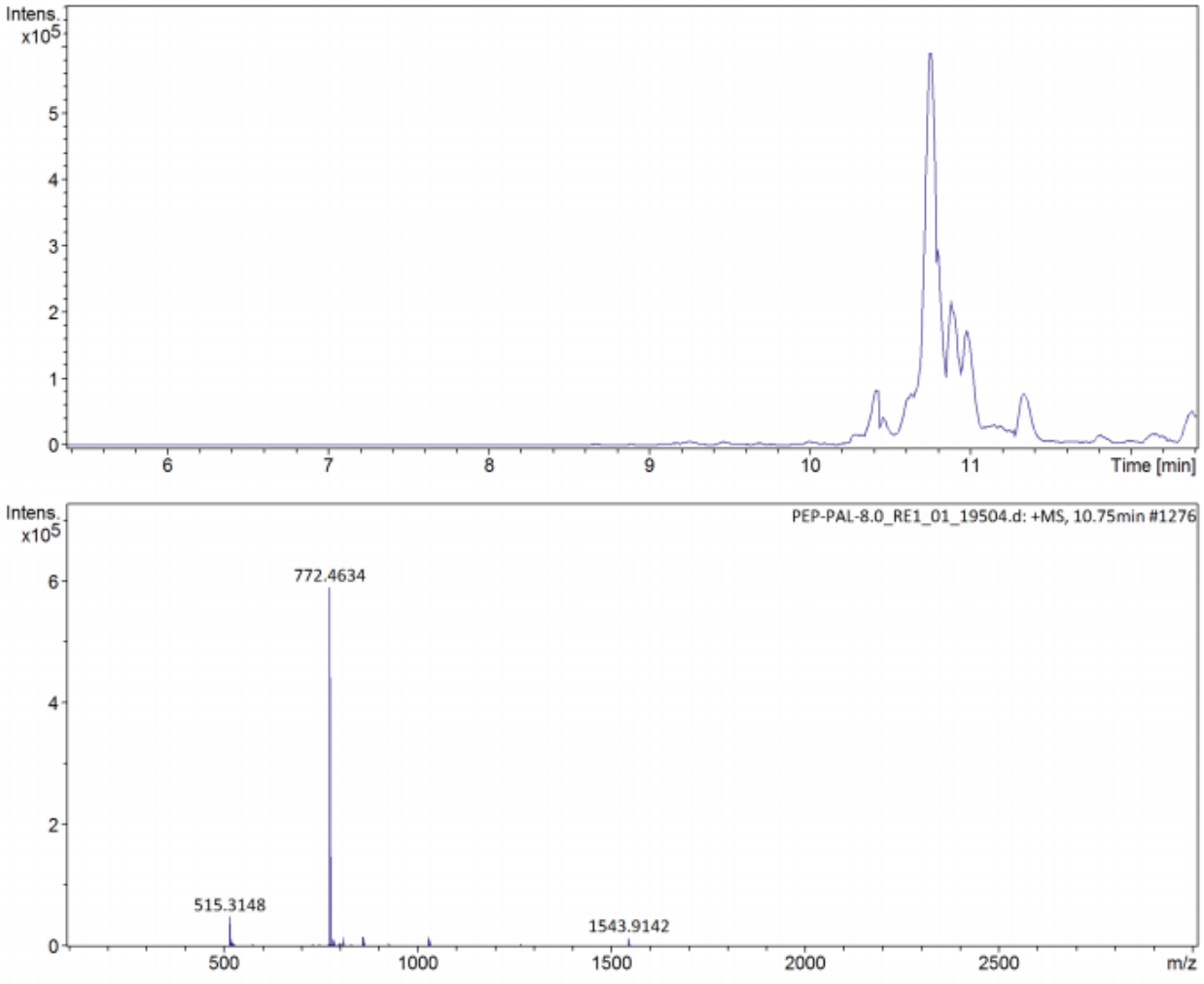


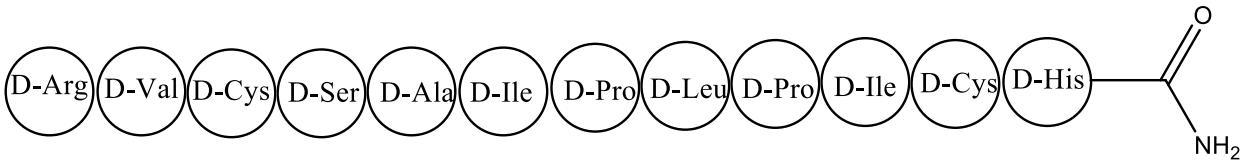
Figure 2. 13 UHPLC TIC chromatogram of purified KM-PEP-cyc-pal peptide with the retention time of 10.75 minutes

2.8 KM-PEP-DAA

2.8.1 Design and synthesis of KM-PEP-DAA peptide

Several attempts have been made to modify the biologically active peptide without significantly changing the structure. A number of researchers have reported that the use of D-amino acids rather than the conventional L amino acids is capable of achieving this goal. However, one of the

limitations of using D-amino acids is that it may lower the activity of peptide because it could possibly change the overall structure of the peptides, which plays a key role in the antimicrobial activity. Therefore, in order to determine whether the activity would be enhanced or decreased, D-amino acids were employed for the synthesis of KM-PEP-DAA.



KM-PEP-DAA

Figure 2. 14 The peptide sequence of KM-PEP-DAA

The peptide KM-PEP-DAA was synthesized using the same method as described in section 2.3.2 and the full peptide sequence was confirmed on the UHPLC (**Figure 2.14**). It was then cleaved off the resin using a cleavage mixture described in section 6.4.9 and the peptide was dissolved in 100% HPLC grade DMSO.

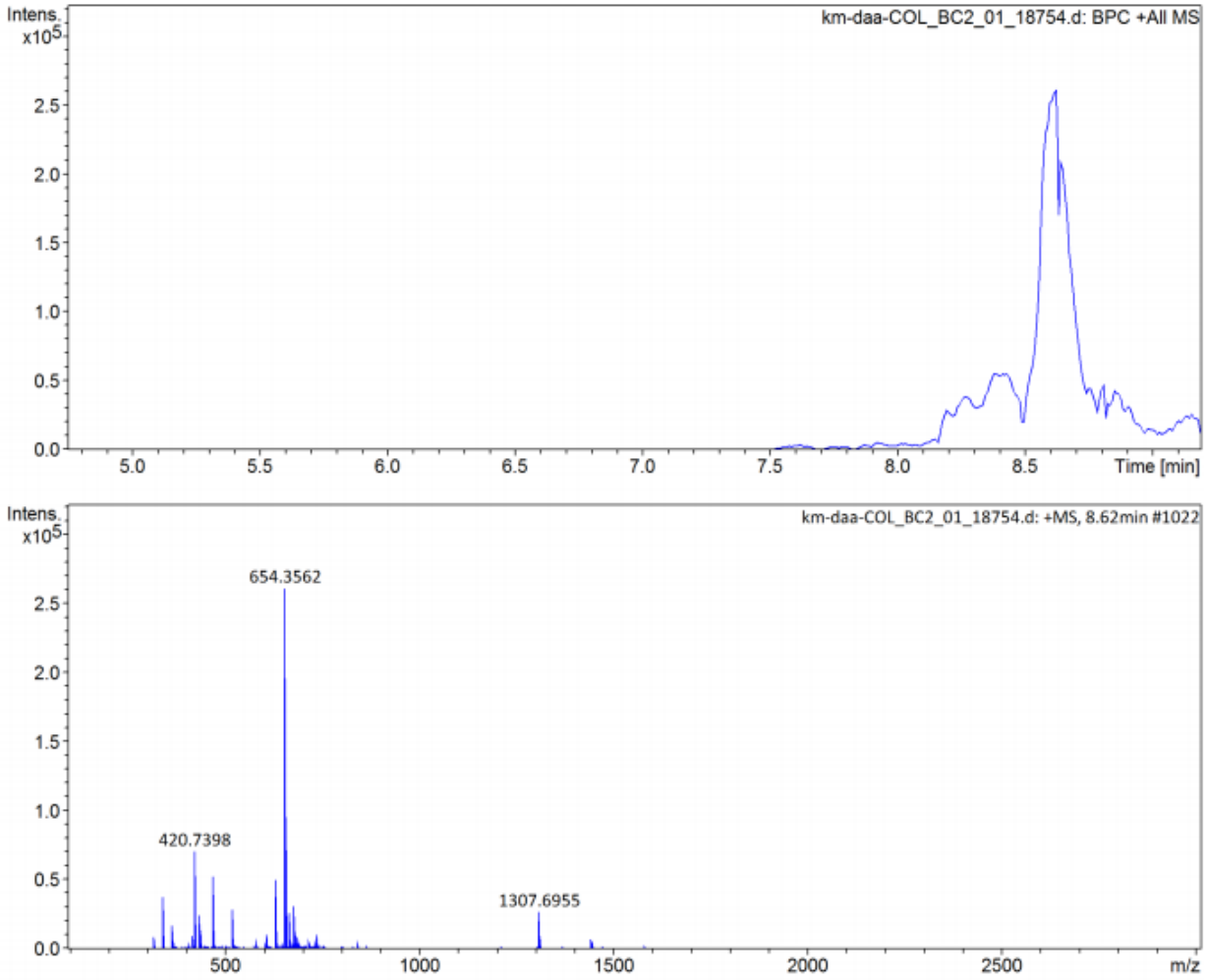


Figure 2. 15 UHPLC TIC chromatogram of purified KM-PEP-DAA peptide with the retention time of 8.62 minutes

2.8.2 Purification of KM-PEP-DAA peptide

The purification of the KM-PEP-DAA peptide was the same as KM-PEP-carb. The peptide had very similar retention as KM-PEP-carb because they are both linear peptide and have the exact same amino acid sequence. The retention time was 5.11 minutes on the prep-HPLC and 8.62 on the UHPLC. The peptide was purified using prep-HPLC however, other impurities co-eluted with the peptide hence further purification is needed. The calculated mass for KM-PEP-DAA was 1306.70 m/*z* (**Figure 2.15)** and the mass found was $[M+H]^+$ 1307.69 m/*z*. The purity was also determined by UHPLC-MS and was found to be 76% thus further purification will be done. This peptide will be evaluated for antimicrobial testing.

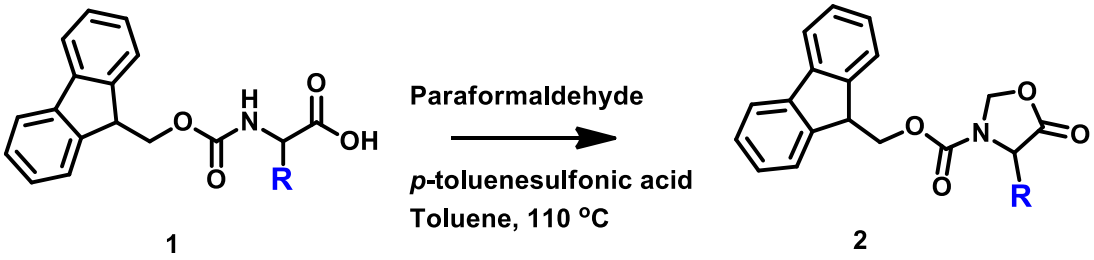
2.9 KM-PEP-Nmethyl peptide

2.9.1 Design and synthesis of KM-PEP-*N*-methyl peptide

Another aspect of the Tigerinin RC1 that needs to be improved is the low metabolic stability and the lack of oral availability. The integration of *N*-Methylated amino acids into peptides has been recognized as a strategy to enhance stability and bioavailability. Moreover, these peptides increase the membrane permeability, proteolytic stability, and rigidity of the peptide. In this section, the attempted synthesis of KM-PEP-*N*-methyl peptide is discussed whereby valine, alanine, isoleucine and leucine were *N*-Methylated and incorporated into the peptide. This *N*-methylated peptide should have better activity than KM-PEP-carb due to the rigidity as well as proteolytic stability.

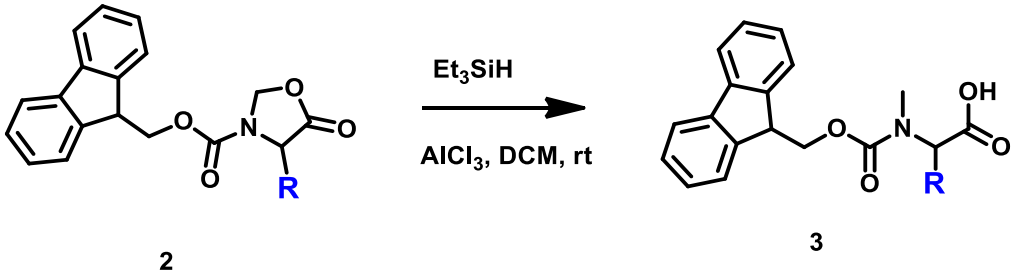
The synthesis of the *N*-methylated amino acids was based on the procedure used by Suode Zhang *et al.* which involves the reduction of 5-oxazolidinones. This method is a two-step synthesis that begins by forming a 5-oxazolidinone from an fmoc-amino acid (**Scheme 2.1**). The ring closure was facilitated by the reaction between the amine in the fmoc-amino acid and the paraformaldehyde under acidic conditions.

Generally, primary amides readily react with formaldehyde or paraformaldehyde in the presence of an acid to produce methylenediamides. However, cyclic products are known to occur when there are functional groups other than the amide present in the molecule. The intramolecular reaction results in methylene bridge formation.



Scheme 2.1 The general synthetic scheme for the formation of the 5-oxazolidinone intermediate

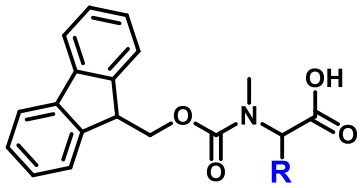
The second step involves the reduction of the 5-oxazolidinone intermediate (**Scheme 2.2**). Triethylsilane was used as a reducing agent because of the active hydride. The reductive opening of the oxazolidinone ring was enabled with the $AlCl_3$ Lewis acid catalyst.



Scheme 2.2 The general synthetic scheme for the formation of the *N*-methylated amino acids

The advantage of using this procedure to form *N*-methylated amino acids was that it tolerates functionalized side chains, assuming that they are protected with protecting groups which are not acid sensitive.

The ^{1}H NMR spectrum of the *N*-methylated amino acids contained signals at 7-8 ppm ascribed to the aromatic regions. The aliphatic region varied from each product however a definitive signal that verified the success of these reactions was the singlet visible at ~3 ppm for the *N*-CH_3 protons in each case. The ^{13}C NMR spectrum of the *N*-methylated amino acids contained 7 signals around 160-120 ppm due to the carbons in the aromatic regions. The carboxylic carbon was very distinct at 172.73 ppm and the aliphatic region had peaks co-relating to the respective amino acids. These compounds were also confirmed on the UHPLC and FTIR (see section 6.4.13-6.4.16).



3

Table 2. 2 *N*-methylated Fmoc amino acids with respective yields

Product	R	Yield %
KM-N-ALA	CH_3	39
KM-N-VAL	$CH(CH_3)_2$	40
KM-N-ISO	$CH_3CH_2CH(CH_3)_2$	55
KM-N-LEU	$CH_2CH(CH_3)_2$	68

Once the *N*-methylated amino acids were synthesized and purified they were integrated into the peptide using solid phase peptide synthesis (SPPS). Fmoc chemistry was utilized for the synthesis of the KM-PEP-*N*-methyl although several features were modified to accommodate for the difficult coupling and side reactions of *N*-methylated amino acids.

The peptide KM-PEP-Nmethyl was synthesized using the same method as described in section 2.3 although the coupling reagent used was HATU and double coupling was used. Coupling the amino acids was much more challenging which can be ascribed to the steric hindrance caused by having *N*-methylated amino acids. The peptide synthesis was closely monitored using UHPLC and as seen in **Figure 2.15** the first 5 amino acids (Leu–Pro–Ile–Cys–His-$CONH_2$) coupled successfully. The calculated mass for KM-PEP-*N*-methyl for the first 5 amino acids was 608.35 and the mass found was $[M+H]^+$ 609.34 *m/z*. When coupling the next two amino acids (proline followed by isoleucine) there was a drastic drop in the coupling efficiency. The intensity of the peak was very low however it was confirmed to be the peptide as the calculated mass of 832.50 *m/z* and the mass found was

$[M+H]^+$ 833.50 m/z. After the 7th amino acid none of the other amino acids coupled to the peptide. This could be due to steric hindrance which can be ascribed to the replacement of the hydrogen atom with the CH_3 group on the nitrogen of the amino acid.

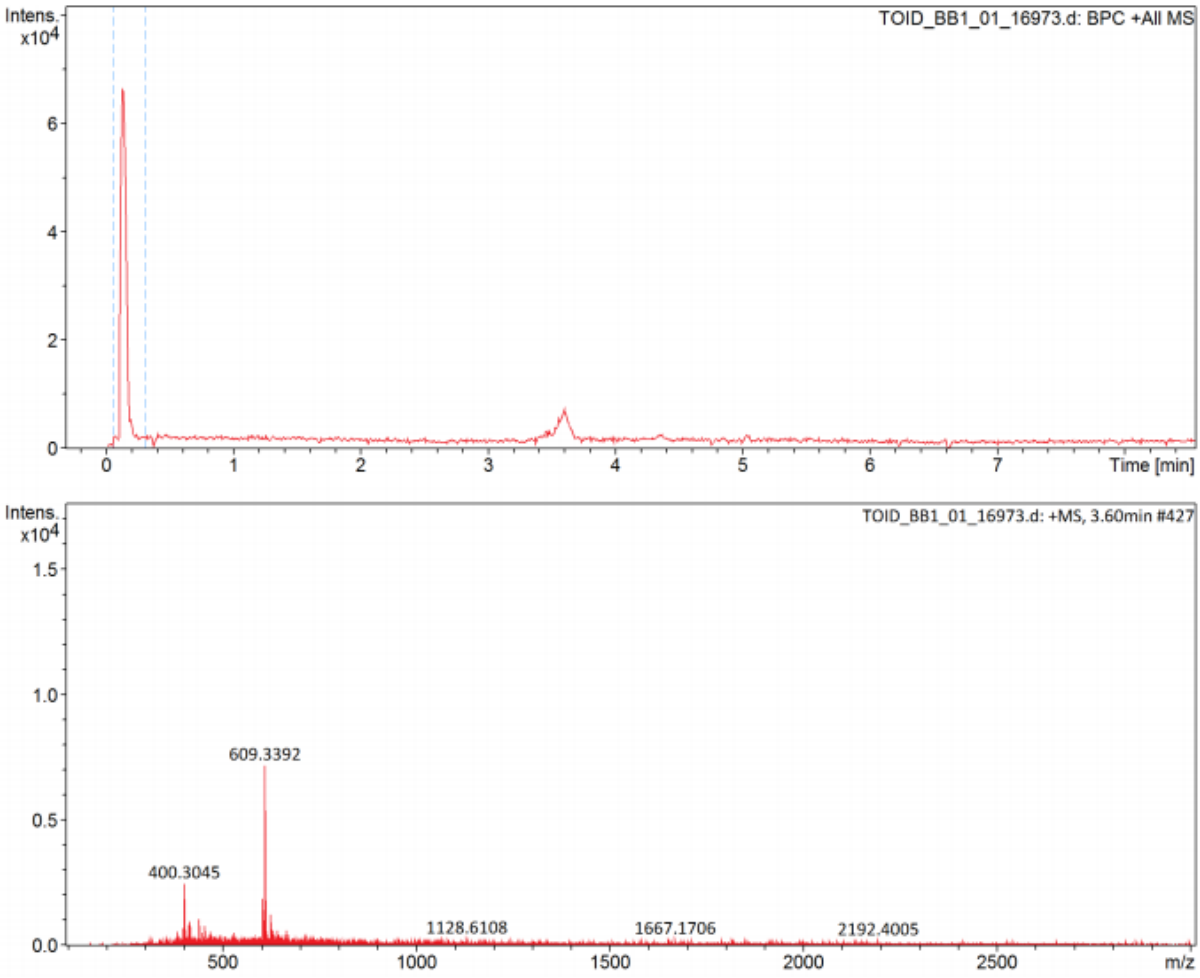


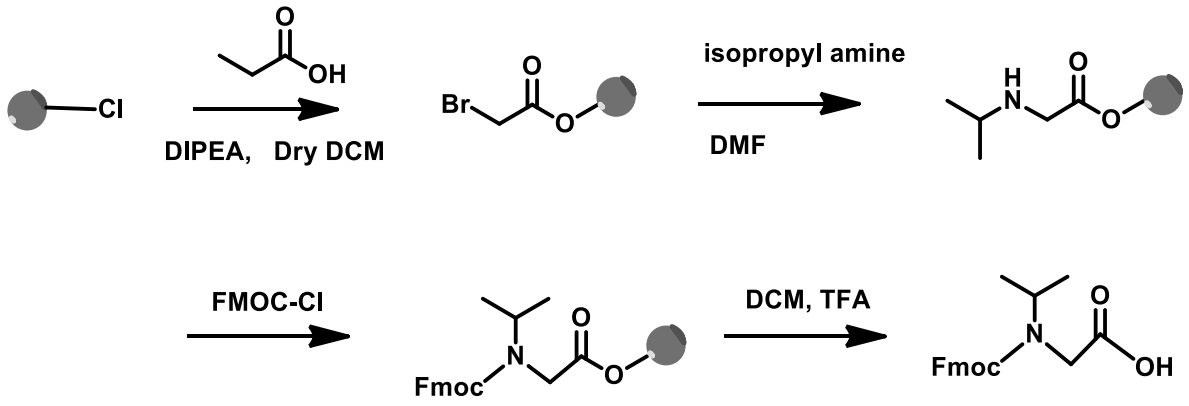
Figure 2. 14 UHPLC chromatogram of crude KM-PEP-Nmethyl peptide of the first 5 amino acids with the retention time of 3.60 minutes

2.9 KM-PEP-toid peptide

2.9.1 Design and synthesis of KM-PEP-toid peptide

In this section, the synthesis of the alkylated poly-*N*-substituted glycine (peptoid) mimic of the Tigerinin RC1 antimicrobial peptide was attempted. Peptoids are known to increase the stability

and the selectivity of the peptide for bacterial membranes.[146] In several cases, alkylation significantly strengthened the selectivity of the peptoids with no notable loss in antimicrobial potency.[147] In order to synthesize the peptoid, the alkylated *N*-substituted amino acids of valine, alanine, isoleucine and leucine were first synthesized with the intention of incorporating them into the peptoid.



Scheme 2.3 Synthetic scheme of the valine peptoid

The synthesis of the *N*-substituted valine amino acid peptoid utilized the method described in section 6.4.11 and was confirmed using UHPLC and NMR spectroscopy however further purification was needed. This *N*-substituted amino acid would have been incorporated in the peptide which could have enhanced the proteolytic stability. The calculated mass was 339.392 m/*z* and the found mass was $[M+Na]^+$ 362.1506 m/*z* which confirmed the synthesis of the *N*-substituted valine amino acid peptoid. The mass spectral data of all the peptides which were successfully synthesized as well as the ones which were attempted is illustrated in Table 2.3. The peptides marked with the asterisks were successfully synthesised however they needed to be purified using prep-HPLC for a second time due to impurities in the product that remained after the first purification attempt.

Table 2. 3 Detailed summary of the masses found on the UHPLC-MS and respective yields of the KM-PEP peptide analogues

Peptide ID	Sequence (C-N terminal)	Calculated mass	Found mass	Molecular ion	Retention time /min	Yield %
KM-PEP-carb	RVCSAIPLPICH-COOH	1307.68 $C_{57}H_{97}N_{17}O_{14}S_2$	1308.687	$[M+H]^+$	8.54	3.5
KM-PEP-cyc-amide	RVCSAIPLPICH-$CONH_2$ (C3-C11)	1304.68 $C_{57}H_{96}N_{18}O_{13}S_2$	1305.6905	$[M+H]^+$	6.63	2.5
KM-PEP-Pal	Pal-RVCSAIPLPICH-$CONH_2$	1544.93 $C_{157}H_{97}N_{17}O_{14}S_2$	773.5997	$[M+2H]^{2+}$	10.18	*
KM-PEP-Ada	Ada-RVCSAIPLPICH-$CONH_2$	1468.80 $C_{68}H_{112}N_{18}O_{14}S_2$	1469.8066	$[M+H]^+$	7.34	3.0
KM-PEP-DAA	RVCSAIPLPICH-NH_2*	1306.68 $C_{157}H_{97}N_{17}O_{14}S_2$	1307.6955	$[M+H]^+$	8.62	*
KM-PEP-Ada-cyc	Ada-RVCSAIPLPICH-$CONH_2$ (C3-C11)	1466.79 $C_{68}H_{102}N_{18}O_{14}S_2$	734.4011	$[M+2H]^{2+}$	10.60	*
KM-PEP-Pal-cyc	Pal-RVCSAIPLPICH-$CONH_2$	1542.91 $C_{157}H_{97}N_{17}O_{14}S_2$	772.4634	$[M+2H]^{2+}$	10.75	*

	(C3-C11)					
KM-PEP-Nmeth	RVCSAIPLPICH-NH_2 (Nmethyl V2,A5,I6,L8,I10)	1307.68 $C_{157}H_{97}N_{17}O_{14}S_2$	N/A	N/A	N/A	¤
KM-PEP-Nmeth 5 Amino Acids	LPICH-$CONH_2$ (Nmethyl L8,I10)	608.35 $C_{28}H_{48}N_8O_5S$	609.3392	$[M+H]^+$	3.60	N/A
KM-PEP-toid	RVCSAIPLPICH-$CONH_2$ (Peptoid V2,A5,I6,L8,I10)	1307.68 $C_{157}H_{97}N_{17}O_{14}S_2$	N/A	N/A	N/A	#

***unsuccessfully purified**

¤ unsuccessful synthesis

 # not synthesized due to time constrains

2.10 Conclusion

The successful synthesis of some peptides was verified using LCMS spectroscopy as shown in **Table 2.3** although some peptides would need to be purified again. The synthesis of KM-PEP-*N*-meth was unsuccessful because none of the amino acids could couple after the 7th amino acid which may be due to steric hindrance. The KM-PEP-toid peptide was incomplete due to time constrains and the *N*-substituted valine amino acid peptoid will be incorporated in the peptide in future. Another aspect that was analysed was the hydrophobic properties of the peptides. The overall hydrophobicity of the peptides was determined using the retention time on UHPLC. This varied significantly due to the modified C-terminals, N-terminals and overall structure. The peptide with the greatest hydrophobicity was KM-PEP-cyc-pal and the least hydrophobicity peptide was KM-PEP-cyc-amide.

The purity of the peptides was measured by UHPLC evaluating the area under all the peaks in the spectrum relative to the area under the peak of the peptide in each case. The purity of KM-PEP-carb, KM-PEP-cyc-amide and KM-PEP-ada was above 98.99%. The purity of KM-PEP-cyc-ada, KM-PEP-pal and KM-PEP-ada was above 90% which is still acceptable for biological testing but the purity of KM-PEP-DAA and KM-PEP-cyc-pal was below 90% which indicates that further purification is needed.

The strong antimicrobial activity of KM-PEP-cyc-amide peptide may be ascribed to the rigid structure of the peptide as well as the amidation of the C-terminal ending. In order to evaluate the relative potency of the KM-PEP-cyc-amide peptide, the minimum inhibitory concentration of the other analogues needs to be determined. That information will assist in the assessment of key moieties in the peptide. Several attempts have been made in other studies to understand the relationship between structure and activity in peptides. Recent evidence has shown that the overall charge and amphipathic properties play a key role but the exact mechanism is a complex concept which is not fully understood.

Chapter 3

Synthesis and characterization of Cationic and RGD Tigerinin RC1 peptide derivatives

In this chapter, two different peptide sequences were designed to specifically bind to the bacterial membrane and also induce the formation of collagen. The first peptide discussed herein is KM-CT (Arg–Lys–Cys–Ser–Lys–Arg–Pro–Lys–Arg–Cys–His-$CONH_2$). This peptide consisted of 11 amino acids and has an overall charge of +6. The charge was strikingly higher than the charge of the peptides discussed in chapter 2 due to the added lysine, arginine and histidine basic residues.

The KM-CT peptide and its analogues were designed on the basis of evaluating if the increased charge could enhance the binding efficiency to the membrane of the bacteria. The hydrophilic section of the membrane consists of the phospholipid head with negatively charged phosphate groups. The cationic KM-CT peptide can bind to the negatively charged phosphate groups, which would result in pore formation and membrane damage. The second peptide discussed is KM-RDG (Arg–Gly–Asp–Gly–Gly–Lys–Cys–Ser–Lys–Arg–Pro–Lys–Arg–Cys–His–$CONH_2$). This peptide is similar to KM-CT peptide however, the RGD motif was incorporated into the peptide. The RGD is the section of the peptide highlighted in blue representing arginine, glycine and aspartic acid. The RGD sequence is known to bind to the $\alpha_2\ \beta_1$ integrin, $\alpha_M\ \beta_2$ integrin, $\alpha_v\ \beta_3$ integrin and $\alpha_{IIB}\ \beta_3$ integrin[151]. This plays a crucial role in inducing matrix macromolecules such as collagen. This integrin homing peptide was designed to promote the wound healing process and collagen formation[152].

3.1 The cationic peptide sequences

3.1.1 Design of the KM-CT peptide analogues

This section details the peptides aimed at the bacterial membrane anionic lipids. Studies have proven that the bacterial membrane is a thriving target in the design of antibacterial compounds which are effective against both Gram-positive and Gram-negative bacteria. In order to develop an effective antimicrobial agent, it is crucial to understand the function and structure of the bacterial membrane.

The bilayer of the phospholipid membrane is characterized by the hydrophilic and hydrophobic portions. The hydrophilic polar head consists of glycerol, phosphate and an ester linker. The hydrophobic portion mainly consists of fatty acid chains. Both Gram-negative and Gram-positive bacteria contain a cytoplasmic membrane. Thus, the amphipathic property of the peptide will play a fundamental role in the bioactivity. Recent evidence shows that numerous cationic peptides have the ability to depolarize the cytoplasmic membrane of their target bacteria, which results in cell death. Since the hydrophilic polar head of the membrane is anionic, the cationic peptide has a high affinity for the hydrophilic portion of the membrane, which was a key aspect for the design of the peptides. In a study by Sun Hee Moon *et al.* a novel linear cationic peptide was discovered. The Paenipeptin C′ peptide caused remarkable membrane potential depolarization in *P. aeruginosa* and *S. aureus* at 32–64 μg/mL.[153] According to their study, the high potency of the peptide was due to the cationic property and the hydrophobicity of the lipid chain of the peptide.[153]

In this study, several amino acids in the Tigerinin RC1 sequence were replaced with positively charged amino acids in an attempt to increase the cationic properties of the peptide. The initial sequence (Arg–Val–Cys–Ser–Ala–Ile–Pro–Leu–Pro–Ile–Cys–His-COOH) was changed to (Arg–Lys–Cys–Ser–Lys–Arg–Pro–Lys–Arg–Cys–His-$CONH_2$) resulting in an overall charge of +6. Analogues of the cationic peptide were also synthesized. Two of the analogues had fatty acids (palmitic acid and adamantane carboxylic acid) attached to the N-terminal of the peptide and one analogue made use of D amino acids only. The benefits of using fatty acids as well as D amino acids such as membrane permeability and selectively were thoroughly discussed in chapter 2.

Thus the aim of this study was to enhance the binding efficiency of the peptide to the membrane by increasing the cationic properties of the peptide in order to effectively bind to the anionic section of the phospholipid bilayer. The other aspect of the strategy was to incorporate fatty acids which would bind to the hydrophobic section of the bilayer.

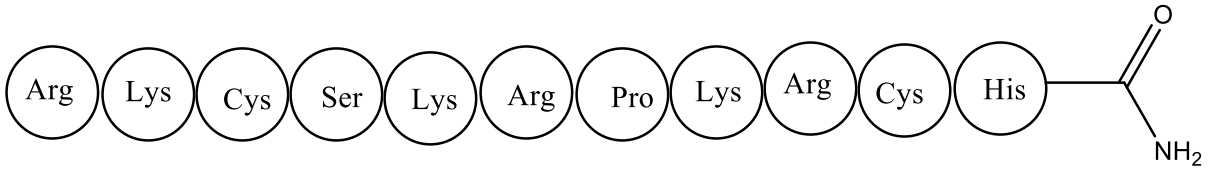
3.1.2 Synthesis of the KM-CT peptide and analogues

The synthesis of these peptides was conducted manually using Fmoc chemistry. The synthesis was conducted using a long-necked reaction vessel with a frit at the bottom. The resin used for this peptide was a rink amide resin (0.4 mmol, 29 8mg) to produce the $CONH_2$ C-terminal. The first amino acid which was coupled was histidine (2 M), using *N, N* diisopropylethylamine (DIPEA) (1 M) in DMF. The following amino acids that were coupled were activated with HBTU (1.9 M) in DMF. The full sequence (**Figure 3.1)** of the peptides were confirmed using mass spectroscopy.

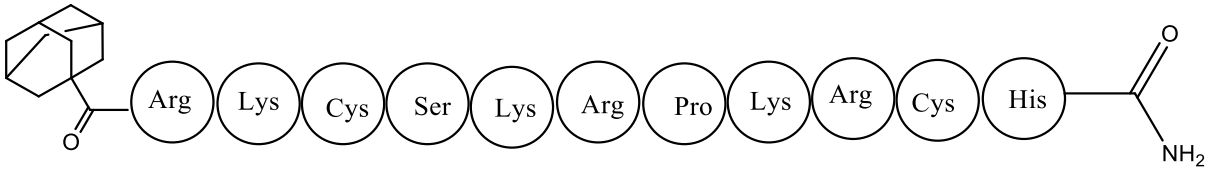
The cleavage of these peptides from the resin was conducted using the procedure described in section 6.4.9. The peptides were dissolved in 50% HPLC grade acetonitrile and 50% HPLC grade H_2O. A gradient elution method employing water and acetonitrile in 15 minutes was used, buffer A, 0.1% formic acid in H_2O; buffer B, 0.1% formic acid in CH_3CN. The column temperature was set at 20 ^oC (as reported in section 2.2). The 5 peptides were followed the same protocol as the peptides in chapter 2 but with a different sequence.

3.1.3 Results and discussion

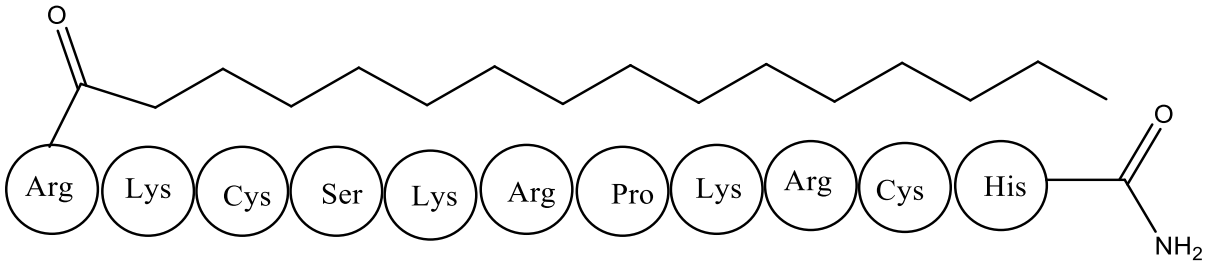
The cationic peptides **(Figure 3.1)** were more soluble than the Tigerinin RC1 analogues. The KM-CT and KM-CT-cyc peptides were relatively hydrophilic due to the presence of charged amino acids. The charged amino acids were all basic amino acids and constitute 55% of the peptide. As a result, the cationic peptides readily dissolved in 1:1 acetonitrile/water, contrary to the Tigerinin RC1 analogues which were insoluble in acetonitrile/water and only dissolved in 100% DMSO.



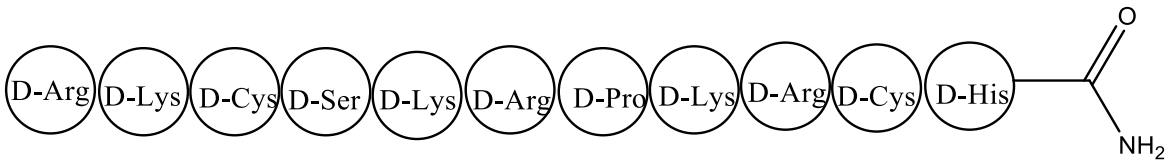
KM-CT



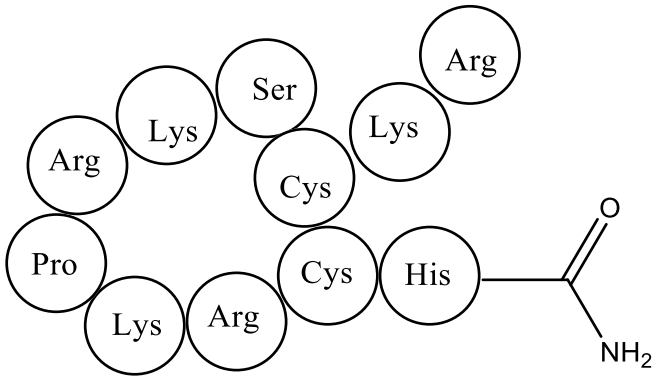
KM-CT-Ada



KM-CT-Pal



KM-CT-DAA



KM-CT-cyc

Figure 3. 1 Sequences of cationic peptides synthesized

Results from the UHPLC revealed that KM-CT and KM-CT-cyc eluted after around 3 minutes with 75% H_2O and 25% acetonitrile. The incorporation of palmitic acid and adamantine increased the hydrophobic nature of the peptides thus resulting in retention of the peptide by the hydrophobic stationary phase, their retention times was 8.00 minutes (**Table 3.1)**.

As such, the peptide analogues containing palmitic acid and adamantane moieties were amphipathic and may have a high affinity for the lipid bilayer of bacterial membranes. In summary, the synthesis of the desired amphipathic peptide analogues was successful. The peptides will need to be purified again on the prep-HPLC and antimicrobial testing will be conducted.

Table 3. 1 Detailed summary of the masses found on the UHPLC-MS and respective retention times of the cationic peptides

Peptide ID	Sequence (C-N terminal)	Calculated mass	Found mass	Molecular ion	Retention time /min
KM-CT	RKCSKRPKRCH-$CONH_2$	1396.74 $C_{55}H_{98}N_{26}O_{13}S_2$	1397.7851	$[M+H]^+$	3.41
KM-CT-cyc	RKCSKRPKRCH-$CONH_2$	1394.72 $C_{55}H_{98}N_{26}O_{13}S_2$	465.9125	$[M+3H]^{3+}$	3.43
KM-CT-Ada	Ada-RKCSKRPKRCH-$CONH_2$	1556.83 $C_{66}H_{112}N_{26}O_{14}S_2$	780.3589	$[M+2H]^{2+}$	8.85
KM-CT-Pal	Pal-RKCSKRPKRCH-$CONH_2$	1632.95 $C_{66}H_{112}N_{26}O_{14}S_2$	817.3392	$[M+2H]^{2+}$	8.25
KM-CT-DAA	RKCSKRPKRCH-$CONH_2$	1396.74 $C_{55}H_{98}N_{26}O_{13}S_2$	1397.7888	$[M+H]^+$	8.07

 # purification was incomplete due to time constrains

3.2 The RGD integrin homing peptide sequence

3.2.1 Design of the KM-RGD peptide

The RGD tri-peptide is fast becoming a key instrument in the biomaterials field. This adhesive peptide, arginine-glycine-aspartate, is an integrin-binding motif which has been widely used to enhance the ability of bioactive agents to bind to receptors in the extracellular matrix (ECM).

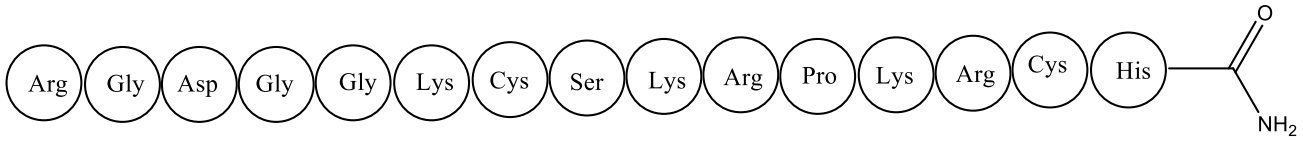
The extracellular matrix (ECM) is the non-cellular component present within all tissues and organs, and provides not only essential physical scaffolding for the cellular constituents but also initiates crucial biochemical and biomechanical cues that are required for tissue morphogenesis, differentiation and homeostasis. The main fibrous ECM proteins are collagens, elastins, fibronectins and laminins. Collagen is the most abundant fibrous protein within the interstitial ECM and constitutes up to 30% of the total protein mass of a multicellular animal. Collagens, which constitute the main structural element of the ECM, provide tensile strength, regulate cell adhesion, support chemotaxis and migration, and direct tissue development.

The KM-RGD peptide was a combination of 2 peptides resulting in a 15 amino acid peptide sequence. The first portion was the RGD sequence for receptor binding while the second portion consists of (Lys–Cys–Ser–Lys–Arg–Pro–Lys–Arg–Cys–His-$CONH_2$), which is the cationic peptide KM-CT mentioned in section 3.1. These two peptides were linked using two glycine amino acids resulting in the sequence (Arg–Gly–Asp–Gly–Gly–Lys–Cys–Ser–Lys–Arg–Pro–Lys–Arg–Cys–His-$CONH_2$). The overall charge of the peptide was +6. The analogues of this peptide were designed the same as the analogues mentioned in section 3.1.1. Fatty acids and D amino acids were incorporated.

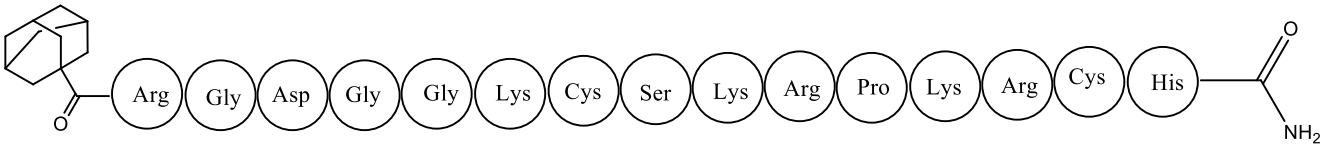
The aim of this section was to synthesis wound healing peptides which also have antimicrobial properties. A key aspect of KM-RGD and its analogues is the integrin-binding arginine-glycine-aspartate sequence. The strategy was to make the peptide bind to the receptors in the ECM in order to induce collagen formation which should promote wound healing.

3.2.2 Synthesis of KM-RGD peptide

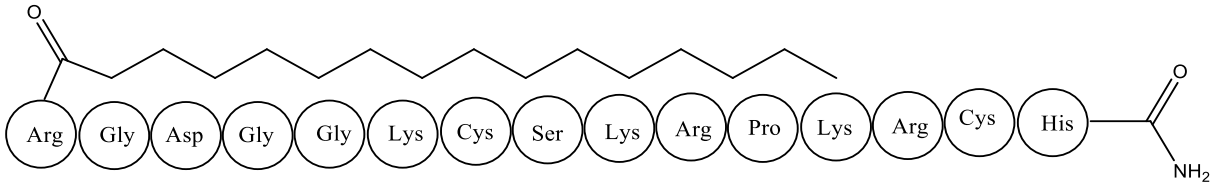
Fmoc chemistry was used in the synthesis of the KM-RGD peptide and its analogues (**Figure 3.2)**. The synthesis was conducted in the same manner as the KM-CT peptide mention in section 3.1.2, however, a stronger coupling reagent was used and the double coupling was employed. Rink amide resin (0.39 mmol, 288 mg) was used to produce the $CONH_2$ C-terminal. The first amino acid which was coupled was histidine (2 M), using *N*, *N* diisopropylethylamine (DIPEA) (1 M) in DMF with HATU (1.9 M) as the coupling reagent. A few challenges occurred during the synthesis of these peptides. The use of double coupling after the sixth amino acid and the use of HATU as a coupling reagent increased the efficacy of the coupling of the amino acids. The full sequence of the peptide chains was confirmed using mass spectroscopy.



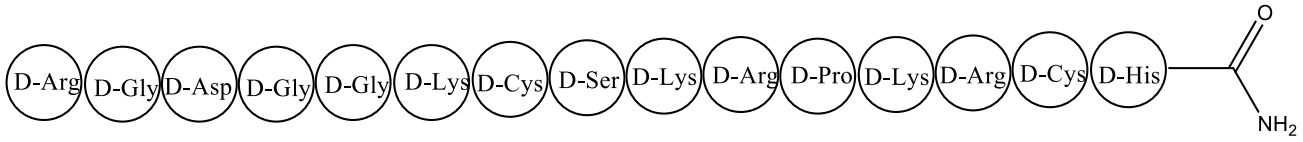
KM-RGD



KM-RGD-Ada



KM-RGD-pal



KM-RGD-DAA

Figure 3. 2 Sequences of integrin binding peptides synthesized

3.2.3 Results and discussion

Due to the RGD sequence, the KM-RGD peptide and its analogues were significantly more difficult to synthesize. Glycine is frequently found in beta turns of peptides and proteins. Since glycine is the smallest amino acid, it is the most sterically flexible causing the peptide to change conformation. According to Pei-Yeh Chen *et al*. the Asp-Gly sequence was used to create a β-structure that favours the formation of a type I′ turn.[154] Therefore, the structural conformation of the RGD peptide may affect efficient coupling. Based on the size of the peptide and the presence

of three glycine amino acids in the peptide, we speculate that the challenges in the coupling of the amino acids are attributed to a possible change in conformation.

Another aspect to consider was the repeated cycles of coupling which could lead to cleavage of side chain protecting groups, in particular for Histidine. The RGD peptides were 15 amino acids long which were much longer than the previously reported peptides. The change in length of the peptides could possibly cause the histidine to be more susceptible to cleavage of the side chain protecting group. Previous studies by Albert Isidro-Llobet, *et al.* have reported the loss of the protecting group from histidine during coupling[155]. Steric hindrance from the side chain protecting groups of the large amino acids such as lysine and arginine also lowers the coupling efficiency.

In this case, both the bulkiness of the side chains and the sequence conformational change caused by the RGD moiety may have affected the coupling efficiency.

In order to overcome these challenges, a stronger coupling reagent was used. The HBTU coupling reagent is known to be well suited for standard coupling reactions but a more effective reagent, HATU, can be used to increase the coupling efficiency. HATU is different from HBTU because of the nitrogen atom in the 6 membered ring (**Figure 3.3**).

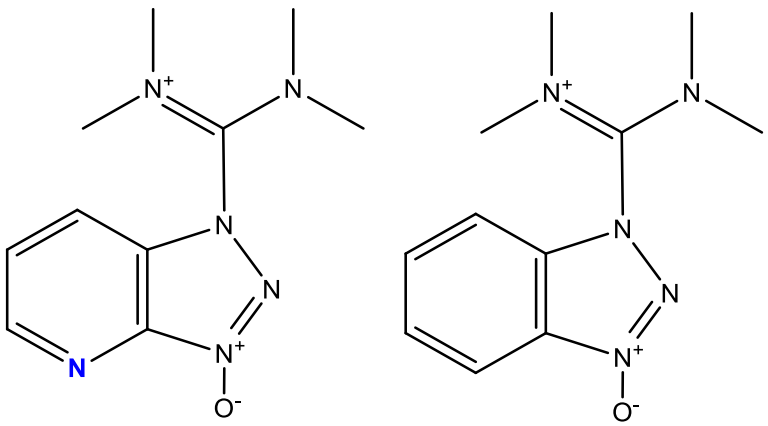


Figure 3. 3 Illustrates the difference between HATU and HBTU

These reagents both react with the carboxylic end of the amino acid to form active esters, which then react with amines of the resin-bound peptide, however, HATU produces less epimerization during coupling and has a higher reaction rate. This is due to the additional nitrogen atom, stabilising the entering amine through an intermediate hydrogen-bonded 7-membered ring (**Figure 3.4**).

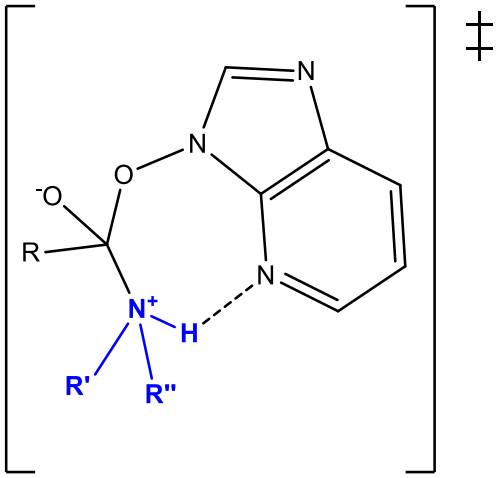


Figure 3. 4 The intermediate hydrogen-bonded 7-membered ring

The overall charge of KM-RGD and its analogues was +6 and 46% of the amino acids in the peptide were basic residues. This was relatively similar to the cationic peptides, however, UHPLC revealed that the RGD peptides were significantly hydrophobic. Despite the high charge of the RGD peptides and the basic residues, the conformation of the peptides possibly caused the peptides to have hydrophobic properties.

Table 3. 2 Detailed summary of the masses found on the UHPLC-MS of the RGD peptides

Peptide ID	Sequence (C-N terminal)	Calculated mass	Found mass	Molecular ion	Retention time /min
KM-RGD	RGDGGKCSKRPKRCH-$CONH_2$	1682.83 $C_{65}H_{114}N_{30}O_{19}S_2$	561.9635	$[M+3H]^{3+}$	7.77
KM-RGD-Ada	Ada-RGDGGKCSKRPKRCH-$CONH_2$	1844.94 $C_{76}H_{128}N_{30}O_{20}S_2$	923.3142	$[M+2H]^{2+}$	8.20
KM-RGD-Pal	Pal-RGDGGKCSKRPKRCH-$CONH_2$	1921.06 $C_{81}H_{144}N_{30}O_{20}S_2$	961.8737	$[M+2H]^{2+}$	8.94
KM-RGD-DAA	RGDGGKCSKRPKRCH-$CONH_2$	1682.83 $C_{65}H_{114}N_{30}O_{19}S_2$	842.9421	$[M+2H]^{2+}$	5.60

 # purification was incomplete due to time constrains

3.3 Conclusion

The synthesis of the KM-CT peptides and the KM-RGD peptides was successful. The UHPLC-MS was used to verify that the desired peptides sequence was achieved for each peptide. The retention time of the respective peptides varied significantly due to the different moieties incorporated as well as the use of D-amino acids. The RGD chains were the most challenging peptides to synthesize. This could be due to the chain length because longer peptides are known to be more difficult to couple. Due to time constrains the peptides were not purified. In this study, the desired sequences were accomplished and will be sent for further antimicrobial tests.

Chapter 4

Silver nanoparticles and peptides

4.1. Introduction

Nanoparticles are continuously being appreciated, especially silver nanoparticles (AgNPs), for having good antimicrobial properties. Consequently, conjugation of AMPs with silver nanoparticles (AgNPs) has been suggested to reinforce the biological activity[156]. Nonetheless, there are some major properties which need to be considered, specifically, the manner in which the AgNP and the peptides interact, and the conformation of cysteine-containing AMPs. This interaction is closely correlated with the stability and activity of the system. The disadvantage of AgNPs is that they are commonly unstable in solution and hence an AgNP-AMP structure having long-term stability with enhanced activity is favourable[157]. The other feature involves the presence of cysteine in peptides. They are usually abundant in a number of groups of AMPs and normally exist in the form of disulfide bridges playing a key role in the structure and function of AMPs[158]. Due to the high binding affinity of silver to sulfur, cysteines are also known to attach directly to AgNPs. Therefore, conjugating a cysteine-containing peptide with AgNP is expected to affect structural conformations and possibly, have an advantageous outcome on the strength and nature of nanoparticle-peptide interactions.

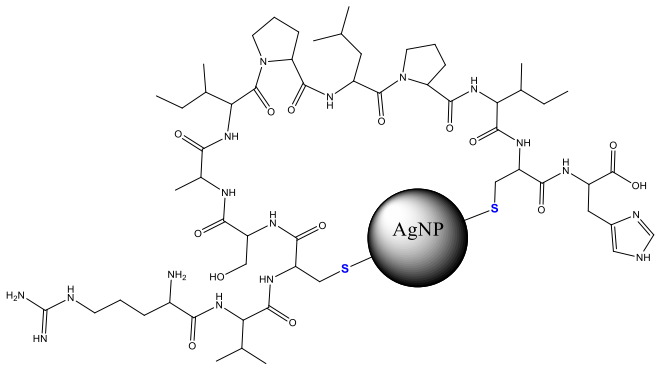


Figure 4. 1 Structure of KM-PEP-carb with two cysteine residues binding to a silver nanoparticle (AgNP)

The linear analogue of the Tigerinin RC1 peptide, KM-PEP-carb, was conjugated to AgNPs. AgNPs are known to bind to cysteine residues and **Figure 4.1** illustrates how KM-PEP-carb could bind to a AgNP. In this study, silver nanoparticle-antimicrobial peptide (AgNP-PEP) conjugates were investigated and analysed using transmission electron microscopy (TEM) and UV–Vis spectroscopy. The aim of this study is to investigate the correlation between NP size and bioactivity as well as cytotoxicity.

According to literature, the antimicrobial properties of silver depends largely on the presence of free silver ions but various mechanisms have been postulated as well. It is suspected that the exchange between positively charged Ag^+ ions and the negatively charged bacterial membranes plays a prominent role in the rupturing of the membrane and breaking down of the cell.[159] It is also proposed that positively charged Ag^+ ions inhibit the replication of DNA.[160] Another antimicrobial mechanism includes the interaction of Ag with thiol groups in proteins as well as blocking and inactivation of respiratory enzymes. Unfortunately, ionic silver is quite toxic to mammalian cells as well. This causes limitations for biomedical and medicinal applications. A study had shown that Ag^+ ions released from all the tested commercial silver dressings induce differential cell death *in vitro*. Contrary to Ag^+ ions, silver nanoparticles (AgNPs) in most cases are reported to be less cytotoxic by mass of silver added[161].

In a response study, the toxicity of silver ions was documented to be approximately 3.4 times higher than that of the silver nanoparticles[162]. The exact mechanism of how AgNPs induce toxicity in prokaryotic cells and mammalian cells is not fully understood but Ag^+ ions could be liberated from AgNPs resulting in the same effect. Another possibility is that AgNPs share the mechanism with Ag^+ in having a high affinity for thiol-group-containing proteins that are abundant in the cell membrane, thus leading to cell death.

Regarding the lower toxicity of AgNPs, one needs to consider the fact that the reduced toxicity may be ascribed to the slowly modulated liberation of the Ag^+ ions and the massive uptake of Ag^+ ions by eukaryotic cells as seen in **Figure 4.2**[163]. Another factor is that the AgNP are sterically hindered and because of their size they may not strongly bind to the cells as opposed to Ag^+ with an ionic radius of 0.137 nm.

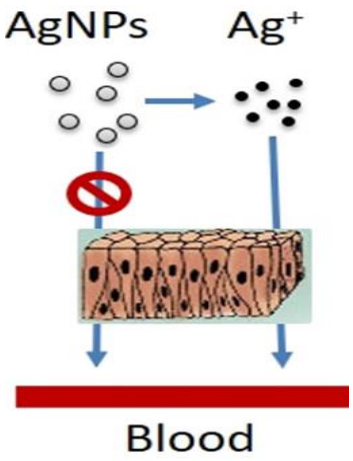


Figure 4. 2 An illustration of how the bulky AgNPs are too sterically hindered to cross the membrane and how Ag^+ ions are small enough the pass the membrane.

Consequently, the surface of the large Ag NPs is blocked from interacting with the mammalian cells. This is why silver nanoparticles have been greatly synthesized and integrated as bactericides in wound dressings, implants and water treatment devices[164]. Without these modifications, silver is as lethal to mammalian cells as it is to bacteria but when converted into nanoparticles their toxicity is reduced.

4.1.1 Surface Plasmon Resonance (SPR)

The Surface Plasmon Resonance has become a very dynamic and robust optical detection method for evaluating, label-free biomolecular interactions in real time. This technique is applied in various disciplines such as life science, electrochemistry, food and environmental science just to mention a few. The most popular commercially available SPR instrument uses a detection scheme known as the Kretschmann configuration.

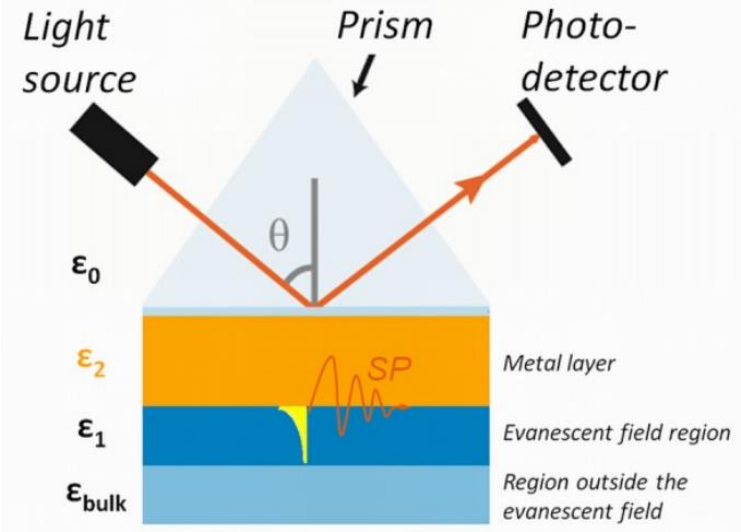


Figure 4. 3 Kretschmann configuration illustrating the light incident at angle θ with respect to the surface normal which hits the silver film deposited on the flat surface of a cylindrical glass lens and is then reflected[165].

In this system, a light source passes through the prism and reflects off the metal layer then travels into the detector as seen in **Figure 4.3**. When the incident angle which is also called the resonance angle is reached, light is absorbed by the electrons in the metal surface of the sensor chip. This causes the electrons to resonate. These resonating electrons are called surface plasmons which are sensitive to the environment around it. This causes a loss of the intensity in the reflective beam which results in a dark band. The shape and position of the dip in the SPR reflection intensity curve provides information about the sensor surface. This can be performed with a standard ultraviolet-visible (UV-Vis) spectrometer as in this study.

In the chapter, we report the synthesis of silver nanoparticles conjugated to a cysteine-containing peptide KM-PEP-carb. These conjugates should exhibit increased stability and bioactivity, in contrast to the individual components. Cytotoxicity and antimicrobial activity studies were conducted in order to assess the improvements in biological activity.

4.2. Results and Discussion

4.2.1 Colour change due to the dielectric environment

The preparation of AgNPs involved the reduction of $AgNO_3$ using the sodium citrate or $NaBH_4$ reduction method in an aqueous solution as shown in **Figure 4.4**. $NaBH_4$ is a stronger reducing agent than sodium citrate, the method using $NaBH_4$ will produce smaller size particles. The AgNPs were centrifuged to remove starting material as described in section 6.4.17 and 6.4.18. These nanoparticles were also modified with KM-PEP-carb by mixing various volumes of the peptide (25 mg/l) with the AgNP. Several sizes were synthesized in order to determine which AgNP size will produce the highest antimicrobial activity.

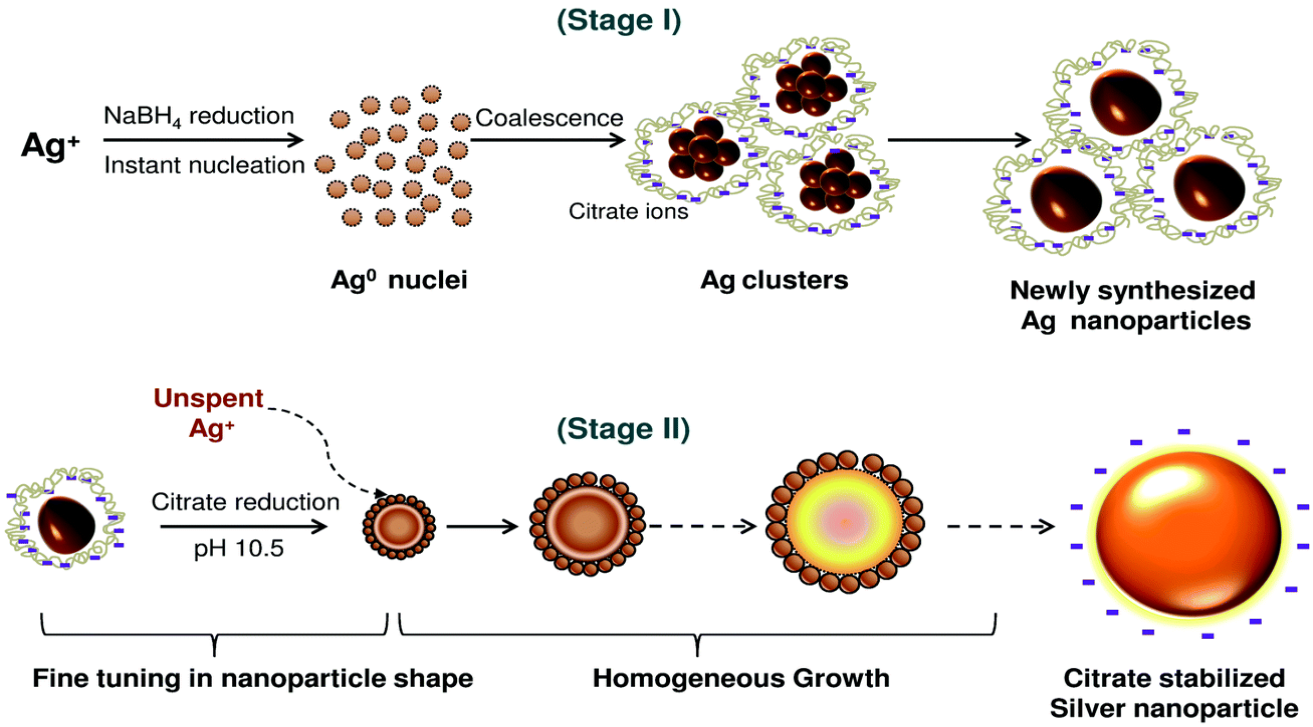


Figure 4. 4 Synthesis of stabilized silver nanoparticles (AgNP)[166]

It is crucial to understand how the AgNPs are stabilized in order to explain the changes that occur when conjugating the nanoparticles to the peptide. As a result of conjugation with KM-PEP-carb,

the colloidal solution changed into different colours ranging from blue to brown-red as shown in **Figure 4.5**. The colour of the colloidal solution was different because of the change in the dielectric environment of AgNPs due to the addition of the peptide and slight aggregation of the particles.

4.2.2 UV-Vis spectroscopy of AgNPs and the conjugates

The conjugation of the AgNPs to the peptide was indicated by the visual appearance of an orange, brown-red and blue solution for AgNP-PEP-$NaBH_4$, AgNP-PEP-0.5ml and AgNP-PEP-1ml respectively, which was confirmed by UV-visible spectroscopy. The compounds were named according to the amount of reducing agent used. UV-Vis spectrometry measures the degree at which light is absorbed by a medium at different wavelengths in the ultraviolet and visible spectra. This is done by irradiating a sample with light of known wavelength and intensity and measuring the intensity of the transmitted light.

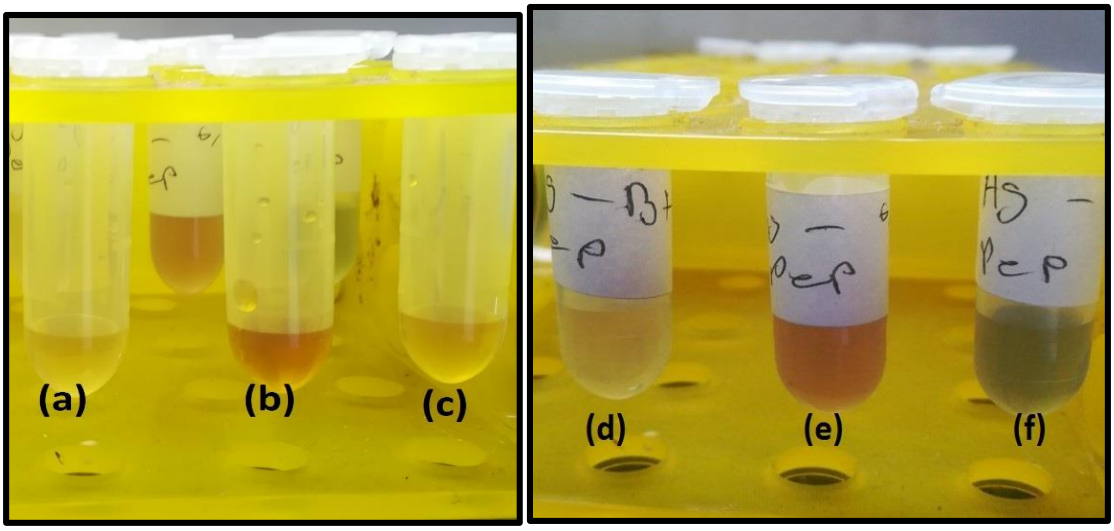


Figure 4. 5 Colour change of silver nanoparticles (a) AgNP-$NaBH_4$ (b) AgNP-0.5ml (c) AgNP-1ml (d) AgNP-PEP- $NaBH_4$ (e) AgNP-PEP-0.5ml (f) AgNP-PEP-1ml

The surface plasmon resonance (SPR) absorption peaks of the conjugated AgNPs and the AgNPs are shown in **Figure 4.6.** The absorption spectrum of the products shows the SPR band ranging from 393 nm to 406 nm, demonstrating the presence of spherical or spherical-like AgNPs. According to literature, the absorbance of a metallic nanoparticle of any shape can be successfully predicted in the visible range for particle sizes ≤ 10 nm. This principle predicted that spherical

AgNPs would have an SPR band around 400nm. The Mie theory first described this occurrence theoretically by solving Maxwell's equations for a radiation field interacting with a spherical metal particle under the fitting circumstances[167]. The absorption spectra theoretically calculated using Mie's Scattering theory is used to calculate the surface plasmon resonance (SPR) derived absorption spectra. The modified Mie's theory was adapted according to the bulk plasmon frequency, bulk collision frequency and Fermi velocity. There are three properties which affect the absorption frequency which is the dielectric constant of the metal, the medium and the size of the particle. For spherical AgNP, the absorbance should appear around 400 nm and the absorbance of larger particles would result in a minor redshift and a minor blue-shift for smaller particles.

In **Table 4.1** the summary of the SPR bands for both nanoparticle and peptide modified AgNPs are shown. The AgNP-0.5ml AgNP-1ml SPR bands had the largest absorbance which was found to be red-shifted at 408 nm and 406 nm respectively, which indicated that it comprised of the largest nanoparticles. This result was anticipated due to the large volume of the citrate reducing agent. These particles were synthesized with 0.5 ml 1 ml of the citrate reducing agent in order to produce larger nanoparticle. The AgNP-2ml had an absorbance of 398 nm which is slightly lower than the absorbance for AgNP-0.5ml and AgNP-1ml. These nanoparticles were synthesized using 2ml of the citrate reducing agent, as a result, the nanoparticles were slightly smaller. The smallest particles were also synthesized using $NaBH_4$ as a reducing agent. Since $NaBH_4$ is a stronger reducing agent than citrate it produced the smallest nanoparticle at an absorbance of 393 nm. The four different sizes produced were used to make three different conjugates.

Table 4. 1 SPR band according to the UV-visible spectra for silver nanoparticles

Product name	SPR bands
AgNp-1ml	406
AgNp-2ml	398
AgNp-$NaBH_4$	393
AgNp-PEP-1ml	399
AgNp-PEP-2ml	404
AgNp-PEP-$NaBH_4$	396

The UV-Vis was also used to determine the conjugation of the peptide to the nanoparticles. **Figure 4.6** demonstrates a slight change in the SPR band which indicates that the peptide is conjugated to the nanoparticles due to the change in the dielectric environment. The absorbance for AgNP-PEP-$NaBH_4$, AgNP-PEP-2ml, AgNP-PEP-1ml and AgNP-0.5ml were recorded at 396 nm, 404 nm, 399 nm and 405 nm respectively. For AgNP-PEP-$NaBH_4$ and AgNP-PEP-2ml there was a redshift and for AgNP-PEP-1ml and AgNP-0.5ml there was a blue shift. Since the SPR band of the conjugates are still within the range for spherical silver nanoparticles, the morphology of the nanoparticles should still be intact.

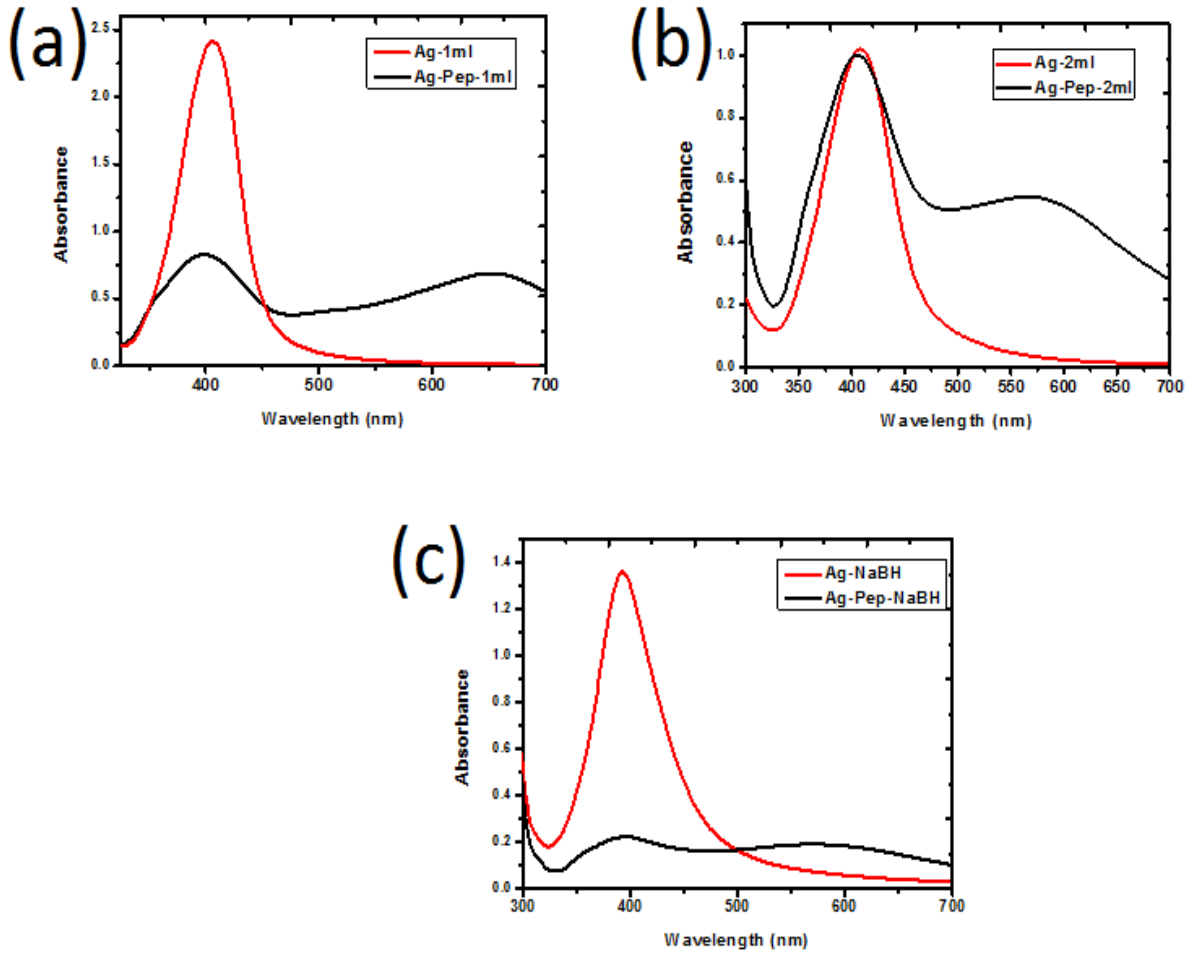


Figure 4. 6 UV–vis absorption spectroscopy showing the SPR band for silver (red line) and Ag-Pep (Black line).

AgNP-PEP shows two plasmon bands, commonly ascribed to light absorption (and scattering) along both the longitudinal axis and the transverse axis, absorption and scattering will cause surface plasmon resonance of the colloidal particles. This occurs when the nanoparticles agglomerate or have an irregular shape. A sphere will equally absorb and scatter light resulting in one band but an irregular shape will have two bands due to the scattering from both the longitudinal axis and the transverse axis. The SPR band appearing around 400nm confirm the presence of Nanospheres and the peak around 600 nm may be attributed to the quadrupole plasmon resonance and due to the non-spherical silver nano-particles. However, a slight agglomeration and aggregation of NPs was observed in the conjugated AgNPs only. This effect may be attributed to the intermolecular forces between the nanoparticles and the peptide.

Studies show that AgNPs have high affinities for AMPs, especially Cys residues.[168] In order to understand the interaction between the peptide and the nanoparticles, there are two aspects which need to be taken into account.

First, collaborative effects over the larger sections of the peptide chain are crucial in governing the affinity for metal surfaces. Secondly, peptides which are selective for AgNP surfaces illustrate that the affinity is not entirely determined by individual amino acids but also by the tertiary structure of the spatial arrangements of the amino acids in the peptide. The stability of the nanoparticles is aided by the negative charges on the surface induced by the citrate ions, resulting in the repulsive force between the nanoparticles which further foster dispersion of the nanoparticles in the aqueous solution. The addition of KM-PEP-carb to the AgNPs in solution results in the displacement of the citrate capping agent as seen in **Figure 4.7.** During the replacement of citrate ions by the cysteine residues of the KM-PEP-carb on the surface of AgNPs, the AgNPs loses its stability to some degree which leads to aggregation.

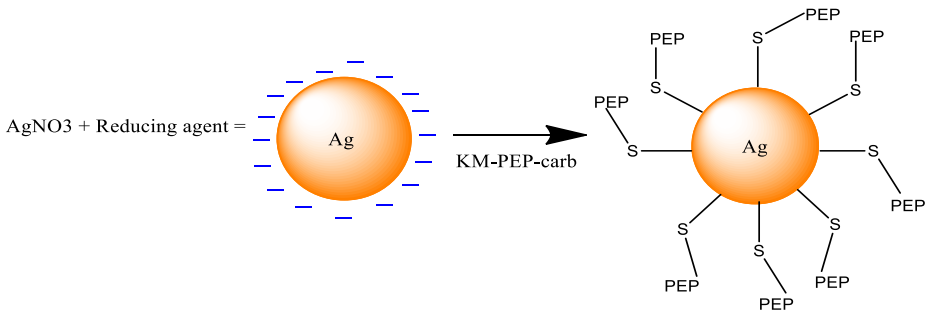


Figure 4. 7 Bio-functionalization of AgNPs achieved via the displacement of citrate with KM-PEP-carb from citrate-capped AgNPs

As the citrate ions were being displaced by the thiol group of the peptide in the reaction, the inter-particle distance between NPs became smaller due to the lack of repulsion which is also known as the proximity effect. This transition results in the susceptibility of nanoparticles to cluster together. Consequently, this phenomenon has corroborated the presence of the SPR band around 600nm in the absorption spectra. The intensity of the peaks is also directly proportional to the concentration of the nanospheres. The concentration of KM-PEP-carb (25 ppm) is further diluted when added to the AgNPs solution and thus results in a smaller SPR bands in all spectra for the conjugates.

4.2.3Transmission electron microscopy (TEM)

A transmission electron microscope (TEM) shoots a beam of electrons through a sample to create a highly magnified image of the sample by using a high-voltage electricity supply to power the cathode. The samples for TEM analysis were prepared by placing the copper TEM grids on a filter paper and drop-coating the AgNPs solution onto the copper TEM grids. The solution was absorbed by the filter paper and the grids containing the nanoparticles were allowed to dry overnight prior to measurement.

Figure 4.8 illustrates the corresponding TEM micrographs for AgNP and peptide functionalized AgNPs. TEM micrographs show monodispersed AgNP-PEP-1ml with spherical-like morphology and the average diameter of about 24 ± 5 nm and 23 ±5 nm for AgNP-1ml. Monodispersity of the particles, which is the amount of uniformity in the size, volume and spherical shape of the particles, confirmed the successful synthesis of the AgNP. The major advantage of monodispersed particles may be attributed to the uniform properties of individual particles, which makes the property of whole particles strictly controllable.

There was no distinct change in the diameters of AgNPs after the modification with KM-PEP-carb. The average diameter of both AgNP-PEP-2ml and AgNP-2ml was 10 nm ± 2 nm **(Figure 4.9)** and the average diameter of AgNP-PEP-$NaBH_4$ and AgNP- $NaBH_4$ was 8 nm ± 2 nm and 9 nm ± 3 nm respectively **(Figure 4.10)**. These images verify the information from the UV-Vis spectra that the AgNP-1ml has the largest particle sizes, followed by AgNP-2ml then AgNP-$NaBH_4$. It also validates the fact that spherical nanoparticles were synthesized. TEM images of aggregated particles can be seen in Appendix **Figure 7. 13**. This verifies the second peak in the UV-Vis spectra of the conjugated samples which are also ascribed to the presence of aggregated AgNPs.

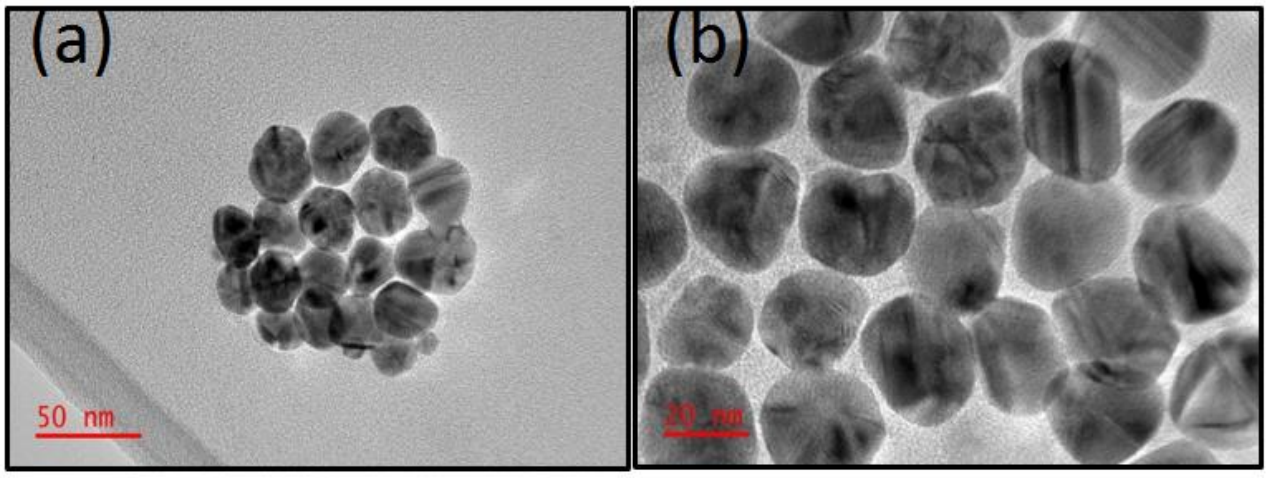


Figure 4. 8 TEM images of citrate capped gold nanoparticles (a) AgNP-1ml (b) AgNP-1ml-PEP

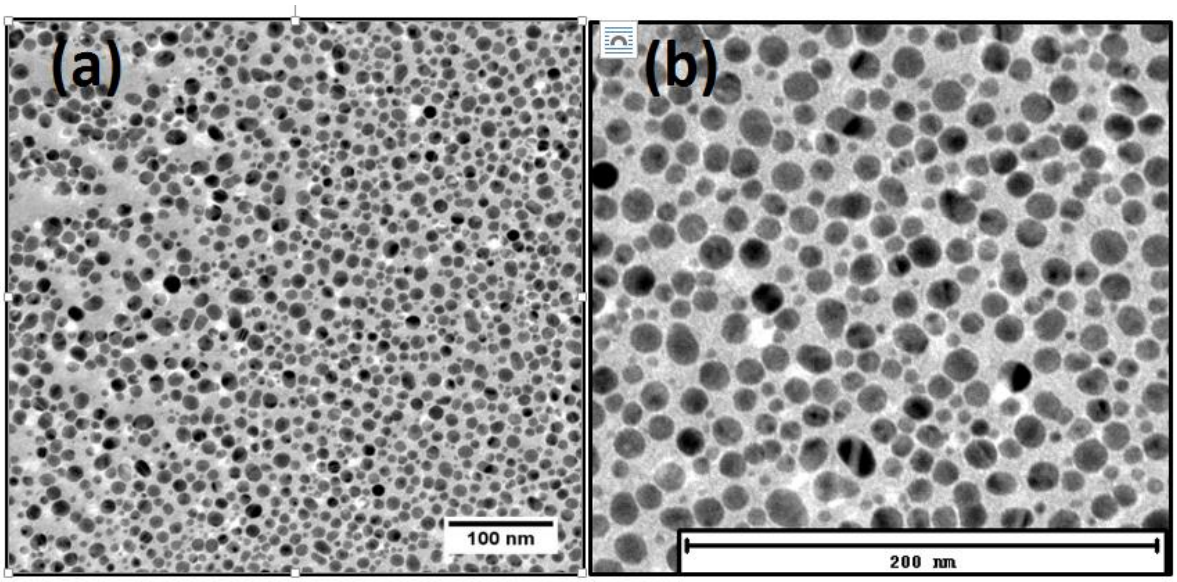


Figure 4. 9 TEM images of citrate capped gold nanoparticles (a) AgNP2ml (b) AgNP-2ml-PEP

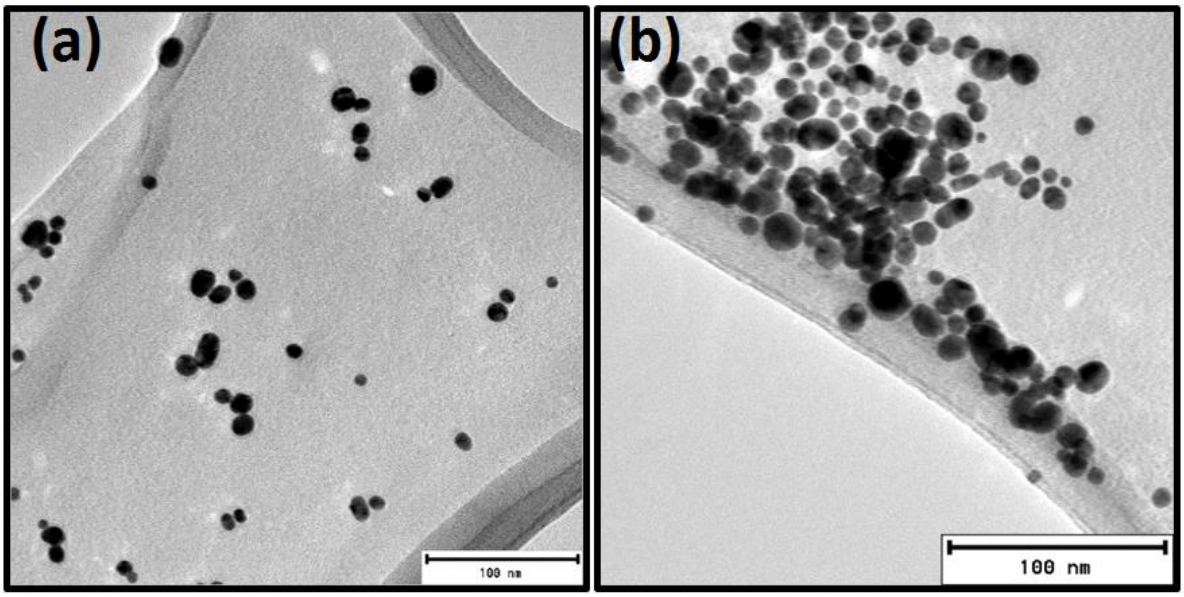


Figure 4. 10 TEM images of citrate capped gold nanoparticles (a) AgNP-$NaBH_4$ (b) AgNP-$NaBH_4$-PEP

4.2.4 Size distribution of silver nanoparticles

The size distribution of the AgNPs was determined using TEM images and ImageJ software. ImageJ is a public domain Java image processing and analysis program which help determine the exact size of all the particle in the TEM image and evaluate standard deviation of the sizes. The histograms give a visual representation of the average size of the particle and how the sizes vary. Uneven sized distribution may occur due to aggregation of the NPs as well as the presence of non-spherical particles. When the silver ions cluster together, non-spherical shaped particles may form. During the synthesis of the nanoparticles, the reducing agent is added drop-wise with vigorous stirring to ensure that the particles are effectively dispersed to avoid aggregation.

According to **Figure 4.11, 12 and 13,** the average size of the AgNPs before conjugation and after conjugation with KM-PEP-carb was very similar. It is important for the size and shape to be consistent in order to have comparable results when biological and analytical tests are being conducted. It also ensures that the chemical and physical properties are relatively the same which will help control and fine-tune the conjugates. The AgNPs and conjugates retained their size and shape. The summary of the average sizes and standard deviation is illustrated in **Table 4.2.**

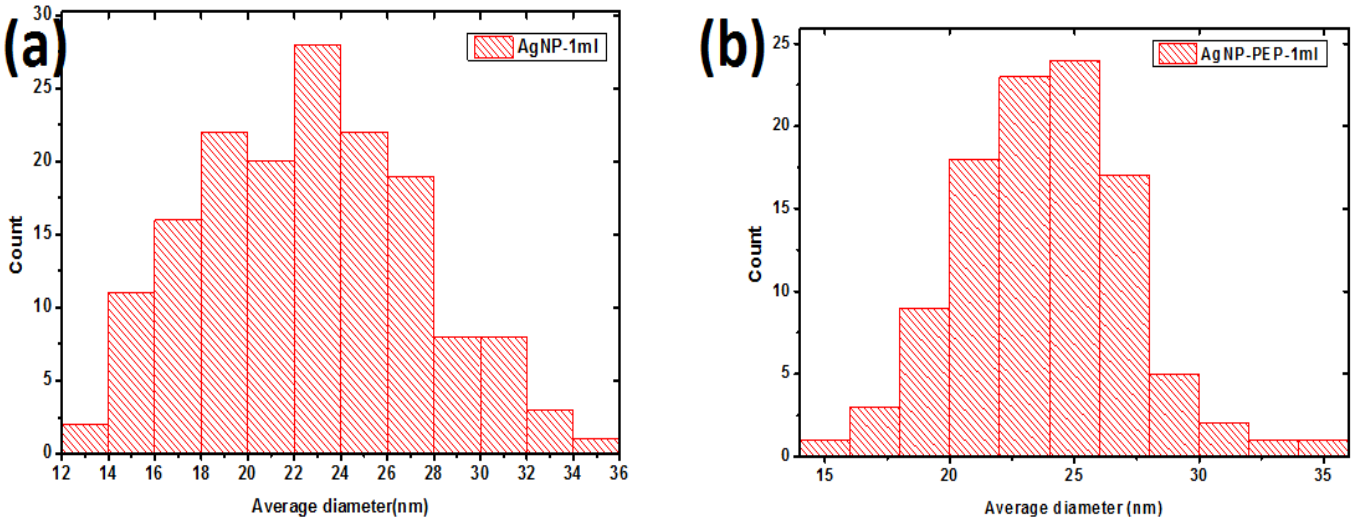


Figure 4. 11 Size distribution of citrate capped gold nanoparticles (a) AgNP-1ml (b) AgNP-1ml-PE

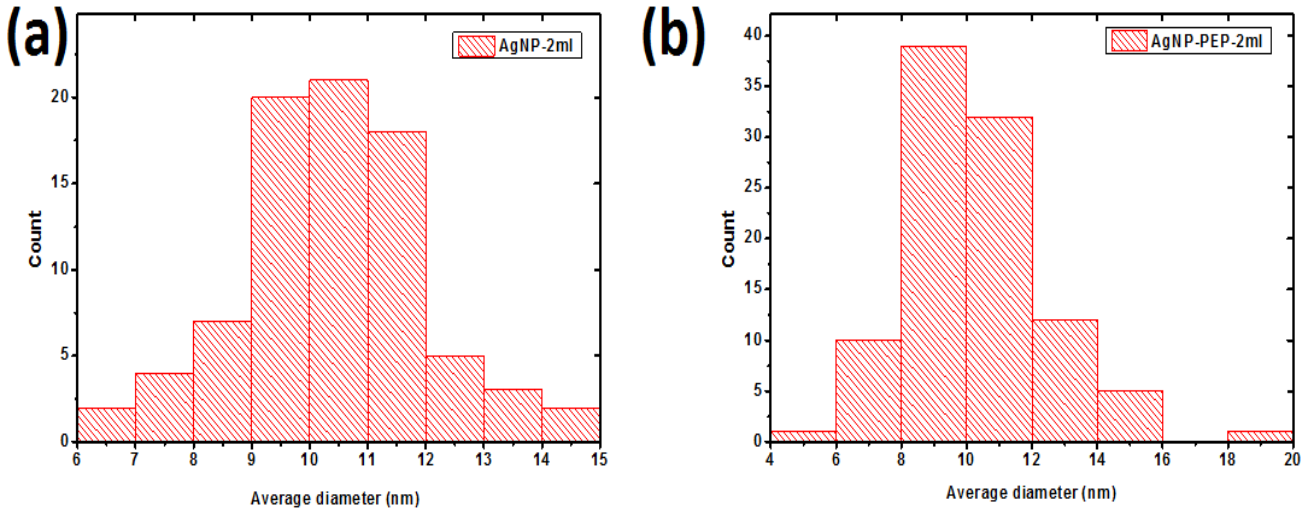


Figure 4. 12 Size distribution of citrate capped gold nanoparticles (a) AgNP-2ml (b) AgNP-2ml-PEP

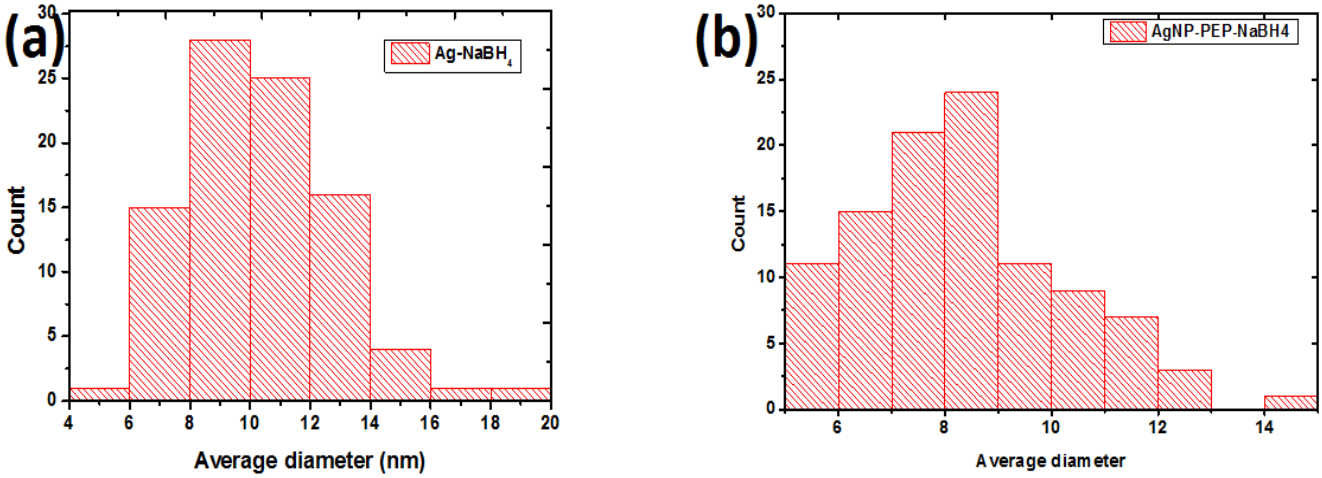


Figure 4. 13 Size distribution of citrate capped gold nanoparticles (a) AgNP-$NaBH_4$ (b) AgNP-PEP-$NaBH_4$

Table 4. 2 Average size and standard deviation for AgNPs

Product name	Average diameter nm
AgNP-1ml	24 ± 5
AgNP-2ml	10 ± 2
AgNP-$NaBH_4$	9 ± 3
AgNP-PEP-1ml	23 ± 5
AgNP-PEP-2ml	10 ± 2
AgNP-PEP-$NaBH_4$	8 ± 2

4.2.5 Cytotoxicity tests

The cytotoxicity test is one of the biological evaluation and screening tests that use tissue cells *in vitro* to observe the effect of potential therapeutics on cell growth, reproduction and morphology.

In this study, the volume of AgNP added, the volume of KM-PEP-carb added and AgNP size was varied in order to evaluate the effect that it may have on the antimicrobial properties as well as the cytotoxicity on human cells. This would help provide information on how to fine-tune conjugates to have enhanced biological properties. In **Table 4.3,** the amount of AgNPs and KM-PEP-carb in each fraction is displayed and the concentration of the KM-PEP-carb was 25 µg/ml. Fraction 1 contained the peptide only and Fraction 8 contained the AgNPs only.

According to a study done by Indrani Pal *et al*. higher stability and activity of the peptide conjugated to nanoparticles was observed compared to the nanoparticles or the peptide alone.[156] The study also revealed that the bridging between AMPs and AgNP can be reinforced through cysteines, which are inherently present in AMPs. In this study, it is evident in **Table 4.4** that the cell viability is very favourable when 20 µl of the sample was tested because all of the fractions were non-toxic. The volume was increased by a magnitude of 5 to assess how it will affect the toxicity. When 100 µl of the sample was added there was a great increase in cytotoxicity. This result was expected because a larger amount of the sample was injected however, this result also revealed that fraction 7 (**Table 4.4**) had a much lower toxic effect compared to the other fractions.

This study revealed that the cytotoxicity of both the KM-PEP-carb peptide and the AgNPs towards MT-4 cells is very low at 20 µl and is very high when the volume is increased to 100 µl. However, it clear that the AgNPs are slightly less toxic when 100 µl of the sample was used. Another observation revealed in these results is the distinct difference in the cytotoxicity of fraction 6 and 7. These samples have the same size AgNPs (9 nm) but the amount of AgNP and KM-PEP-carb added in each fraction differed as seen in **Table 4.3.** Fraction 6 was the most cytotoxic sample at 109.31% toxicity and fraction 7 was the least cytotoxic sample at 64.83% toxicity. The cytotoxicity improved by 44.48% when comparing fraction 6 to fraction 7. The evidence from this study suggests that the most favourable size for AgNPs is approximately 9 nm and that the concentration of KM-PEP-carb which plays a crucial role in controlling the cytotoxicity.

Table 4. 3 The amount of AgNP and KM-PEP-carb added in each fraction when preparing the samples.

Product name	Volume of AgNP added	Volume of KM-PEP-carb added	AgNP size
Fraction 1	0	2 ml	N/A
Fraction 2	100 µl	400 µl	25 nm
Fraction 3	10 ml	200 µL	25 nm
Fraction 4	100 µL	400 µL	*
Fraction 5	10 ml	200 µL	*
Fraction 6	100 µL	400 µL	9 nm
Fraction 7	10 ml	200 µL	9 nm
Fraction 8	2 ml	0	25 nm

*Synthesized using 0.5 ml of citrate reducing agent

Table 4. 4 Cytotoxicity test of silver nanoparticles conjugated to KM-PEP-carb evaluated on MT4 cell.

Table 1: Cytotoxicity studies of the samples at 20 µl

Test Compound	Volume used (µl)	Cell viability (%)	% Toxicity
Fraction 1	20	98.14	1.86
Fraction 2	20	96.95	3.05
Fraction 3	20	99.80	0.20
Fraction 4	20	93.91	6.09
Fraction 5	20	93.91	6.09
Fraction 6	20	99.27	0.73
Fraction 7	20	90.39	9.61
Fraction 8	20	95.10	4.90
Auranofin (control)	20	0	100
H_2O (control)		100	0

Table 2: Cytotoxicity studies of the samples at 100 µl

Test Compound	Volume used (µl)	Cell viability (%)	% Toxicity
Fraction 1	100	-1.48	101.48
Fraction 2	100	3.57	96.43
Fraction 3	100	3.21	96.79
Fraction 4	100	-8.41	108.41
Fraction 5	100	4.40	95.60
Fraction 6	100	-9.31	109.31
Fraction 7	100	35.17	64.83
Fraction 8	100	14.57	85.43
Auranofin (control)	100	0	100
H_2O (control)	100	100	0

4.2.6 Antibacterial activity

The conjugate of 4-Ag-PEP-$NaHBH_4$ and 8-Ag-PEP-$NaHBH_4$ were tested for antibacterial activity. The volume of the reducing agent, $NaBH_4$, was 4ml and 8 ml respectively in order to synthesize and analyse AgNPs with a diameter ranging between 9 nm and 15 nm. This is because the conjugate which had the highest cell viability was 9 nm. Their minimum inhibitory

concentration (µg/ml) against *E.coli, P. aeruginosa, S.aureus and B.subtilis* were evaluated. The well-characterized strain of Escherichia coli ATCC 25922 is recommended and widely used as a control for Gram-negative bacterium for various laboratory experiments, *Pseudomonas aeruginosa* is a common bacterium that can cause diseases in animals and humans. It is found in soil, water, skin flora, and most man-made environments throughout the world. It is an opportunistic pathogen for both humans and plants. *Pseudomonas aeruginosa* ATCC 27853 is usually used to test antimicrobial activity and *S.aureus* ATCC29913 is a gram-positive bacteria which causes abscess of the skin. *B.subtilis* ATCC 2002 is also a gram-positive strain of bacteria which can form a biofilm. According to the results, the minimum inhibitory concentration could not be determined due to the very low concentration of the conjugates.

Table 4. 5 Minimum inhibitory concentration (µg/ml) for conjugates against different organisms

Minimum inhibitory concentration (µg/ml) for different organisms					
Compound	Starting concentration (µg/ml)	*E.coli*	*P. aeruginosa*	*S.aureus*	*B.subtilis*
		ATCC25922	ATCC 27853	ATCC29913	ATCC 2002
4-Ag-PEP $NaHBH_4$	2	>2	>2	>2	>2
8-Ag-PEP $NaBH_4$	2	>2	>2	>2	>2

4.3 Conclusion

In summary, the study suggests that cytotoxicity decreases when the particle size is approximately 9 nm. This study also revealed that concentration of the KM-PEP-carb peptide influences cytotoxicity. Finally, it is evident that the conjugation of KM-PEP-carb to AgNPs improves cytotoxicity and the cytotoxicity of the conjugate was significantly better than its counterparts.

Chapter 5

Summary and conclusion

The Tigerinin RC1 provided an appropriate starting point for the design of antimicrobial wound healing peptides. Several techniques were employed to synthesize peptides and the objective was to improve stability, permeability and activity of the Tigerinin RC1 peptide. In this study 18 peptide analogues were synthesized and characterized using HRMS.

The incorporation of palmitic acid and adamantane made a prominent difference in the polarity of the peptides. The UHPLC revealed that when fatty acids are integrated into the peptide, the retention time increases and the peptide becomes more hydrophobic. This property plays a key role for the attachment of the anionic bacterial membrane. This property is also crucial for antimicrobial peptides because the bacterial membrane consists of lipids that possess a polar head and hydrophobic tail. Since the KM-PEP analogues are basic and have an overall charge of +2, integration of the hydrophobic groups may improve the affinity of the peptides to the hydrophobic section of the membrane.

The rigidity of the peptide also played a distinct role in the antimicrobial activity. Previous studies have shown that cyclization of peptides increases the binding energy towards the target molecule. This can be seen when comparing the antimicrobial activity of KM-PEP-carb and KM-PEP-cyc-amide. Despite the fact that the sequence of both peptides was precisely the same, the MIC antimicrobial activity of the KM-PEP-cyc-amide was 128 µg/ml and KM-PEP-carb was not active at that concentration. The maximum concentration used for KM-PEP-carb was 256 µg/ml. This implies that the KM-PEP-carb has a much high MIC value or the peptide is not active at all. The lack of antimicrobial activity of the other analogue may be due to the conformation of the peptides. The *N*-methylated peptide was not fully synthesized. The UHPLC revealed that after the 7th amino acid, other amino acids are not able to couple. This could be due to steric hindrance or the conformation of the peptide.

The second series of peptides (KM-CT and KM-RGD) were also successfully synthesized. The aim was to design membrane penetrating peptides which can bind to the integrin. A few challenges arose during the synthesis of the RGD analogues due to steric hindrance and the possible β-turns induced by the glycine amino acids. The use of HATU and double coupling enhanced the efficiency of the coupling. The AgNP study revealed that cytotoxicity improves when peptides are conjugated to AgNPs however the size of the particle and the concentration of the mixture plays a significant role.

This multidiscipline study gives insight into the structure-activity relationship of the Tigerinin RC1 peptide and showed that the disulfide bridge cyclic conformation plays a significant role in the antimicrobial activity.

Future work

Antimicrobial testing will be conducted on other bacterial strains which are found in wounds. Wound healing studies will be carried out in future on all the peptides using the scratch assay. Techniques such as 2D NMR spectroscopy will be used to determine the 3D structure of the peptides. Further studies will also focus on developing a method for coupling N-methylated amino acids into the Tigerinin RC1 peptide sequence.

Chapter 6

Experimental procedures

6.1 Reagents and chemicals

6.1.1 Reagents for peptides

Piperidine, *N,N,N′,N′*-tetramethyl-O-(1H-benzotriazol-1-yl)uronium hexafluorophosphate (HBTU), Fmoc amino acids, paraformaldehyde, *p*-toluenesulfonic acid, toluene, $NaHCO_3$, anhydrous $MgSO_4$, hexane, ethylacetate, aluminium chloride, triethylsilane, chlorotrityl resin, triisopropylsilane (TIS), formic acid, trifluoroacetic acid (TFA), 1,2-ethanedithiol (EDT), diisopropylethylamine (DIPEA), were purchased from Dld Scientific. Iodine, ascorbic acid and dichloromethane (DCM) were purchased from Sigma Aldrich and the DCM was dried upon distillation over calcium hydride. Dimethylformamide (DMF), methanol, acetonitrile, hexane, dimethyl sulfoxide and ether were purchased from Radchem.

6.1.2 Reagents for AgNP-PEP

Silver nitrate ($AgNO_3$, 99%), trisodium citrate ($C_6H_5Na_3O_7$, $2H_2O$, 99.9%), sodium borohydride ($NaBH_4$) were all purchased from Sigma Aldrich and used as received. All glassware was washed with aquaregia solution, and all the solutions were made up with distilled water. Glycerol 69 [$C_3H_5(OH)_3$] was purchased from Associated Chemical Enterprises (PTY) LTD, South Africa.

6.2 Instrumentation

Instrumentation used for peptides and amino acids

6.2.1 Ultra High Pressure Liquid Chromatography (UHPLC)

Analytical analysis was performed on a Thermo Scientific Dionex Ultimate 3000 Ultra High Pressure Liquid Chromatography (UHPLC) with a flowrate of 0.30 ml/min on C18 column (5 μm, 100 Å, 4.60 mm x 150 mm) coupled to a Diode Array Detector (215 nm and 254 nm). A solvent system applying formic acid as the ion-pairing agent was utilized. Solvent A consisted of 0.1% formic acid /H_2O (v/v) and solvent B consisted of 0.1% formic acid acid/Acetonitrile (v/v).

6.2.2 Preparative High Pressure Liquid Chromatography (PREP-HPLC)

Purification of the peptides were carried out on an Agilent 1260 Infinity preparative instrument with a flowrate of 15 mL/min on an Agilent Prep- C18 (5 μm, 100 Å 250 mm x 21.2 mm) and Phenomenex HPLC/SFC C-18 (5 μm, 100 Å 250 mm x 21.2 mm) with a UV/VIS detector (215 nm and 254 nm) and an automated fraction collector. A two-buffer system was employed, utilizing formic acid as the ion-pairing agent. Buffer A consisted of 0.1% formic acid/H_2O (v/v) and buffer B consisted of 0.1% formic acid/acetonitrile (v/v).

6.2.3 Peptide automated synthesis

Peptides were synthesized on an automated Protein Technologies, Inc PS-3TM Peptide Synthesizer.

6.2.4 Ultraviolet–visible spectroscopy

The absorption spectra were acquired using an Agilent Technologies Cary Series UV-Vis spectrophotometer. The theoretical yield of the peptides were obtained using the absorbance at 301 nm see section 6.4.3 below for full calculations.

6.2.5 Mass spectroscopic analysis

Analysis of amino acids and small portions of peptides was performed on the applied Advion expression-MS (ESI) mass spectrometer in positive mode.

The Thermo Scientific Ultimate 3000 UHPLC was used for sample analysis. It was coupled to a Bruker compact Qq TOF high-resolution mass spectrometer instrument. The autosampler was at 5 °C with an injection volume of 5 µL. The ionization technique used was an electrospray ionization (ESI) and the ion source was kept at 220 °C in the positive ion mode

6.2.6 Nuclear magnetic resonance spectroscopy (NMR)

The structural elucidation of compound were conducted using 1D (^{1}H, ^{13}C) and 2D (COSY, HSQC) NMR spectra on Bruker AVANCE III 300 MHz spectrometer and solutions in deuterated solvents. All chemical shifts were reported in δppm. ^{1}H chemical shifts were internally referenced to tetramethylsilane (δ 0.00) for $CDCl_3$ or to the residual proton resonance in CD_3OD (δ 3.31) and DMSO-d_6 (2.49). Carbon chemical shifts were internally referenced to the solvent resonances in CD_3OD (49.15), DMSO-d_6 (39.51), or $CDCl_3$ (77.16). The multiplicity of the peaks were abbreviated as follows: s, singlet; d, doublet; t, triplet; q, quartet; m, multiplet; br, broad; *J*, coupling constant in Hz.

Instrumentation used for silver nanoparticle and its conjugates

6.2.7 Transmission electron microscopy (TEM)

Transmission electron microscopy (TEM) images were acquired from the FEI Tecnai-12 microscopy at an electron acceleration voltage of 200 KV and beam sport size of 10-100 nm.

6.2.8 Ultraviolet–visible spectroscopy

The absorption spectra were attained using a Varian Cary Eclipse (Cary 50) UV-Vis spectrophotometer. All the samples were diluted with distilled water in order to achieve the optical density (OD) of 1 for analysis.

6.3 Biological screening

6.3.1 Cytotoxicity

Cytotoxicity studies were outsourced to Mintek- Advanced Material Division and the following general procedure was used:

On the day that the cytotoxicity test was conducted, cells were counted and seeded (1 x 106 cells/ml). A 96 well cell culture plate was used and the cells (100 µl) were placed in each of the wells for testing. The 96 well plate was then put into the incubator to equilibrate to 37°C and 5% CO_2. While the equilibration was occurring, test samples were made up in 10% RPMI solution in the desired concentration. The test samples (100 µl) were then added to wells containing cells. The mixture was mixed thoroughly to ensure the solution was homogeneous with the cells. Then the plate was placed into the incubator (37 °C) for 5 days. On the 5th day 10 µl of MTS was added and mixed. The plates were then incubated for a further 4 hours, and read at 450 nm (xMARKTM, Bio-Rad,USA.).

6.3.2 Antimicrobial tests

Antimicrobial studies using the micro dilution method.were outsourced to the University of Kwa-Zulu Natal, pharmaceutical sciences department

The minimum inhibitory concentration (MIC) is described as the lowest amount of the antimicrobial agent needed to prevent the growth of a microorganism under defined experimental conditions, resulting in a quantitative measure of bacterial susceptibility. The MIC of the peptides against the four bacterial strains, which are Gram-positive and Gram-negative bacteria, was determined by the micro dilution method. When conducting MIC testing, peptide stock solutions

were prepared in sterile water for all experiments before performing a series of two-fold serial dilutions. Bacterial cultures were grown and diluted before seeding an equal volume into each well. The plates were incubated and read for Gram-positive and Gram-negative bacteria. The MIC was defined as the concentration at which no microbial growth was observed visually or spectrophotometrically. Growth media containing only microbial cells was used as the negative control.

6.4 General procedures

6.4.1 General procedure for the swelling, activation and coupling of the first amino acid to 2-chlorotitryl resin

2-Chlorotrityl-chloride resin (600 mg, 0.174 mmol/g) was added to a 15 ml centrifuge tube. Dry DCM (10.0 ml) and 1ml of thionylchloride were added to the tube. The mixture was shaken overnight then filtered and washed with dry DCM (3 ×15.0 ml). In order to avoid deactivation of the water sensitive resin, it was immediately added to dry DCM (20.0 ml), 1 ml of DIPEA (2.0 M, 2.0 ml) and the first amino acid which was histidine (2.0M, 1.49 g). This mixture was reacted for 30 minutes then dried using suction. Finally the resin was washed with DMF (3 ×15 ml).

6.4.2 General procedure for the swelling, activation and coupling of the first amino acid to rink amide resin

The rink amide resin (600 mg, 0.160 mmol/g) was swollen in DMF (20.0 ml) for 3 hours in a 15 ml centrifuge tube. The resin was then dried in a reaction fitted with a fritted filter vessel using suction. 20% piperidine in DMF was added twice for 5 min to deprotect the resin which was then washed with DMF (3 × 15 ml) and DCM (3 × 15 ml). A solution of DIPEA (1.0 M, 20.0 ml), HBTU (0.863 g) and the first amino acid which was histidine (2.0 M, 1.49 g) were added to the reaction vessel. This mixture was reacted for 30 minutes then dried under suction. Finally the resin was washed with DMF (3 × 15.0 ml).

6.4.3 General procedure for analysing the substitution of the first amino acid

The resin, with the first amino acid attached, was weighed out in duplicate samples of 5 to 10 mg in an eppendorf tube then 20% piperidine in DMF (1.0 ml) was added to the resin to remove the Fmoc protecting group and was shaken for 20 min then centrifuged down. From the centrifuged sample, 100 µl of the supernatant was transferred into a tube with DMF (10.0 ml). The mixture was thoroughly mixed and the solution (2.0 ml) was pipetted into one cuvette cell and DMF (2.0 ml) was added into another cuvette cell. The cuvette containing DMF was used to zero the spectrophotometer. The sample was checked for absorbance at 301 nm three times and used to calculate the substitution using the following equation:

$$Subs = 101(A)/7.8(w)$$

A = absorbance

w = mg of resin

The Substitution of Fmoc-Amino Acid Loaded was then used to calculate the loading capacity and the theoretical yield:

Theoretical yield = sub (mmol/g) × mass of resin (g) × Mr of peptide (g/mol)

6.4.4 General procedure for the synthesis of peptides

The resin attached to the first amino acid (histidine) was treated with 20% piperidine in DMF (20.0 ml) twice for 5 minutes to deprotect the amino acid. Then the resin was then washed with DMF (6 × 15.0 ml). The resin was then mixed with DIPEA (1.0 M, 20 ml), HBTU (0.863 g) and the second amino acid, cysteine (2.0 M, 1.41 g). This mixture was reacted for 30 minutes then dried using suction. The resin was washed with DMF (3 × 15.0 ml) and treated with 20% piperidine in DMF (20.0 ml) twice for 5 minutes and then the resin was then washed again with DMF (6 × 15.0 ml). The resin was then mixed with DIPEA (1 M, 20 ml), HBTU (0.863 g) and the next amino acid (2 M). This mixture was reacted for 30 minutes, and dried using suction which after the resin was washed with DMF (3 × 15.0 ml). This method was repeated until the full peptide was synthesized.

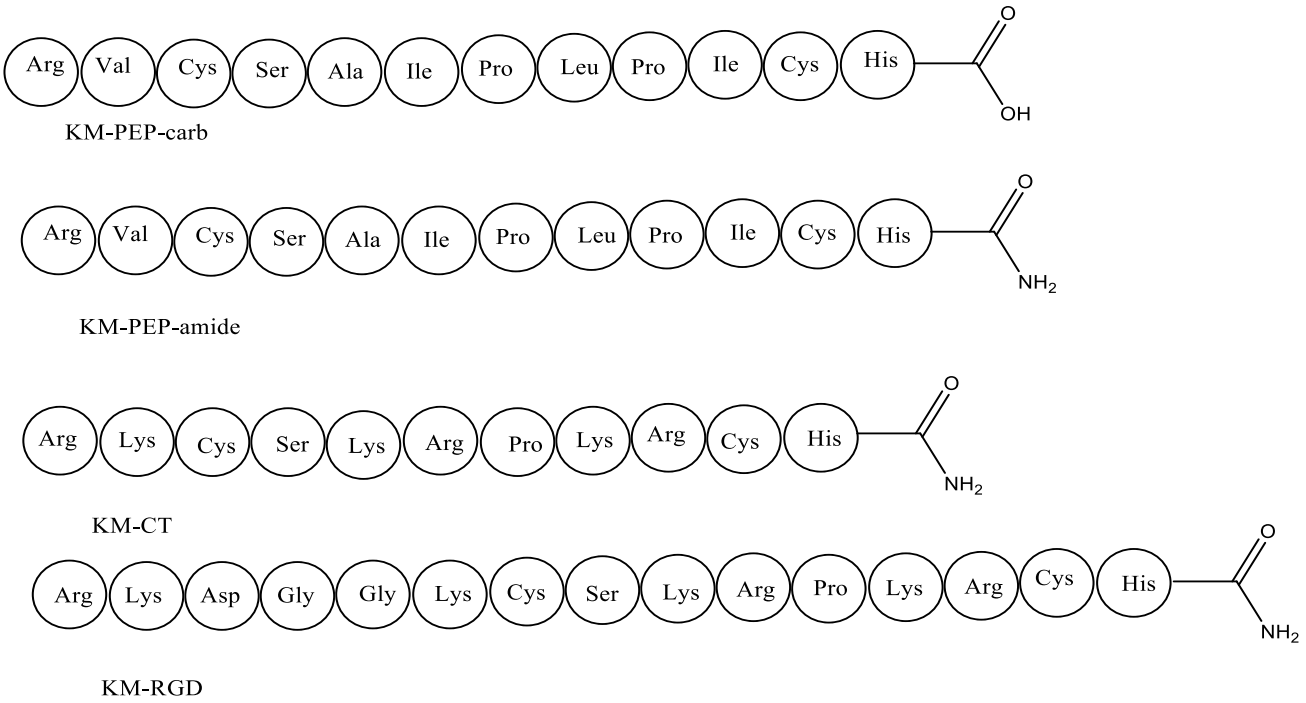


Figure 6. 1 Sequences of original peptides

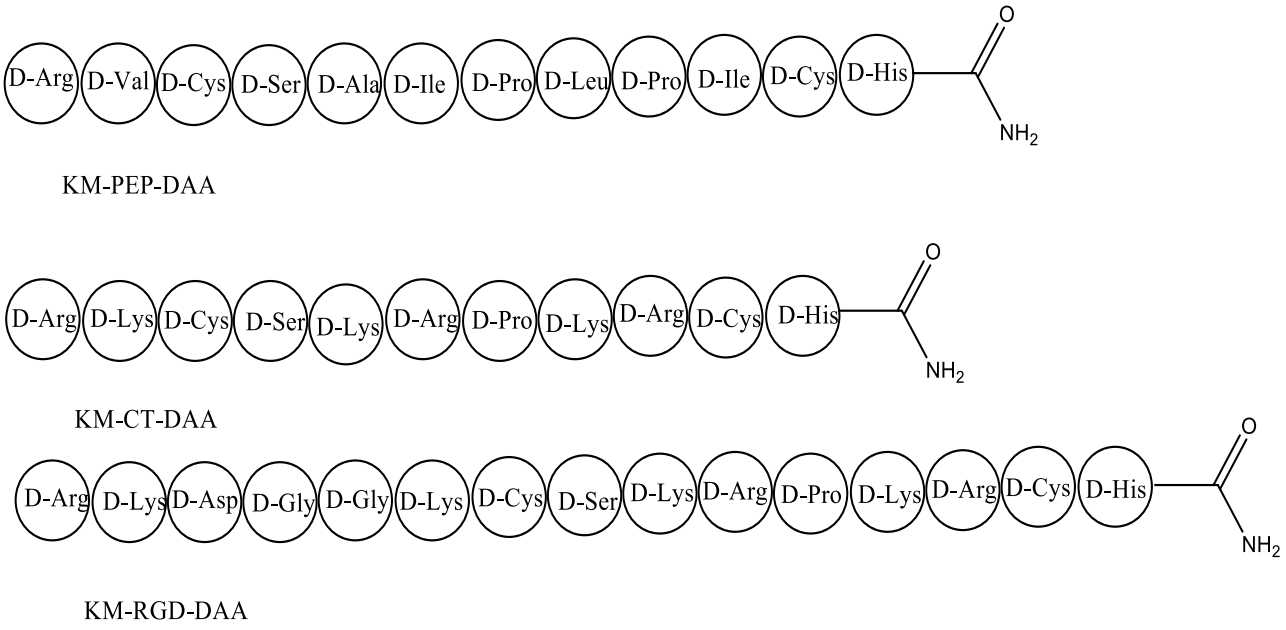


Figure 6. 2 Sequences of peptides containing D amino acids

6.4.6 General procedure for the synthesis of peptides containing adamantane and palmitic acid on the N-terminal

The resin attached to the first amino acid (histidine) was treated with 20% piperidine in DMF (20.0 ml) twice for 5 minutes to deprotect the amino acid. The resin was then washed with DMF (6 × 15.0 ml) and mixed with DIPEA (1.0 M, 20.0 ml), HBTU (0.863 g) and the second amino acid, cysteine (2.0 M, 1.41 g). This mixture was reacted for 30 minutes and dried using suction. The resin was washed with DMF (3 × 15.0 ml) and treated with 20% piperidine in DMF (20.0 ml) twice for 5 minutes to deprotect the amino acid and again washed with DMF (6 × 15.0 ml). The resin was then mixed with DIPEA (1.0 M, 20 ml), HBTU (0.863 g) and the next amino acid (2.0 M). This mixture was reacted for 30 minutes and dried using suction. The resin was washed with DMF (3 × 15.0 ml). This method was repeated until all of the amino acids in the peptide were coupled. The resin was treated with 20% piperidine in DMF (20.0 ml) twice for 5 minutes to deprotect the amino acid and washed again with DMF (6 × 15.0 ml) and dried using suction.

Adamantane carboxylic acid (2 M, 443 mg), DIPEA (1.0 M, 20.0 ml) and HBTU (0.863 g) were then added to the resin attached to the full peptide. This mixture was reacted for 30 minutes and the resin was washed in DMF (3 × 15.0 ml) and finally dried using suction.

The analogues with palmitic acid on the N-terminal were synthesized by adding palmitic acid (2.0 M, 615 mg) and DIPEA (1.0 M, 20.0 ml) and HBTU (0.863 g) to the resin attached to the full peptide. This mixture was reacted for 30 minutes then the resin was washed in DMF (3 × 15.0 ml) and finally dried using suction.

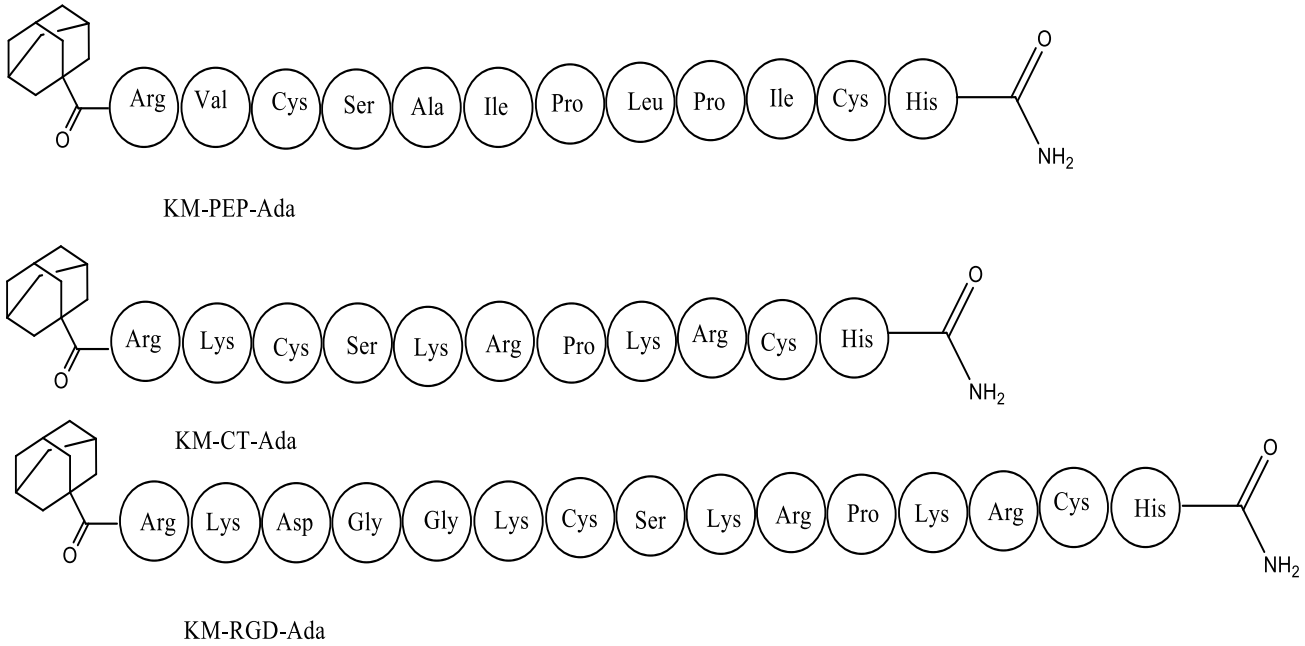
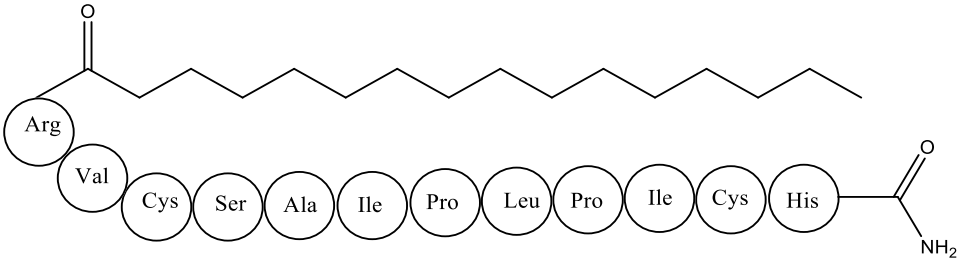
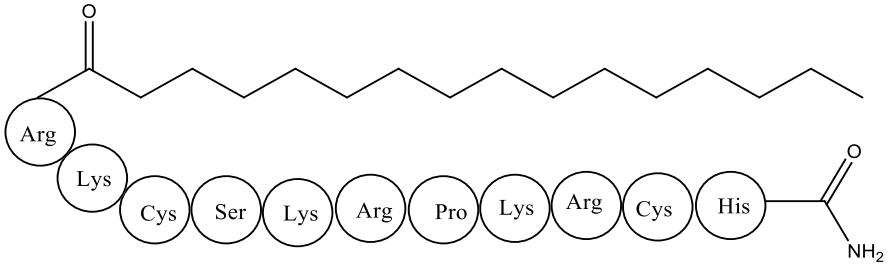


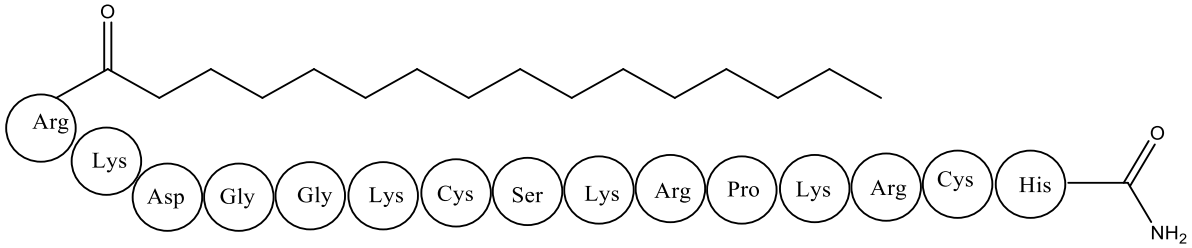
Figure 6. 3 Sequences of peptides containing adamantane group



KM-PEP-Pal



KM-CT-Pal

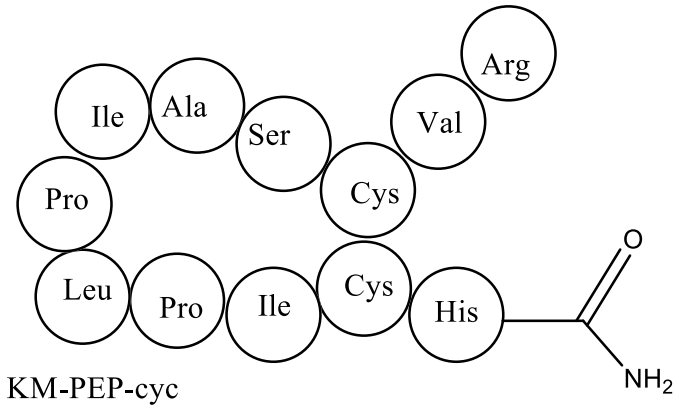


KM-RGD-Pal

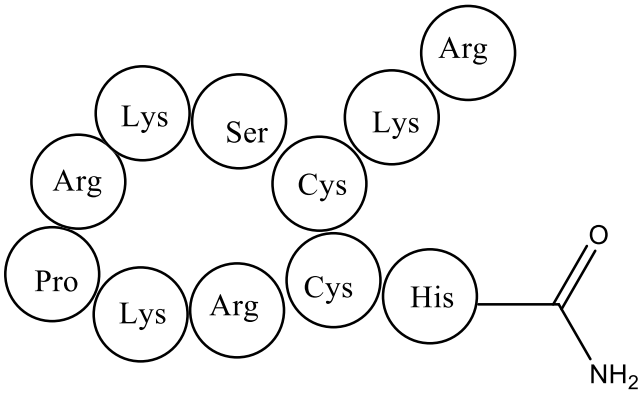
Figure 6. 4 Sequences of peptides containing palmitic group

6.4.8 General procedure for the cyclization of the peptides

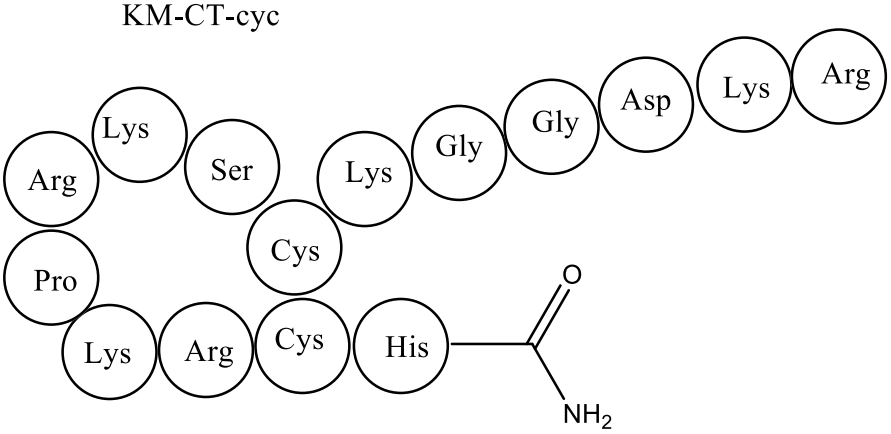
The peptides were cyclized while still attached to the resin. Iodine (0.26 g) was dissolved in 4:1 DMF/H_2O (10.0 ml) and added to the resin. This mixture was reacted for 4 hours. The resin was then washed with 2% ascorbic acid in DMF (1 g in 50 ml of DMF) to neutralise the residual iodine. The resin was then washed twice with 10 ml of DMF and 10 ml of DCM.



KM-PEP-cyc



KM-CT-cyc



KM-RGD

Figure 6. 5 Sequences of cyclic peptides

6.4.9 General procedure for the cleavage of the peptides from the resin

The resin attached to the peptide was removed from the reaction vessel and transferred to a manual peptide synthesis reaction vessel for the final cleavage. It was then washed with DMF (3 x 15.0 mL) then DCM (3 x 15.0 mL) and dried under suction. A cleavage mixture was prepared by mixing 95:2.5:2.5:1 % (v/v) TFA: H_2O: EDT: TIS in a 50 ml centrifuge tube. The dry resin was then transferred into the 50 ml centrifuge tube containing 20 ml of the cleavage mixture and was placed in a shaker for 3 hours. The resin was filtered and washed with 5 ml of the cleavage mixture followed by the addition of 60 ml of cold diethyl ether (which caused the peptide to precipitate). The filtrate was centrifuged several times and the precipitate was washed with cold diethyl ether. The white powder was then dissolved and purified using prep-HPLC.

6.4.10 General procedure for the purification of the peptides

The crude peptide samples were first dissolved in an acetonitrile/water solution or 100% DMSO. These samples were purified using an Agilent 1260 Infinity semi-preparative instrument with a flowrate of 15 ml/min on a C18 column.

Table 6. 1 Summary of peptides synthesized in chapter 2

Peptide ID	Sequence (C-N terminal)	Calculated mass	Found mass	Molecular ion	Retention time /min	Yield %
KM-PEP-carb	RVCSAIPLPICH-COOH	1307.68 $C_{57}H_{97}N_{17}O_{14}S_2$	1308.687	$[M+H]^+$	8.54	3.5
KM-PEP-cyc-amide	RVCSAIPLPICH-$CONH_2$	1304.68 $C_{57}H_{96}N_{18}O_{13}S_2$	1305.6905	$[M+H]^+$	6.63	2.5
KM-PEP-Pal	Pal-RVCSAIPLPICH-$CONH_2$	1544.93 $C_{157}H_{97}N_{17}O_{14}S_2$	773.5997	$[M+2H]^{2+}$	10.18	#
KM-PEP-Ada	Ada-RVCSAIPLPICH-$CONH_2$	1468.80 $C_{68}H_{112}N_{18}O_{14}S_2$	1469.8066	$[M+H]^+$	7.34	3.0
KM-PEP-DAA	RVCSAIPLPICH-$CONH_2$*	1306.68 $C_{157}H_{97}N_{17}O_{14}S_2$	1307.6955	$[M+H]^+$	8.62	#
KM-PEP-Ada-cyc	Ada-RKCSKRPKRCH-$CONH_2$	1466.79 $C_{68}H_{102}N_{18}O_{14}S_2$	734.4011	$[M+2H]^{2+}$	10.60	#
KM-PEP-Pal-cyc	Pal-RKCSKRPKRCH-$CONH_2$	1542.91 $C_{157}H_{97}N_{17}O_{14}S_2$	772.4634	$[M+2H]^{2+}$	10.75	#
KM-PEP-Nmeth	-RKCSKRPKRCH-$CONH_2$	1307.68 $C_{157}H_{97}N_{17}O_{14}S_2$	N/A	N/A	*	

KM-PEP-Nmeth 5 Amino Acids	LPICH-$CONH_2$	608.35 $C_{28}H_{48}N_8O_5S$	609.3392	$[M+H]^+$	3.60	#
KM-PEP-toid	RKCSKRPKRCH-$CONH_2$*	1307.68 $C_{157}H_{97}N_{17}O_{14}S_2$	N/A	N/A	*	

***unsuccessful**

*** not synthesized**

 # purification was incomplete due to time constrains

Table 6. 2 Summary of peptides synthesized in chapter 3

Peptide ID	Sequence (C-N terminal)	Calculated mass	Found mass	Molecular ion	Retention time /min
KM-CT	RKCSKRPKRCH-$CONH_2$	1396.74 $C_{55}H_{98}N_{26}O_{13}S_2$	1397.7851	$[M+H]^+$	3.41
KM-CT-cyc	RKCSKRPKRCH-$CONH_2$	1394.72 $C_{55}H_{98}N_{26}O_{13}S_2$	465.9125	$[M+3H]^{3+}$	3.43
KM-CT-Ada	Ada-RKCSKRPKRCH-$CONH_2$	1556.83 $C_{66}H_{112}N_{26}O_{14}S_2$	780.3589	$[M+2H]^{2+}$	8.85
KM-CT-Pal	Pal-RKCSKRPKRCH-$CONH_2$	1632.95 $C_{66}H_{112}N_{26}O_{14}S_2$	817.3392	$[M+H]^+$	8.25
KM-CT-DAA	RKCSKRPKRCH-$CONH_2$	1396.74 $C_{55}H_{98}N_{26}O_{13}S_2$	1397.7888	$[M+H]^+$	8.07

KM-RGD	RGDGGKCSKRPKRCH-$CONH_2$	1682.83 $C_{65}H_{114}N_{30}O_{19}S_2$	561.9635	$[M+3H]^{3+}$	7.77
KM-RGD-Ada	Ada-RGDGGKCSKRPKRCH-$CONH_2$	1844.94 $C_{76}H_{128}N_{30}O_{20}S_2$	923.3142	$[M+2H]^{2+}$	8.20
KM-RGD-Pal	Pal-RGDGGKCSKRPKRCH-$CONH_2$	1921.06 $C_{81}H_{144}N_{30}O_{20}S_2$	961.8737	$[M+2H]^{2+}$	8.94
KM-RGD-DAA	RGDGGKCSKRPKRCH-$CONH_2$	1682.83 $C_{65}H_{114}N_{30}O_{19}S_2$	842.9421	$[M+2H]^{2+}$	5.60

 # purification was incomplete due to time constrains

6.4.11 General procedure for the synthesis of the peptoids

Activated 2-chlorotrityl chloride resin (1 g, 1.33 mmol) was swelled in dry DCM (10 ml) for 10 minutes in a sintered glass reaction vessel. Bromoacetic acid (1.6 g) in DMF (final concentration of (1.2 M) and DIPEA (2 ml) was added to the reaction vessel and the mixture was mixed by bubbling nitrogen gas for 2 hours. The solvent was removed by filtration and the resin washed with DCM (3 x 10 mL) and DMF (3 x 10 mL). A solution of the amine (1 M) in DMF was added to the reaction vessel and mix by bubbling nitrogen through the mixture for 1 hour. The solvent was removed by filtration and the resin was washed with DCM (3 x 10 ml) and DMF (3 x 10 ml). Bromoacetic acid (1.6 g) in DMF (final concentration of 1.2 M) and DIC (2 ml) was added to the reaction vessel and bubbled for 2 hours using nitrogen. These steps were repeated for the desired sequences. Final cleavage of the peptoid from the resin was carried out similarly as that of peptides described above.

6.4.12 General procedure for the cleavage of the peptoids

After the completion of the synthesis of the peptoid, the resin was washed 3 times with 10 ml of DMF to remove impurities and unreacted starting material and also washed 6 times with 10 ml DCM to remove the DMF. The resin was dried under suction for 10 min and a solution of 5% TFA solution in DCM was added. After 15 min the resin was filtered and washed with DCM. Diethyl ether was added and when a precipitated formed, the crude peptoid would be centrifuged and if the peptoid did not form a precipitate then the filtrate was placed in the rotary evaporator to remove the solvent.

6.4.13 General procedure for the synthesis of the *N*-methylated Fmoc leucine

For the synthesis of the oxazolidinone intermediate, Fmoc leucine (7.07 g, 20 mmol), paraformaldehyde (4.0 g, 40 mmol) and *p*-toluenesulfonic acid (400 mg, 40 mmol) were dissolved in toluene (350 ml). The mixture was refluxed in a Dean-Stark setup until all the starting material was no longer visible by TLC (10:3 DCM:MeOH). Once the solution cooled to room temperature, it was washed with saturated aqueous $NaHCO_3$ and dried over anhydrous $MgSO_4$. The product was then concentrated on a rotary-evaporator. Purification of the product was conducted via crystallization. The product was dissolved in warm acetonitrile and an equal amount of hexane was gently added. The product formed crystals overnight.

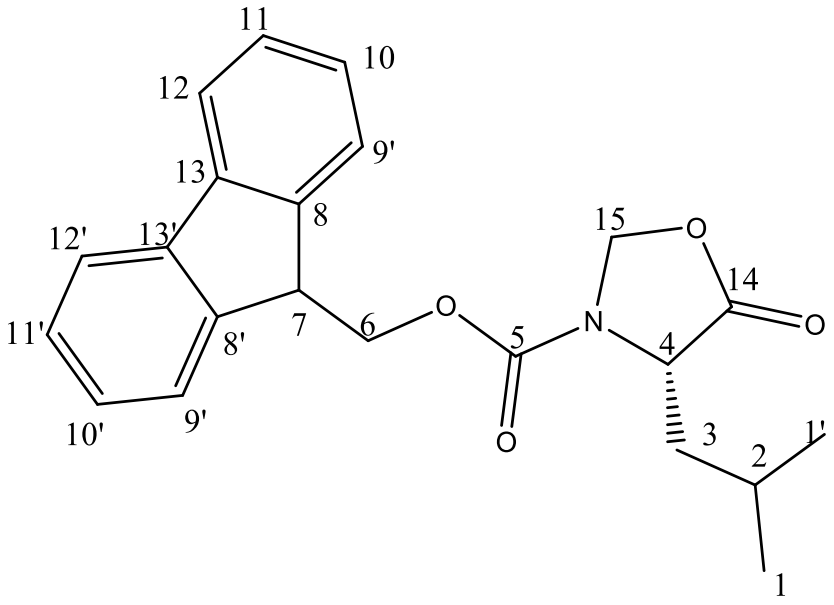


Figure 6. 6 oxazolidinone of Fmoc leucine

For the synthesis of the *N*-methylated leucine, the oxazolidinone was dissolved in dry DCM (400 ml) then aluminium chloride (2.67 g, 40 mmol) and triethylsilane (2.33 g, 40 mmol) were added to the mixture. The mixture was stirred at room temperature until TLC (1:3 Ethylacetate:hexane) showed the complete consumption of the starting material. Once the reaction was complete, an additional amount of DCM (200 ml) was added and the organic phase was washed with 1M HCl and then it was dried over anhydrous $MgSO_4$. The product was then concentrated on a rotary-evaporator. Column chromatography (25% EtOAc/hexane) was used then further purification of the product was conducted via crystallization. The product was dissolved in warm acetonitrile and an equal amount of hexane was gently added. The product formed crystals overnight to afford yellow crystals (5.02 g, 68%).

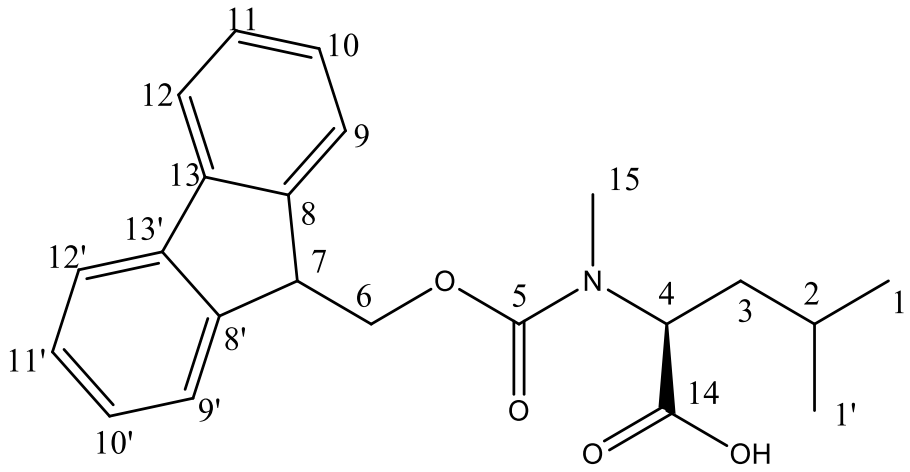


Figure 6. 7 *N*-methylated Fmoc-leucine

R_f (50% EtOAc/hexane) 0.83.***mp***: 141-143°C. **$[\alpha]^{20}_D$** (-) 9.863 (*c* 0.73, DMSO). **^{1}H NMR (300 MHz, DMSO-d6)** δ , 8.03 – 7.79 (2H, m, H12, H12'), 7.63 (2H, td, *J* = 7.6, 3.6 Hz, H9, H9'), 7.35 (4H, m, *J* = 22.9, 9.4, 7.9, 6.1, 1.5 Hz, H10, H10', H11, H11'), 4.63 (1H, dd, *J* = 11.4, 4.5 Hz, H7), 4.49 – 4.35 (2H, m, CH_2-H6), 4.33 – 4.18 (1H, m, H4), 2.71 (3H, s, CH_3-H15), 1.83 – 1.47 (2H, m, CH_2-H3), 1.41 – 1.25 (1H, m, H2), 0.96 – 0.58 (6H, m, CH_3-H1, CH_3-H1'). **^{13}C NMR (75 MHz, DMSO-d6)** δ 172.94 (C14), 156.03 (C5), 143.72 (C8, C8'), 140.74 (C13, C13'), 127.58 (C12, C12'), 127.04 (C11, C11'), 124.81 (C10, C10'), 120.05 (C9, C9'), 66.66 (C4), 56.09 (C6), 46.71 (C7), 29.86 (C3), 24.38 (C15), 22.96 (C2), 20.89 (C1). **IR (ν_{max}/cm^{-1}):** 3010 (OH); 2985 (ArC-H); 2865 (C-H); 1751 (Ester C=O); 1649 (Carboxylic C=O). **HRMS m/z:** calculated for $C_{22}H_{25}NO_4$: 367.18, found: $[M + H]^+$ 368.1853

6.4.14 General procedure for the synthesis of the *N*-methylated Fmoc isoleucine

The Fmoc isoleucine (7.07 g, 20 mmol), paraformaldehyde (4 g, 40 mmol) and *p*-toluenesulfonic acid (400 mg, 40 mmol) were dissolved in toluene (350 ml). The mixture was refluxed in a Dean-Stark setup until all the starting material was no longer visible by TLC (10:3 DCM:MeOH). Once the solution cooled to room temperature, it was washed with saturated aqueous $NaHCO_3$ and dried over anhydrous $MgSO_4$. The product was concentrated on a rotary-evaporator. Purification of the product was then conducted via crystallization. The product was dissolved in warm acetonitrile then an equal amount of hexane was gently added using a pasture pipette. The product formed crystals overnight.

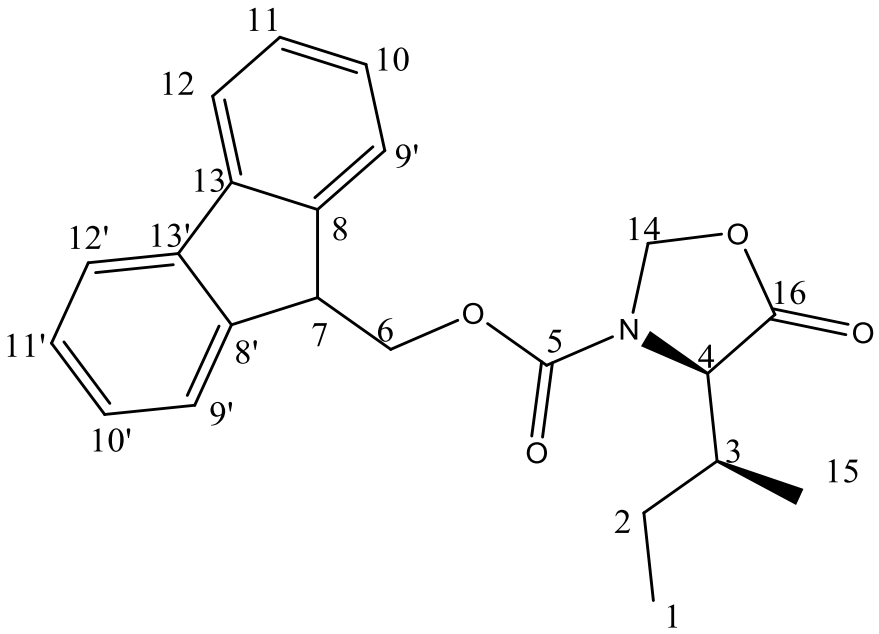


Figure 6. 8 Oxazolidinone of Fmoc-isoleucine

For the synthesis of the *N*-methylated isoleucine, a quantitative amount of the oxazolidinone was dissolved in dry DCM (400 ml) then aluminium chloride (2.67 g, 40 mmol) and triethylsilane (2.33 g, 40 mmol) were added to the mixture. The mixture was stirred at room temperature until TLC (1:3 Ethylacetate:hexane) showed the non-appearance of starting material. Once the reaction was complete, an additional amount of DCM (200 ml) was added and the organic phase was washed with 1M HCl and then it was dried over anhydrous $MgSO_4$. The product was then concentrated on a rotary-evaporator. Column chromatography (25% EtOAc/hexane) was used then further purification of the product was conducted via crystallization. The product was dissolved in warm acetonitrile and an equal amount of hexane was gently added using a pasture pipette. The product formed crystals overnight to afford yellow crystals (3.74 g, 55%).

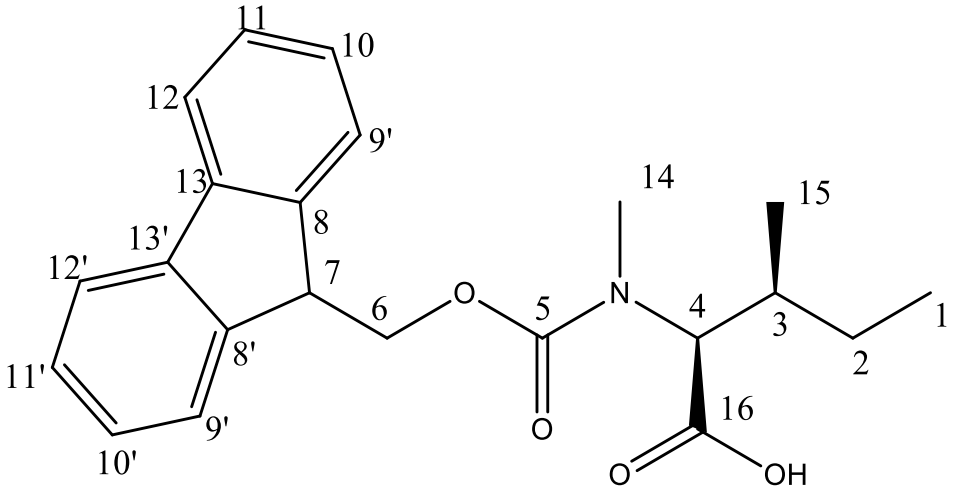


Figure 6. 9 *N*-methylated Fmoc-isoleucine

R_f (50% EtOAc/hexane) 0.80. ***mp*:** 178-180°C. **$[\alpha]^{20}_D$** (-) 41.87 (*c* 0.48, DMSO). **^{1}H NMR (300 MHz, DMF-d7)** δ 8.31 (2H,d, *J* = 7.2 Hz, H12, H12'), 8.07 (2H,dt, *J* = 12.4, 6.1 Hz, H9, H9'), 7.79 (4H, m, *J* = 26.1, 7.2 Hz, H10, H10', H11, H11'), 4.93 – 4.66 (4H, m, H4, H5 , H6, H7), 3.14 (3H, d, *J* = 2.8 Hz, H14), 2.37 – 2.15 (1H, m, H3), 1.81 – 1.64 (1H, m, H2), 1.57 (1H, q, *J* = 11.9, 8.4 Hz, H2), 1.34 – 1.13 (6H, m, H1, H15). **^{13}C NMR (75 MHz, DMSO-d6)** δ 171.99 (C16), 156.93 (C5), 143.72 (C8, C8'), 140.77 (C13, C13'), 127.57 (C12, C12'), 127.03 (C11, C11'), 124.88 (C10, C10'), 120.02 (C9, C9'), 66.68 (C4), 62.41 (C6), 46.73 (C7), 32.63 (C3), 29.93 (C14), 24.54 (C2)15.62 (C15), 10.58 (C16).**IR (ν_{max}/cm^{-1}):** 3039 (OH); 2960 (ArC-H); 2875 (C-

H); 1733 (Ester C=O); 1620 (Carboxylic C=O). **HRMS m/z:** calculated for $C_{22}H_{25}NO_4$: 367.18, found: $[M + H]^+$ 368.1856

6.4.15 General procedure for the synthesis of the *N*-methylated Fmoc alanine

The Fmoc alanine (6.23 g, 20 mmol), paraformaldehyde (4.0 g, 40 mmol) and *p*-toluenesulfonic acid (400 mg, 40 mmol) were suspended in toluene (350 ml). The mixture was refluxed in a Dean-Stark setup until all the starting material was no longer visible by TLC (10:3 DCM:MeOH). Once the solution cooled to room temperature, it was washed with saturated aqueous $NaHCO_3$ and dried over anhydrous $MgSO_4$. The product was then concentrated on a rotary-evaporator. Purification of the product was conducted via crystallization. The product was dissolved in warm acetonitrile then an equal amount of hexane was gently added using a pasture pipette. The product formed crystals overnight.

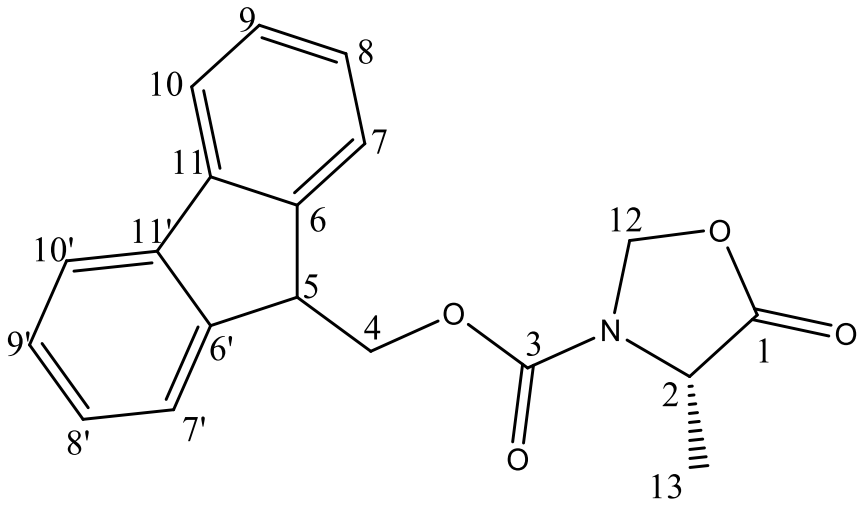


Figure 6. 10 Oxazolidinone of Fmoc-alanine

For the synthesis of the *N*-methylated alanine, a quantitative amount of the oxazolidinone was dissolved in dry DCM (400 ml) then aluminium chloride (2.67 g, 40 mmol) and triethylsilane (2.33

g, 40 mmol) were added to the mixture. The mixture was stirred at room temperature until TLC (1:3 Ethylacetate:hexane) showed the non-appearance of starting material. Once the reaction was complete, an additional amount of DCM (200 ml) was added and the organic phase was washed with 1M HCl and then it was dried over anhydrous $MgSO_4$. The product was then concentrated on a rotary-evaporator. Column chromatography (25% EtOAc/hexane) was used then further purification of the product was conducted via crystallization. The product was dissolved in warm acetonitrile and an equal amount of hexane was gently added using a pasture pipette. The product formed crystals overnight to afford white crystals (2.51 g, 39%).

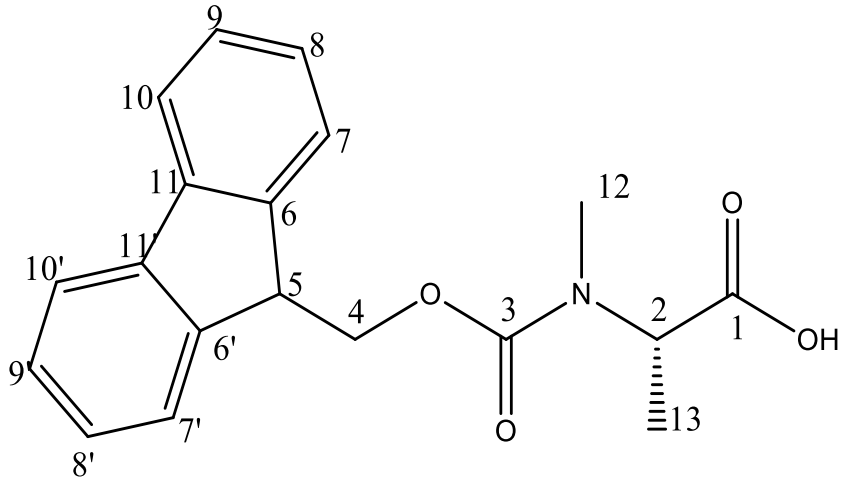


Figure 6. 11 *N*-methylated Fmoc-alanine

R_f (50% EtOAc/hexane) 0.62. ***mp*:** 135-140°C. **$[\alpha]^{20}_D$** (-) 5.083 (*c* 1.20, DMSO). **^{1}H NMR (300 MHz, DMSO-d_6)** δ 7.89 (2H, d, *J* = 7.5 Hz, H10, H10'), 7.64 (2H, t, *J* = 7.8 Hz, H7, H7'), 7.46 – 7.31 (4H, m, H8, H8' ,H9 ,H9'), 4.67 – 4.51 (1H, m, H5), 4.31 (3H, dt, *J* = 13.4, 5.9 Hz, H2, CH_2-4), 2.78 (3H, s, CH_3-H12), 1.30 (3H, d, *J* = 7.3 Hz, CH_3-H13). **^{13}C NMR (75 MHz, Chloroform-d)** δ 177.35 (C1), 156.78 (C3), 143.88 (C6), 141.33 (C11), 127.70 (C10), 127.06 (C9), 125.02 (C8), 119.97 (C7), 67.91 (C4), 54.23 (C2), 47.24 (C5), 30.50 (C12), 14.56 (C13)**. IR (v_{max}/cm^{-1}):** 3065 (OH); 2944 (ArC-H); 2842 (C-H); 1738 (Ester C=O); 1650 (Carboxylic C=O). **HRMS m/z:** calculated for $C_{19}H_{19}NO_4$: 325.13, found: $[M + H]^+$ 326.1404

6.4.16 General procedure for the synthesis of the *N*-methylated Fmoc valine

The Fmoc valine (6.78 g, 20 mmol), paraformaldehyde (4.0 g, 40 mmol) and *p*-toluenesulfonic acid (400 mg, 40 mmol) were suspended in toluene (350 ml). The mixture was refluxed in a Dean-Stark setup until all the starting material was no longer visible by TLC (10:3 DCM:MeOH). Once the solution cooled to room temperature, it was washed with saturated aqueous $NaHCO_3$ and dried over anhydrous $MgSO_4$. The product was then concentrated on a rotary-evaporator. Column chromatography (25% EtOAc/hexane) was used then further purification of the product was conducted via crystallization. The product was dissolved in warm acetonitrile and an equal amount of hexane was gently added. The product formed crystals overnight.

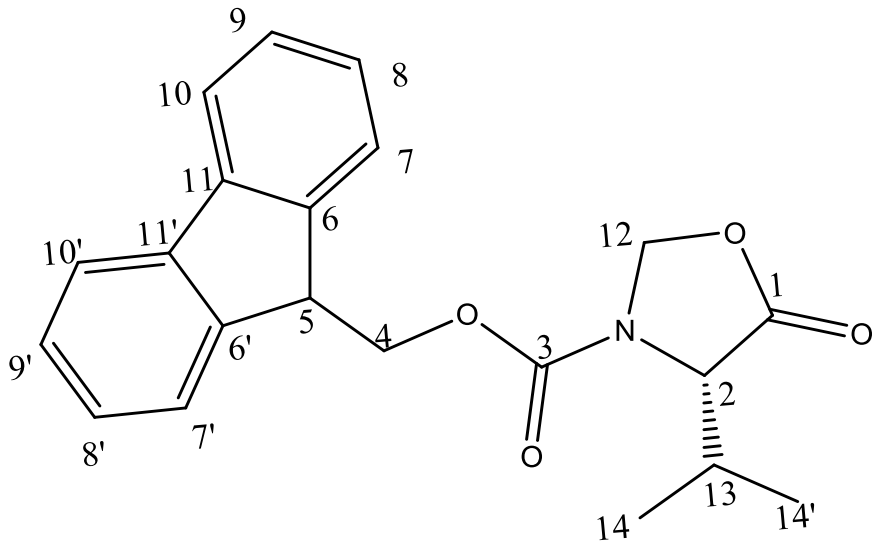


Figure 6. 12 Oxazolidinone of Fmoc-valine

For the synthesis of the *N*-methylated valine, a quantitative amount of the oxazolidinone was dissolved in dry DCM (400 ml) then aluminium chloride (2.67 g, 40 mmol) and triethylsilane (2.33 g, 40 mmol) were added to the mixture. The mixture was stirred at room temperature until TLC (1:3 Ethylacetate:hexane) showed the complete consumption of the starting material. Once the

reaction was complete, an additional amount of DCM (200 ml) was added and the organic phase was washed with 1M HCl and then it was dried over anhydrous $MgSO_4$. The product was then concentrated on a rotary-evaporator. Column chromatography (25% EtOAc/hexane) was used then further purification of the product was conducted via crystallization. The product was dissolved in warm acetonitrile and an equal amount of hexane was gently added. The product formed crystals overnight to afford yellow crystals (2.84 g, 40%).

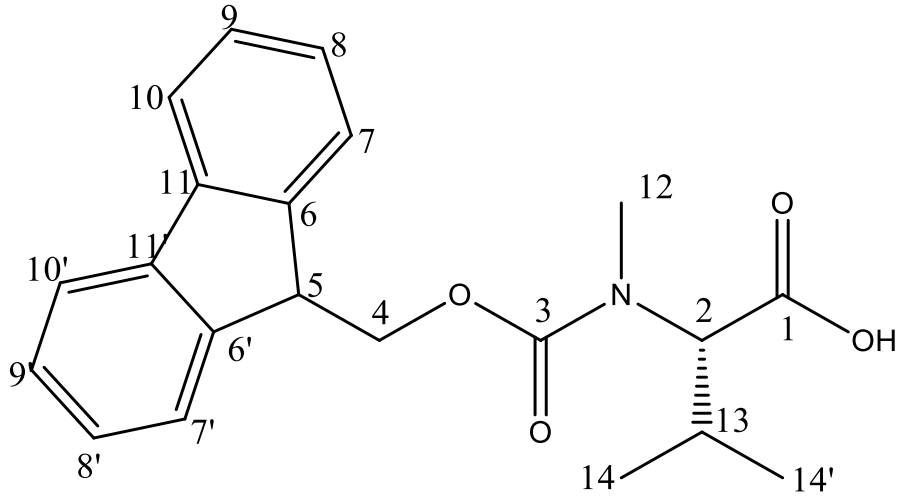


Figure 6. 13 *N*-methylated Fmoc-valine

R_f (50% EtOAc/hexane) 0.48. ***mp*:** 171-173°C. **$[\alpha]^{20}_D$** (-) 49.20 (*c* 0.50, DMSO). **^{1}H NMR (300 MHz, DMSO-d6)** δ 7.89 (2H, d, *J* = 7.6 Hz, H10, H10'), 7.65 (2H, q, *J* = 6.8, 4.9 Hz, H7, H7'), 7.53 – 7.24 (4H, m, H8, H8', H9, H9'), 4.64 – 4.38 (2H, m, CH_2-H4), 4.38 – 4.28 (1H, m, H5), 4.18 (1H, d, *J* = 10.3 Hz, H2), 2.72 (3H, d, *J* = 7.5 Hz,CH_3-H12), 2.25 – 1.85 (1H, m, H13), 1.03 – 0.46 (6H, m, CH_3-H14, CH_3-H14'). **^{13}C NMR** (75 MHz, DMSO-d6) δ 172.73 (C1), 143.36 (C3), 140.21 (C6), 138.22 (C11), 136.19 (C10), 130.29 (C9, C8), 129.74 (C7), 128.10 (C2), 124.74 (C4), 122.18 (C5), 121.99 (C12), 120.82 (C13), 110.55 (C14) **IR (v_{max}/cm^{-1}):** 3020 (OH); 2958 (ArC-H); 2845 (C-H); 1734 (Ester C=O); 1643 (Carboxylic C=O). **HRMS m/z:** calculated for $C_{22}H_{25}NO_4$: 353.16, found: $[M + H]^+$ 354.1697.

6.4.17 General procedure for the synthesis of the silver nanoparticles (AgNPs)

AgNPs Nano spheres were synthesized using two different techniques. In a procedure using citrate as a reducing agent, $AgNO_3$ (10 mg) was dissolved in a 40% glycerol-water solution. The solution was brought to a boiling temperature at about 97^oC while stirring. Once the solution started boiling 3% trisodium citrate solution (0.3 ml) was added drop-wise. The clear solution changed from colorless to pale yellow after 5 min of reacting which was an indication of the formation of AgNPs. The colloidal solutions of AgNPs were centrifuged at 15000 rpm, for 15 min in order to concentrate the dispersed particles to the bottom of the centrifuge tube and to remove excess unreacted ions and starting material in the supernatant. The AgNPs were placed in glass vials for storage and wrapped with aluminium foil to avoid the interactions with light which may cause aggregation of the particle. The second technique made use of sodium borohydride ($NaBH_4$) as a reducing agent. In this procedure (2 mM, 40 ml) solution was prepared and cooled to 0 degrees then $AgNO_3$ (1 mM, 30 ml) was added to the solution drop-wise with stirring. The solution turned yellow and was stirred for another 5 min. The AgNP's which formed were centifuged and stored in the same manner as the previous procedure.

6.4.18 General procedure for the synthesis of the silver nanoparticles (AgNPs) conjugated to KM-PEP-carb peptide

AgNP-PEP was synthesized by first dissolving the KM-PEP-carb (1 mg) in 40 ml of distilled water. The AgNPs were prepared by adding distilled water to the concentrated stored AgNP solution up to the 50 ml mark. For fraction 3, 5 and 7 AgNPs (10 ml) were mixed with 200 µl of the KM-PEP-carb solution. For fraction 2, 4, 6 100 µl of AgNP was mixed with 400 µl of the KM-PEP-carb solution. Fraction 1 consisted of 25 ppm of KM-PEP only and fraction 8 of the AgNP only with an average diameter of 25 nm. The AgNP size for fraction 2 and 3 was 25 nm; for fraction 4 and 5 was 50 nm.

Table 6. 3 Summary of AgNPs and KM-PEP-carb volume used for each sample and the particle sizes

Product name	Volume of AgNP added	Volume of KM-PEP-carb added	AgNP size
Fraction 1	0	2 ml	N/A
Fraction 2	100 µl	400 µl	25 nm
Fraction 3	10 ml	200 µl	25 nm
Fraction 4	100 µl	400 µl	50 nm
Fraction 5	10 ml	200 µl	50 nm
Fraction 6	100 µl	400 µl	9 nm
Fraction 7	10 ml	200 µl	9 nm
Fraction 8	2 ml	0	25 nm

References

1. O.E. Sorensen, J.B. Cowland, K. Theilgaard-Mönch, L. Liu, T. Ganz, N. Borregaard. Wound healing and expression of antimicrobial peptides/polypeptides in human keratinocytes, a consequence of common growth factors. *The Journal of Immunology*. **2003**, 170(11):5583-5589.
2. S.C. Mansour, O.M. Pena, R.E.W. Hancock. Host defense peptides: front-line immunomodulators. *Trends in Immunology* **2014**, 35 (9), 443–450.
3. M. Davis, A. Whittaker, M. Lindgren, M. Djerf-Pierre, L. Manderson, P. Flowers. Understanding media publics and the antimicrobial resistance crisis. *Global Public Health* **2018**, 13 (9), 1158–1168.
4. P.-H. Wang, B.-S. Huang, H.-C. Horng, C.-C. Yeh, Y.-J. Chen. Wound healing. *Journal of the Chinese Medical Association* **2018**, 81 (2), 94–101.
5. K.A. Walters, M.S. Roberts. The structure and function of skin. *In Design of Biomedical Devices and Systems.* **2002**, 18-58.
6. S. Guo, L.A. DiPietro. Factors affecting wound healing. *Journal of Dental Research* **2010**, 89 (3), 219–229.
7. G. Broughton, J.E. Janis, C.E. Attinger. The basic science of wound healing. *Plastic and Reconstructive Surgery* **2006**, 117 (7), 12-34
8. J. Li, J. Chen, R. Kirsner. Pathophysiology of acute wound healing. *Clinics in Dermatology* **2007**, 25 (1), 9–18.
9. A.J. Mellott, D.S. Zamierowski, B.T. Andrews. Negative pressure wound therapy in maxillofacial applications. *Dentistry Journal* **2016**, 4 (3), 463-467.
10. C.M. Minutti, J.A. Knipper, J.E. Allen, D.M.W. Zaiss. Tissue-specific contribution of macrophages to wound healing. *Seminars in Cell & Developmental Biology* **2017**, 61, 3–11.
11. P. Martin, S.J. Leibovich. Inflammatory cells during wound repair: the good, the bad and the ugly. *Trends in Cell Biology* **2005**, 15 (11), 599–607.
12. G.B. Greenburg, T.K. Hunt. The proliferative response *in vitro* of vascular endothelial and smooth muscle cells exposed to wound fluids and macrophages. *Journal of Cellular Physiology* **1978**, 97 (3), 353–360.
13. T.J. Koh, L.A. DiPietro. Inflammation and wound healing: the role of the macrophage. *Expert Reviews in Molecular Medicine* **2011**, 13.
14. S.A. Eming, T. Krieg, J.M. Davidson. Inflammation in wound repair: molecular and cellular mechanisms. *Journal of Investigative Dermatology* **2007**, 127 (3), 514–525.
15. S. Barrientos, O. Stojadinovic, M.S. Golinko, H. Brem, M. Tomic-Canic. PERSPECTIVE ARTICLE: Growth factors and cytokines in wound healing. *Wound Repair and Regeneration* **2008**, 16 (5), 585–601.
16. S. Werner, R. Grose. Regulation of wound healing by growth factors and cytokines. *Physiological Reviews* **2003**, 83 (3), 835–870.
17. S. Jettanacheawchankit, S. Sasithanasate, P. Sangvanich, W. Banlunara, P. Thunyakitpisal. Acemannan stimulates gingival fibroblast proliferation; expressions of keratinocyte growth factor-1, vascular endothelial growth factor, and type I collagen; and wound healing. *Journal of Pharmacological Sciences* **2009**, 109 (4), 525–531.
18. H.M. Kagan, W. Li. Lysyl oxidase: Properties, specificity, and biological roles inside and outside of the cell. *Journal of Cellular Biochemistry* **2003**, 88 (4), 660–672.

19. X. Liu, Y. Zhao, J. Gao, Elastic fiber homeostasis requires lysyl oxidase–like 1 protein. *Nature Genetics* **2004**, 36 (2), 178–182.
20. G.F. Pierce, J. Vande Berg, R. Rudolph, J. Tarpley, T.A. Mustoe. Platelet-derived growth factor-BB and transforming growth factor beta 1 selectively modulate glycosaminoglycans, collagen, and myofibroblasts in excisional wounds. *The American Journal of Pathology* **1991**, 138 (3), 629–646.
21. K. Hotary, E. Allen, A. Punturieri, I. Yana, S.J. Weiss. Regulation of cell invasion and morphogenesis in a three-dimensional type I collagen matrix by membrane-type matrix Metalloproteinases 1, 2, and 3. *The Journal of Cell Biology* **2000**, 149 (6), 1309–1323.
22. M.C. Robson, D.L. Steed, M.G. Franz. Wound healing: Biologic features and approaches to maximize healing trajectories. *Current Problems in Surgery* **2001**, 38 (2), A1-140.
23. T. Kondo, Y. Ishida. Molecular pathology of wound healing. *Forensic Science International* **2010**, 203 (1–3), 93–98.
24. B. Hinz, V. Dugina, C. Ballestrem, B. Wehrle-Haller, C. Chaponnier. Maturation in myofibroblasts V. *Molecular Biology of the Cell* **2003**, 14 (6), 2508-2519.
25. J.M. Goffin, P. Pittet, G. Csucs. Focal adhesion size controls tension-dependent recruitment of α-smooth muscle actin to stress fibers. *The Journal of Cell Biology* **2006**, 172 (2), 259–268.
26. B. Hinz, G. Celetta, J.J. Tomasek, G. Gabbiani, C. Chaponnier. Alpha-smooth muscle actin expression upregulates fibroblast contractile activity. *Molecular Biology of the Cell* **2001**, 12 (9), 2730–2741.
27. U.M.E. Wikesjö, R.E. Nilvéus, K.A. Selvig. Significance of early healing events on periodontal repair: A Review. *Journal of Periodontology* **1992**, 63 (3), 158–165.
28. C.K. Sen, G.M. Gordillo, S. Roy, Human skin wounds: A major and snowballing threat to public health and the economy. *Wound Repair and Regeneration* **2009**, 17 (6), 763–771.
29. J. Tripette, L.-C. Nguyen, L. Allard, P. Robillard, G. Soulez, G. Cloutier.. *In Vivo* Venous assessment of red blood cell aggregate sizes in diabetic patients with a quantitative cellular ultrasound imaging method: proof of concept. *PLoS ONE* **2015**, 10 (4), 1–12.
30. R.F. Alhabshan, M.S. Bin Huwaymil, O.A. Alsaqabi, A.N. Alzaid, A.I. Almasoud. Assessment of knowledge toward complications of diabetic septic foot among diabetics patients in Saudi Arabia. *Egyptian Journal of Hospital Medicine* **2017**, 69 (6), 2557–2561.
31. N.C. Schaper, J.J.V. Netten, J. Apelqvist, B.A. Lipsky, K. Bakker. Prevention and management of foot problems in diabetes: a summary guidance for daily practice 2015, based on the IWGDF guidance documents. *Diabetes/Metabolism Research and Reviews* **2016**, 32 (S1), 7–15.
32. T.N. Demidova-Rice, M.R. Hamblin, I.M. Herman. Acute and impaired wound healing: pathophysiology and current methods for drug delivery, Part 1: Normal and chronic wounds: biology, causes, and approaches to care. *Advances in Skin & Wound Care* **2012**, 25 (7), 304–314.
33. S. Schreml, R.M. Szeimies, L. Prantl, S. Karrer, M. Landthaler, P. Babilas. Oxygen in acute and chronic wound healing. *British Journal of Dermatology* **2010**, 163 (2), 257–268.
34. U.V. Wesley, P.F. Bove, M. Hristova, S. McCarthy, A. van der Vliet. Airway epithelial cell migration and wound repair by ATP-mediated activation of dual Oxidase 1. *Journal of Biological Chemistry* **2007**, 282 (5), 3213–3220.

35. B. Chiang, E. Essick, W. Ehringer, Enhancing skin wound healing by direct delivery of intracellular adenosine triphosphate. *The American Journal of Surgery* **2007**, 193 (2), 213–218.
36. K.R. Thistlethwaite, K.J. Finlayson, P.D. Cooper, B. Brown, M.H. Bennett, G. Kay, M.T. O'reilly, H.E Edwards. The effectiveness of hyperbaric oxygen therapy for healing chronic venous leg ulcers: A randomized, double-blind, placebo-controlled trial: Hyperbaric oxygen therapy for healing chronic venous leg ulcers. *Wound Repair and Regeneration* **2018**, 26 (4), 324–331.
37. T.C. Tu, M. Nagano, T. Yamashita, H, Hamada, K. Ohneda, K. Kimura, O. Ohneda. A chemokine receptor, CXCR4, which is regulated by hypoxia-inducible factor 2α, is crucial for functional endothelial progenitor cells migration to ischemic tissue and wound repair. *Stem Cells and Development* **2016**, 25 (3), 266–276.
38. Q. Zhang, Y. Wu, C.H. Chau, Crosstalk of hypoxia-mediated signaling pathways in upregulating plasminogen activator inhibitor-1 expression in keloid fibroblasts. *Journal of Cellular Physiology* **2004**, 199 (1), 89–97.
39. T.D. Nauta, V.W.M. van Hinsbergh, P. Koolwijk. Hypoxic signaling during tissue repair and regenerative medicine. *International Journal of Molecular Sciences* **2014**, 15 (11), 19791–19815.
40. C. Dunnill, T. Patton, J. Brennan, J. Barrett, M. Dryden, J. Cooke, D. Leaper, N.T Georgopoulos. Reactive oxygen species (ROS) and wound healing: the functional role of ROS and emerging ROS-modulating technologies for augmentation of the healing process: Reactive oxygen species and wound healing. *International Wound Journal* **2017**, 14 (1), 89–96.
41. N. Chang, W.H. Goodson, F. Gottrup, T.K. Hunt. Direct measurement of wound and tissue oxygen tension in postoperative patients. *Annals of Surgery* **1983**, 197 (4), 470–478.
42. A. Carreau, B.E. Hafny-Rahbi, A. Matejuk, C. Grillon, C. Kieda. Why is the partial oxygen pressure of human tissues a crucial parameter? Small molecules and hypoxia. *Journal of Cellular and Molecular Medicine* **2011**, 15 (6), 1239–1253.
43. F. Gottrup. Oxygen in Wound healing and infection. *World Journal of Surgery* **2004**, 28 (3), 312–315.
44. C.D. Pericone, S. Park, J.A. Imlay, J.N. Weiser. Factors contributing to hydrogen peroxide resistance in streptococcus pneumoniae Include pyruvate oxidase (SpxB) and avoidance of the toxic effects of the fenton reaction. *Journal of Bacteriology* **2003**, 185 (23), 6815–6825.
45. T. Yamazaki, C. Kawai, A. Yamauchi, F. Kuribayashi. A highly sensitive chemiluminescence assay for superoxide detection and chronic granulomatous disease diagnosis. *Trop Med Health* **2011**, 39 (2), 41–45.
46. A.R. Siddiqui, J.M. Bernstein. Chronic wound infection: Facts and controversies. *Clinics in Dermatology* **2010**, 28 (5), 519–526.
47. C. Frank, I. Bayoumi, C. Westendorp. Approach to infected skin ulcers. *Canadian family physician* **2005**, 51(10), 1352-9.
48. P. Ferretti, S. Farina, M. Cristofolini, Experimental metagenomics and ribosomal profiling of the human skin microbiome. *Experimental Dermatology* **2017**, 26 (3), 211–219.
49. S. Selwyn, H. Ellis. Skin Bacteria and Skin disinfection reconsidered. *British Medical Journal* **1972**, 1 (5793), 136–140.
50. B.A. Lipsky, C. Hoey. Topical Antimicrobial therapy for treating chronic wounds. *Clinical Infectious Diseases* **2009**, 49 (10), 1541–1549.

51. S. Roy, S. Santra, A. Das, S. Dixith, M. Sinha, S. Ghatak, N. Ghosh, P. Banerjee, S. Khanna, S. Mathew-Steiner, P.D Ghatak. Staphylococcus aureus Biofilm infection compromises wound healing by causing deficiencies in granulation tissue collagen. *Annals of Surgery* **2019**, Publish Ahead of Print.
52. S. Malic, K.E. Hill, A. Hayes, Detection and identification of specific bacteria in wound biofilms using peptide nucleic acid fluorescent *in situ* hybridization (PNA FISH). *Microbiology* **2009**, 155 (8), 2603–2611.
53. R.G. Sibbald, H. Orsted, G.S. Schultz, P. Coutts, D. Keast. Preparing the wound bed 2003: focus on infection and inflammation. *Ostomy Wound Management* **2003**, 49(11),24-51.
54. A. De, H.J. Raj, J. Haldar, P. Mukherjee, P.K. Maiti. Biofilm colonization in chronic treatment refractory infections presenting with discharging sinuses: A study in a tertiary care hospital of Eastern India. *Journal of Laboratory Physicians* **2017**, 9 (2), 125–131.
55. P. Merckoll, T.Ø. Jonassen, M.E. Vad, S.L. Jeansson, K.K. Melby. Bacteria, biofilm and honey: A study of the effects of honey on 'planktonic' and biofilm-embedded chronic wound bacteria. *Scandinavian Journal of Infectious Diseases* **2009**, 41 (5), 341–347.
56. P.D. Thomson. Immunology, microbiology, and the recalcitrant wound. *Ostomy Wound Manage* **2000**, 46 (1), 83-84.
57. D.J. Leaper, P. Durani. Topical antimicrobial therapy of chronic wounds healing by secondary intention using iodine products. *International Wound Journal* **2008**, 5 (2), 361–368.
58. D.J. Leaper. Silver dressings: their role in wound management. *International Wound Journal* **2006**, 3 (4), 282–294.
59. J.A. Molnar, M.J. Underdown, W.A. Clark. Nutrition and chronic wounds. *Advances in Wound Care* **2014**, 3 (11), 663–681.
60. W.K. Stadelmann, A.G. Digenis, G.R. Tobin. Impediments to wound healing. *The American Journal of Surgery* **1998**, 176 (2, Supplement 1), 39S-47S.
61. J.K. Stechmiller. Understanding the role of nutrition and wound healing. *Nutrition in Clinical Practice* **2010**, 25 (1), 61–68.
62. J.D. Bauer, E. Isenring, M. Waterhouse. The effectiveness of a specialised oral nutrition supplement on outcomes in patients with chronic wounds: a pragmatic randomised study. *Journal of Human Nutrition and Dietetics* **2013**, 26 (5), 452–458.
63. A.A. Shepherd. Nutrition for optimum wound healing. *Nursing standard* **2003**, 18 (6), 55–58.
64. M. Arnold, A. Barbul. Nutrition and wound healing. *Plastic and Reconstructive Surgery* **2006**, 117 (7 Suppl), 42S-58S.
65. A.C.L. Campos, A.K. Groth, A.B. Branco. Assessment and nutritional aspects of wound healing. *Current Opinion in Clinical Nutrition and Metabolic Care* **2008**, 11 (3), 281–288.
66. U.Z. Muhammet, B.A. Christophe, S. Jockenhoevel, S. anand, S.H. Tahir SH. A short overview on nutrition, wound healing and medical textiles. *Marmara Fen Bilimleri Dergisi* **2015**, 27, 61-65.
67. M. Pompeo. Misconceptions about protein requirements for wound healing: results of a prospective study. *Ostomy Wound Manage* **2007**, 53 (8), 30–32
68. G. Gabbiani. The role of contractile proteins in wound healing and fibrocontractive diseases. *Methods and achievements in experimental pathology* **1979**, 9, 187–206.
69. A. Godwin, A. Sharma, W.-L. Yang, Receptor-Interacting Protein Kinase 3 Deficiency Delays Cutaneous Wound Healing. *PLOS ONE* **2015**, 10 (10), e0140514.

70. M. van der Rest, R. Garrone. Collagen family of proteins. *The FASEB Journal* **1991**, 5 (13), 2814–2823.
71. P.G. Rodriguez, F.N. Felix, D.T. Woodley, E.K. Shim. The Role of oxygen in wound healing: A Review of the Literature. *Dermatologic Surgery* **2008**, 34 (9), 1159–1169.
72. A. Barbul, S.A. Lazarou, D.T. Efron, H.L. Wasserkrug, G. Efron. Arginine enhances wound healing and lymphocyte immune responses in humans. *Surgery* **1990**, 108 (2), 331–336.
73. A. Barbul. Proline precursors to sustain mammalian collagen synthesis. *The Journal of Nutrition* **2008**, 138 (10), 2021S-2024S.
74. J.K. Stechmiller, B. Childress, L. Cowan. Arginine supplementation and wound healing. *Nutrition in Clinical Practice* **2005**, 20 (1), 52–61.
75. R.J. Smith, D.W. Wilmore. Glutamine Nutrition and requirements. *Journal of Parenteral and Enteral Nutrition* **1990**, 14 (4_suppl), 94-99.
76. R. D'Souza. Glutamine supplements in the critically Ill. **2004**, 97, 3.
77. S.C. Blass, H. Goost, R.H. Tolba, Time to wound closure in trauma patients with disorders in wound healing is shortened by supplements containing antioxidant micronutrients and glutamine: a PRCT. *Clinical nutrition* **2012**, 31 (4), 469–475.
78. G.T. Voss, M.S. Gularte, A.G. Vogt, J.L. Giongo, R.A. Vaucher, J.V. Echenique, M.P. Soares, C. Luchese, E.A. Wilhelm, A.R. Fajardo. Polysaccharide-based film loaded with vitamin C and propolis: A promising device to accelerate diabetic wound healing. *International Journal of Pharmaceutics* **2018**, 552 (1–2), 340–351.
79. S. Chokesuwattanaskul, S. Sukpat, J. Duangpatra, High dose oral vitamin C and mesenchymal stem cells aid wound healing in a diabetic mouse model. *Journal of Wound Care* **2018**, 27 (5), 334–339.
80. A.N. Otterço, P. Brassolatti, A.L.M. Andrade, L.R. Avó, P.S. Bossin, N.A. Parizotto. Effect of photobiomodulation (670 nm) associated with vitamin A on the inflammatory phase of wound healing. *Lasers in Medical Science* **2018**, 33 (9), 1867–1874.
81. A.I. Rojas, T.J. Phillips. Patients with chronic leg ulcers show diminished levels of vitamins A and E, Carotenes, and Zinc: *Dermatologic Surgery* **1999**, 25 (8), 601–604.
82. R. Pop-Busui, A.J.M. Boulton, E.L. Feldman, Diabetic neuropathy: A position statement by the American Diabetes Association. *Diabetes Care* **2017**, 40 (1), 136–154.
83. M.L. Grayson, G.W. Gibbons, K. Balogh, E. Levin, A.W. Karchmer. Probing to bone in infected pedal ulcers: A clinical sign of underlying osteomyelitis in diabetic patients. *Journal of the American Medical Association* **1995**, 273 (9), 721–723.
84. R.B. Paisey, A. Abbott, R. Levenson, R, A. Harrington, D. Browne, J. Moore, M. Bamford, M. Roe, South-West Cardiovascular Strategic Clinical Network peer diabetic foot service review team.. Diabetes-related major lower limb amputation incidence is strongly related to diabetic foot service provision and improves with enhancement of services: peer review of the South-West of England. *Diabetic Medicine* **2018**, 35 (1), 53–62.
85. M.M. Kasiya, G.D. Mang'anda, S. Heyes, R. Kachapila, L. Kaduya, J. Chilamba, P. Goodson, K. Chalulu, T.J. Allain. The challenge of diabetic foot care: Review of the literature and experience at Queen Elizabeth Central Hospital in Blantyre, Malawi. *Malawi Med J* **2017**, 29 (2), 218–223.
86. R.G. Frykberg. Epidemiology of the diabetic foot: Ulcerations and amputations. *Advances in Wound Care; Springhouse* **1999**, 12 (3), 139.

87. K. Wikblad, B. Smide, A. Bergström, J. Kessi, F. Mugusi. Outcome of clinical foot examination in relation to self-perceived health and glycaemic control in a group of urban Tanzanian diabetic patients. *Diabetes Research and Clinical Practice* **1997**, 37 (3), 185–192.
88. A. Ramachandran. Specific problems of the diabetic foot in developing countries. *Diabetes/Metabolism Research and Reviews* **2004**, 20 (S1), S19–S22.
89. A. Omar, J.B. Wright, G. Schultz, R. Burrell, P. Nadworny. Microbial Biofilms and Chronic Wounds. *Microorganisms* **2017**, 5 (1), 9.
90. S.L. Percival, M. Malone, D. Mayer, A.-M. Salisbury, G. Schultz. Role of anaerobes in polymicrobial communities and biofilms complicating diabetic foot ulcers. *International Wound Journal* **2018**, 15 (5), 776–782.
91. D.G. Metcalf, P.G. Bowler. Biofilm delays wound healing: A review of the evidence. *Burns & Trauma* **2013**, 1 (1), 5.
92. C. Scali, B. Kunimoto. An update on chronic wounds and the role of biofilms. *Journal of Cutaneous Medicine and Surgery* **2013**, 17 (6), 371–376.
93. S.P. Galanakos, S.A. Papadakis, K. Kateros, I. Papakostas, G. Macheras. Biofilm and orthopaedic practice: the world of microbes in a world of implants. *Orthopaedics and Trauma* **2009**, 23 (3), 175–179.
94. E.P. Greenberg. Bacterial communication and group behavior. *J Clin Invest* **2003**, 112 (9), 1288–1290.
95. R.D. Wolcott, D.D. Rhoads. A study of biofilm-based wound management in subjects with critical limb ischaemia. *Journal of Wound Care* **2008**, 17 (4), 145–155.
96. M. Azevedo, S. Alla. Diabetes in Sub-Saharan Africa: Kenya, Mali, Mozambique, Nigeria, South Africa and Zambia. *International Journal of Diabetes in Developing Countries* **2008**, 28 (4), 101–108.
97. K. Ismail, K. Winkley, D. Stahl, T. Chalder, M. Edmonds. A cohort study of people with diabetes and their first foot ulcer: the role of depression on mortality. *Diabetes Care* **2007**, 30(6), 1473-1479
98. R.T. Crews, K.L. Schneider, S.V. Yalla, N.D. Reeves, L. Vileikyte. Physiological and psychological challenges of increasing physical activity and exercise in patients at risk of diabetic foot ulcers: a critical review: physical activity and foot ulcers. *Diabetes/Metabolism Research and Reviews* **2016**, 32 (8), 791–804.
99. A. Persoon, M.M. Heinen, C.J.M. van der Vleuten, M.J. De Rooij, P.C. Van De Kerkhof, T. Van Achterberg. Leg ulcers: a review of their impact on daily life. *Journal of Clinical Nursing* **2004**, 13 (3), 341–354.
100. (uSpiked Investigative Team) https://www.uspiked.com/health/2017/05/01/the-chronic-wounds-money-spinner!/ on accessed 24 Mar 2019
101. B.S. Atiyeh, S.A. Dibo, S.N. Hayek. Wound cleansing, topical antiseptics and wound healing. *International Wound Journal* **2009**, 6 (6), 420–430.
102. M. Klebes, C. Ulrich, F. Kluschke, A. Patzelt, S. Vandersee, H. Richter, A. Bob, J. von Hutten, J.T. Krediet, A. Kramer, J. Lademann. Combined antibacterial effects of tissue-tolerable plasma and a modern conventional liquid antiseptic on chronic wound treatment: Antiseptic effects of TTP and liquid antiseptic. *Journal of Biophotonics* **2015**, 8 (5), 382–391.
103. D.A. Williamson, G.P. Carter, B.P. Howden. Current and emerging topical antibacterials and antiseptics: agents, action, and resistance patterns. *Clinical Microbiology Reviews* **2017**, 30 (3), 827–860.

104. T. Bjarnsholt. The role of bacterial biofilms in chronic infections. *Acta pathologica, microbiologica, et immunologica Scandinavica* **2013**, 121, 1–58.
105. N. Høiby, T. Bjarnsholt, M. Givskov, S. Molin, O. Ciofu. Antibiotic resistance of bacterial biofilms. *International Journal of Antimicrobial Agents* **2010**, 35 (4), 322–332.
106. D.J. Leaper, G. Schultz, K. Carville, Extending the time concept: what have we learned in the past 10 years? *. *International Wound Journal* **2012**, 9, 1–19.
107. V. Falanga, M. Sabolinski. A bilayered living skin construct (APLIGRAF®) accelerates complete closure of hard-to-heal venous ulcers. *Wound Repair and Regeneration* **1999**, 7 (4), 201–207.
108. M. Edmonds, European and Australian Apligraf Diabetic Foot Ulcer Study Group. Apligraf in the treatment of neuropathic diabetic foot ulcers. *The International Journal of Lower Extremity Wounds* **2009**, 8 (1), 11–18.
109. W.H. Eaglstein, V. Falanga. Tissue engineering and the development of Apligraf, a human skin equivalent. *Clinical Therapeutics* **1997**, 19 (5), 894–905.
110. T. Gibson, P.B. Medawar. THE FATE OF SKIN HOMOGRAFTS IN MAN. 16.
111. M.P. Curran, G.L. Plosker. Bilayered bioengineered skin substitute (Apligraf): A review of its use in the treatment of venous leg ulcers and diabetic foot ulcers. *BioDrugs* **2002**, 16 (6), 439–455.
112. T. Mustoe. Understanding chronic wounds: a unifying hypothesis on their pathogenesis and implications for therapy. *The American Journal of Surgery* **2004**, 187 (5), S65–S70.
113. W.K. Redekop, J. McDonnell, P. Verboom, K. Lovas, Z. Kalo. The Cost effectiveness of Apligraf: Treatment of diabetic foot ulcers: *PharmacoEconomics* **2003**, 21 (16), 1171–1183.
114. M. Streit, L.R. Braathen. Apligraf – A living human skin equivalent for the treatment of chronic wounds. *The International Journal of Artificial Organs* **2000**, 23 (12), 831–833.
115. M. Noguchi, K. Eishi, S. Yamachika, S. Hazama. Three cases of ischemic ulcer due to arteriosclerosis obliterans responding to basic fibroblast growth factor spray. *Heart and Vessels* **2004**, 19(5):252-256.
116. J. Gupta, N. Mitra, R.R. Townsend, M. Fischer, J.R. Schelling, D.J. Margolis. Variants in genes belonging to the fibroblast growth factor family are associated with lower extremity amputation in non-Hispanic whites: Findings from the chronic renal insufficiency cohort study: Angiogenesis/wound repair genes and lower extremity amputation. *Wound Repair and Regeneration* **2016**, 24 (4), 705–711.
117. M. Fujioka. Combination treatment with basic fibroblast growth factor and artificial dermis improves complex wounds in patients with a history of long-term systemic corticosteroid Use: *Dermatologic Surgery* **2009**, 35 (9), 1422–1425.
118. A. Mollica, F. Pinnen, S. Azzurra, R. Costante. The evolution of peptide synthesis: from early days to small molecular machines. *Current Bioactive Compounds* **2014**, 9 (3), 184–202.
119. I. Martin-Loeches, G.E. Dale, A. Torres. Murepavadin: a new antibiotic class in the pipeline. *Expert Review of Anti-infective Therapy* **2018**, 16 (4), 259–268.
120. S.J. Aston, J. Rylance. Community-acquired pneumonia in sub-saharan Africa. *Seminars in respiratory and critical care medicine* **2016**, 37 (6), 855–867.
121. A.T.Y. Yeung, S.L. Gellatly, R.E.W. Hancock. Multifunctional cationic host defence peptides and their clinical applications. *Cellular and Molecular Life Sciences* **2011**, 68 (13), 2161.
122. L.T. Nguyen, E.F. Haney, H.J. Vogel. The expanding scope of antimicrobial peptide structures and their modes of action. *Trends in Biotechnology* **2011**, 29 (9), 464–472.

123. K. Matsuzaki. Control of cell selectivity of antimicrobial peptides. *Biochimica et Biophysica Acta (BBA) - Biomembranes* **2009**, 1788 (8), 1687–1692.
124. G. Diamond, N. Beckloff, A. Weinberg, K.O. Kisich. The roles of antimicrobial peptides in innate host defense. *Current Pharmaceutical Design.* **2009**, 15 (21), 2377–2392.
125. R.E. Hancock. Cationic peptides: effectors in innate immunity and novel antimicrobials. *The Lancet Infectious Diseases* **2001**, 1 (3), 156–164.
126. B.M. Peters, M.E. Shirtliff, M.A. Jabra-Rizk. Antimicrobial peptides: primeval molecules or future drugs? *PLOS Pathogens* **2010**, 6 (10), e1001067
127. P. Verdu. African Pygmies. *Current Biology* **2016**, 26 (1), 12–14.
128. R. Conde, M. Arguello, J. Izquierdo, R. Noguez, M. Moreno, H. Lanz.. Natural antimicrobial peptides from eukaryotic organisms. In *Antimicrobial Agents*; Bobbarala, V., Ed.; InTech, **2012**. IntechOpen
129. L. Zhang, R.L. Gallo. Antimicrobial peptides. *Current Biology* **2016**, 26 (1), R14–R19.
130. Y. Lai, R.L. Gallo. AMPed Up immunity: how antimicrobial peptides have multiple roles in immune defense. *Trends in Immunology* **2009**, 30 (3), 131–141.
131. S. Mai, M.T. Mauger, L.-N. Niu, Potential applications of antimicrobial peptides and their mimics in combating caries and pulpal infections. *Acta Biomaterialia* **2017**, 49, 16–35.
132. J.-H. Lin, A. Baumgaertner. Stability of a melittin pore in a lipid bilayer: a molecular dynamics study. *Biophysical Journal* **2000**, 78 (4), 1714–1724.
133. D.R. Laver. The barrel-stave model as applied to alamethicin and its analogs reevaluated. *Biophysical Journal* **1994**, 66 (2), 355–359.
134. Y. Shai, Z. Oren. From "carpet" mechanism to de-novo designed diastereomeric cell-selective antimicrobial peptides. *Peptides* **2001**, 22 (10), 1629–1641.
135. D. Sengupta, H. Leontiadou, A.E. Mark, S.-J. Marrink. Toroidal pores formed by antimicrobial peptides show significant disorder. *Biochimica et Biophysica Acta (BBA) - Biomembranes* **2008**, 1778 (10), 2308–2317.
136. N. Rodríguez-Vázquez, H.L. Ozores, A. Guerra, Membrane-targeted self-assembling cyclic peptide nanotubes. *Current Topics in Medicinal Chemistry* **2014**, 14 (23), 2647–2661.
137. S.-C. Park, Y. Park, K.-S. Hahm. The role of antimicrobial peptides in preventing multidrug-resistant bacterial infections and biofilm formation. *International Journal of Molecular Sciences* **2011**, 12 (9), 5971–5992.
138. J. Tanwar, S. Das, Z. Fatima, S. Hameed. Multidrug Resistance: An emerging crisis https://www.hindawi.com/journals/ipid/2014/541340/abs/ (accessed Jan 21, 2019).
139. A.A. Bahar, D. Ren. Antimicrobial Peptides. *Pharmaceuticals* **2013**, 6 (12), 1543–1575.
140. M. Leippe, R. Herbst. Ancient weapons for attack and defense: the pore-forming polypeptides of pathogenic enteric and free-living amoeboid protozoa1. *Journal of Eukaryotic Microbiology* **2004**, 51 (5), 516–521.
141. S.S. Usmani, G. Bedi, J.S. Samuel, THPdb: Database of FDA-approved peptide and protein therapeutics. *PLOS ONE* **2017**, 12 (7), e0181748.
142. W. Aoki, K. Kuroda, M. Ueda. Next generation of antimicrobial peptides as molecular targeted medicines. *Journal of Bioscience and Bioengineering* **2012**, 114 (4), 365–370.
143. H.H. Guan, W. Budzynski, R.R. Koganty, Liposomal formulations of Synthetic MUC1 peptides: effects of encapsulation versus surface display of peptides on immune responses. *Bioconjugate Chemistry* **1998**, 9 (4), 451–458.

144. P. Schönfeld, R. Bohnensack. Fatty acid-promoted mitochondrial permeability transition by membrane depolarization and binding to the ADP/ATP carrier. *FEBS Letters* **1997**, 420 (2–3), 167–170.
145. M. Grillaud, A. Bianco. Multifunctional adamantane derivatives as new scaffolds for the multipresentation of bioactive peptides. *Journal of Peptide Science* **2015**, 21 (5), 330–345.
146. S. A. Fowler, H. E. Blackwell. Structure–function relationships in peptoids: Recent advances toward deciphering the structural requirements for biological function. *Organic & Biomolecular Chemistry* **2009**, 7 (8), 1508–1524.
147. R.N. Zuckermann, J.M. Kerr, S.B.H. Kent, W.H. Moos. Efficient method for the preparation of peptoids [oligo(N-substituted glycines)] by submonomer solid-phase synthesis. *Journal of the American Chemical Society* **1992**, 114 (26), 10646–10647.
148. E. Biron, J. Chatterjee, O. Ovadia, D. Langenegger, J. Brueggen, D. Hoyer, H.A. Schmid, R. Jelinek, C. Gilon, A. Hoffman, H. Kessler. Improving oral bioavailability of peptides by multiple *N*-methylation: somatostatin analogues. *Angewandte Chemie International Edition* **2008**, 47 (14), 2595–2599.
149. M. Sela, E. Zisman. Different roles of D-amino acids in immune phenomena. *The FASEB Journal* **1997**, 11 (6), 449–456.
150. Y. Song, Y. Lu, L. Wang, Purification, characterization and cloning of two novel tigerinin-like peptides from skin secretions of Fejervarya cancrivora. *Peptides* **2009**, 30 (7), 1228–1232.
151. E. Ruoslahti. Rgd and other recognition sequences for integrins. *Annual Review of Cell and Developmental Biology* **1996**, 12 (1), 697–715.
152. J.D. Hood, D.A. Cheresh. Role of integrins in cell invasion and migration. *Nature Reviews Cancer* **2002**, 2 (2), 91–100.
153. S.H. Moon, E. Huang. Novel linear lipopeptide paenipeptin C′ binds to lipopolysaccharides and lipoteichoic acid and exerts bactericidal activity by the disruption of cytoplasmic membrane. *BMC Microbiology* **2019**, 19 (1), 6.
154. P.-Y. Chen, C.-K. Lin, C.-T. Lee, H. Jan, S.I. Chan. Effects of turn residues in directing the formation of the β-sheet and in the stability of the β-sheet. *Protein Science* **2001**, 10 (9), 1794–1800.
155. A. Isidro-Llobet, M. Álvarez, F. Albericio. Amino acid-protecting groups. *Chemical Reviews* **2009**, 109 (6), 2455–2504.
156. I. Pal, V.P. Brahmkhatri, S. Bera, Enhanced stability and activity of an antimicrobial peptide in conjugation with silver nanoparticle. *Journal of Colloid and Interface Science* **2016**, 483, 385–393.
157. K. R, G. G, J. A, G. M. Rapid green synthesis of silver nanoparticles (AgNPs) using (prunus persica) plants extract: exploring its antimicrobial and catalytic activities. *Journal of Nanomedicine & Nanotechnology* **2017**, 08 (04).
158. E. Jorgenson, A. Ianoul. Biofunctionalization of plasmonic nanoparticles with short peptides monitored by SERS. *Journal of Physical Chemistry* **2017**, 121 (5), 967–974.
159. A. Abbaszadegan, Y. Ghahramani, A. Gholami, The effect of charge at the surface of silver nanoparticles on antimicrobial activity against Gram-Positive and Gram-Negative bacteria: a Preliminary Study https://www.hindawi.com/journals/jnm/2015/720654/ (accessed Mar 22, 2019).

160. A. Kędziora, M. Speruda, E. Krzyżewska, Similarities and Differences between Silver Ions and Silver in Nanoforms as Antibacterial Agents. *International Journal of Molecular Sciences.* **2018**, 19 (2), 444
161. S. Marin, G.M. Vlasceanu, R.E. Tiplea, Applications and toxicity of silver nanoparticles: a recent review. *Current Topics in Medicinal Chemistry.* **2015**, 15 (16), 1596–1604.
162. K. Bilberg, M.B. Hovgaard, F. Besenbacher, E. Baatrup. *In Vivo* Toxicity of Silver Nanoparticles and Silver Ions in Zebrafish (Danio rerio). *International Journal of Toxicology.* **2012**, 2012.
163. L. Liu, J. Yang, J. Xie, Z. Luo, J. Jiang, Y.Y. Yang,S. Liu. The potent antimicrobial properties of cell penetrating peptide-conjugated silver nanoparticles with excellent selectivity for Gram-positive bacteria over erythrocytes. *Nanoscale* **2013**, 5 (9), 3834-3834.
164. L. Ge, Q. Li, M. Wang, Nanosilver particles in medical applications: synthesis, performance, and toxicity. *International Journal of Nanomedicine*. **2014**, 9, 2399–2407.
165. T. Viitala, N. Granqvist, S. Hallila, M. Raviña. M. Yliperttula, M. Elucidating the signal responses of multi-parametric surface plasmon resonance living cell sensing: a comparison between optical modeling and drug–MDCKII cell interaction measurements. *PloS one*, , **2013,** 8(8), e72192.
166. S. Agnihotri, S. Mukherji, S. Mukherji. Size-controlled silver nanoparticles synthesized over the range 5–100 nm using the same protocol and their antibacterial efficacy. *RSC Advances* **2014**, 4 (8), 3974–3983.
167. E. Cottancin, G. Celep, J. Lermé, M. Pellarin, J.R. Huntzinger, J.L. Vialle, M. Broyer.Optical properties of noble metal clusters as a function of the size: comparison between experiments and a semi-quantal theory. *Theoretical Chemistry Accounts*.**2006**, 116 (4), 514–523.
168. H. Poblete, A. Agarwal, S.S. Thomas, C. Bohne, R. Ravichandran, J. Phopase, J. Comer, E.I. AlarcoN. New insights into peptide-silver nanoparticle interaction: deciphering the role of cysteine and lysine in the peptide sequence. *Langmuir* **2016**, 32 (1), 265–273.
169. B.P. Tu, J.S. Weissman. Oxidative protein folding in eukaryotes: mechanisms and consequences. *The Journal of cell biology* **2004**, 164(3), 341-346.
170. B.P. Tu, S.C. Ho-Schleyer, K.J. Travers, J.S. Weissman. Biochemical basis of oxidative protein folding in the endoplasmic reticulum. *Science* **2000**, 290(5496),1571-1574.

Appendix

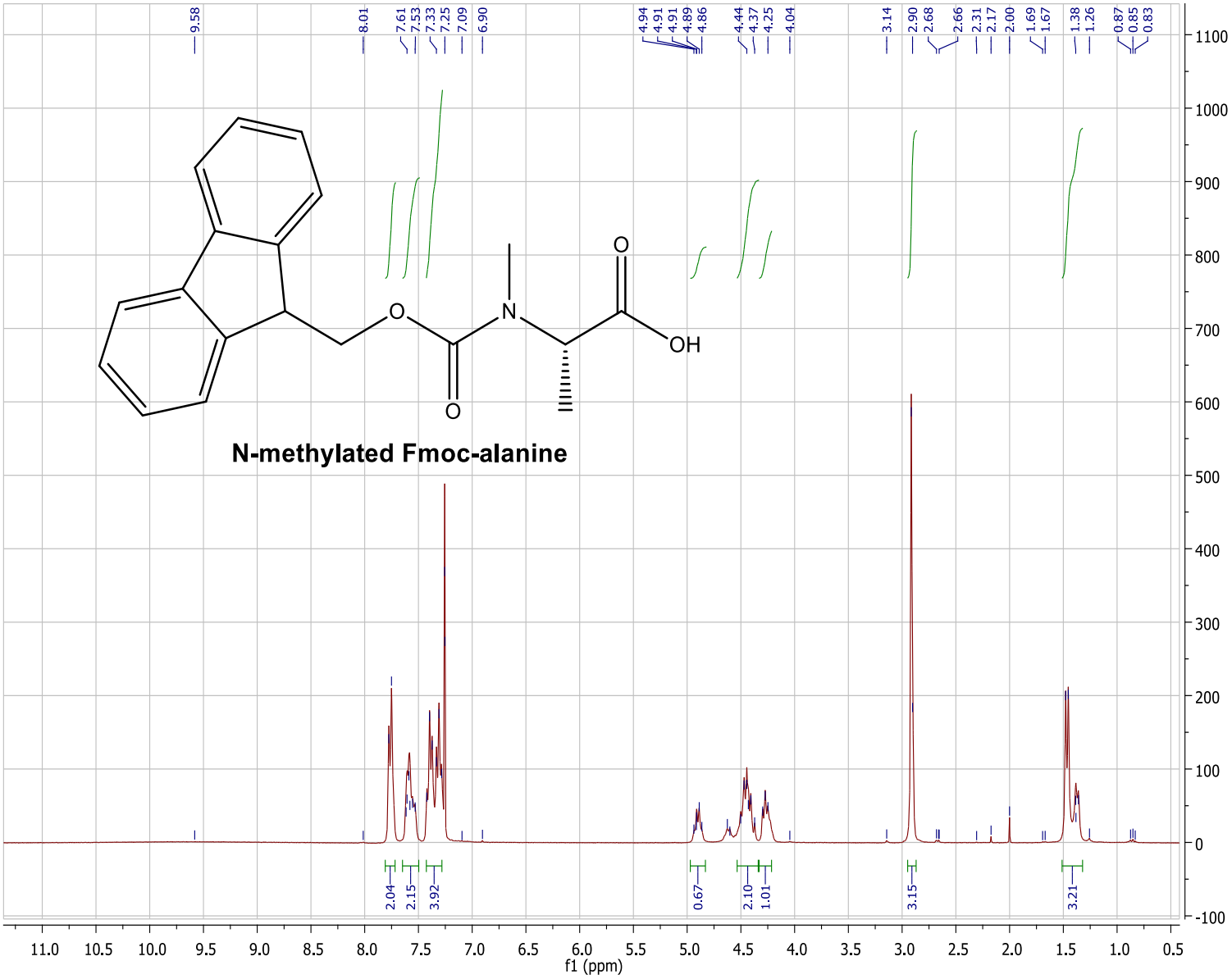


Figure 7.1 1 ^{1}H NMR of N-menthylated F-moc alanine

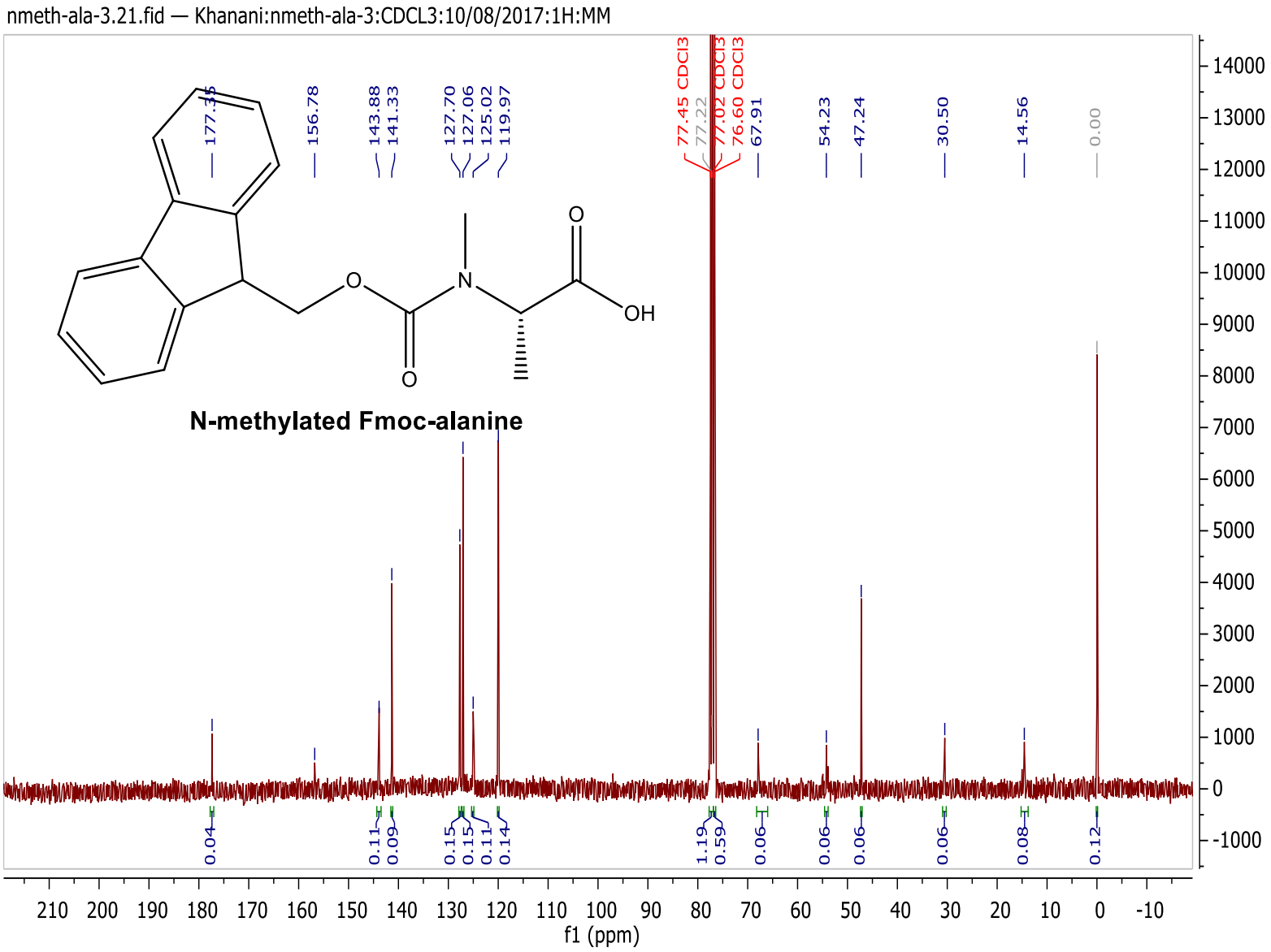


Figure 7.1 2 ^{13}C NMR of N-menthylated F-moc alanine

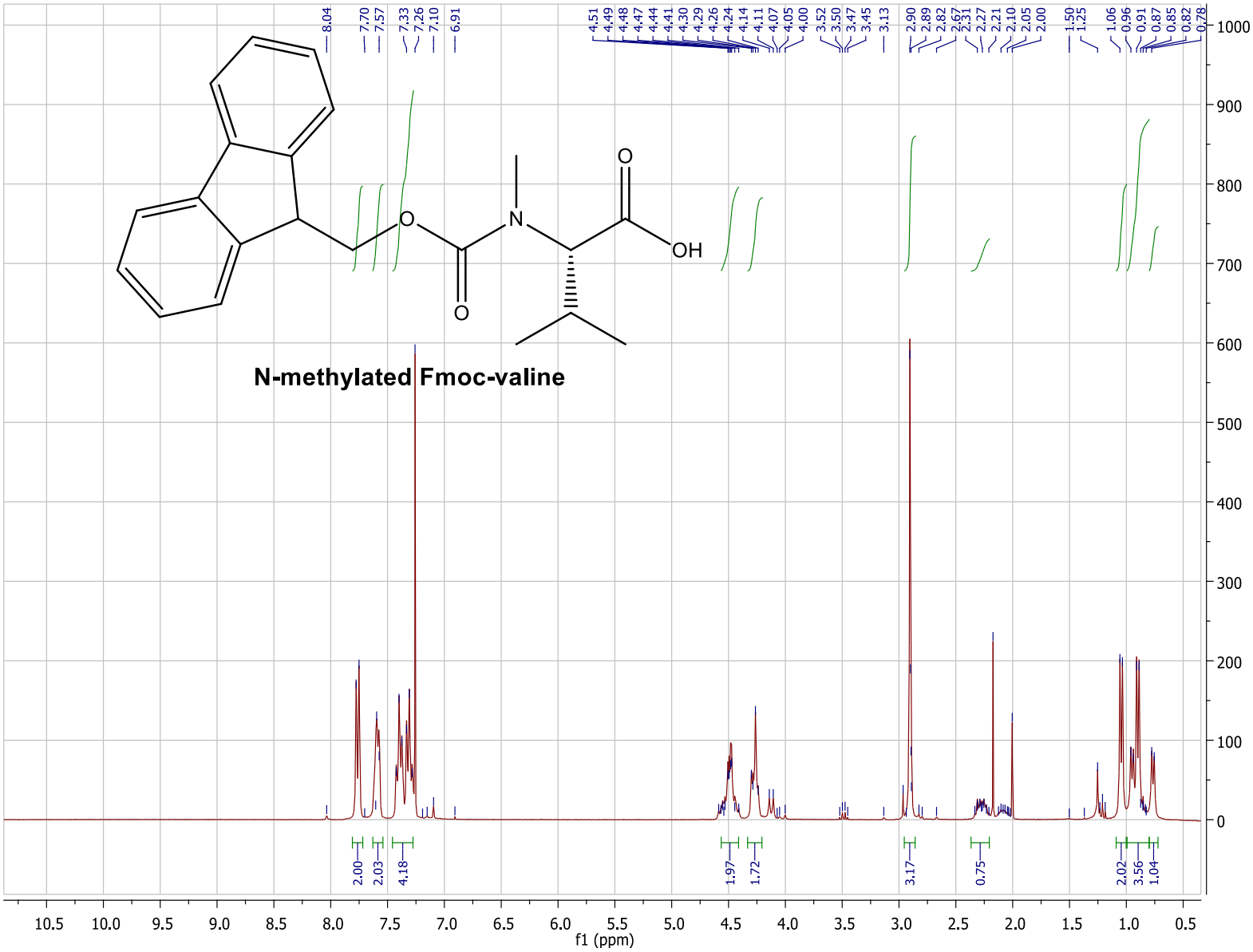


Figure 7.1 3 ^{1}H NMR of N-menthylated F-moc valine

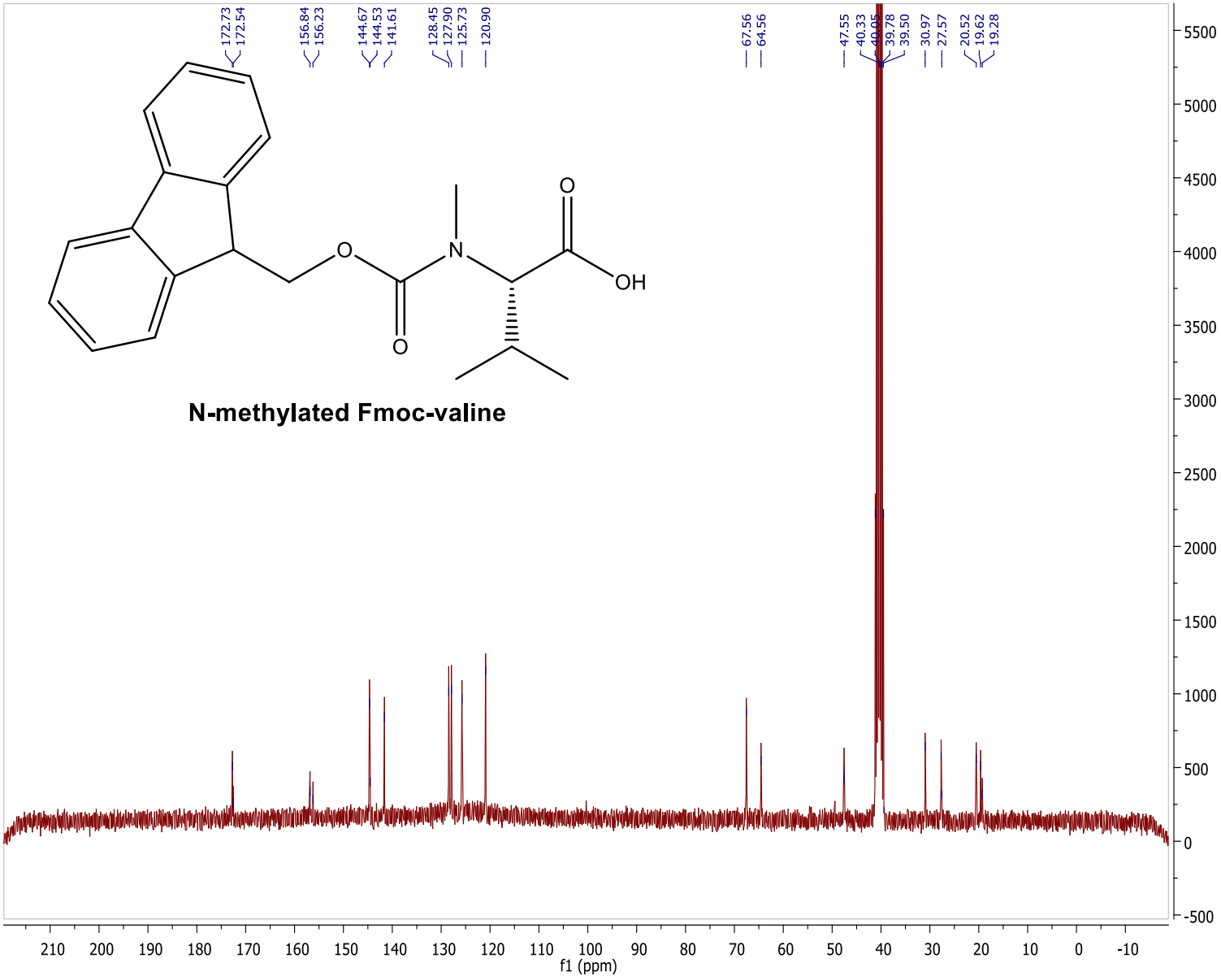


Figure 7.1 4 ^{13}C NMR of N-menthylated F-moc valine

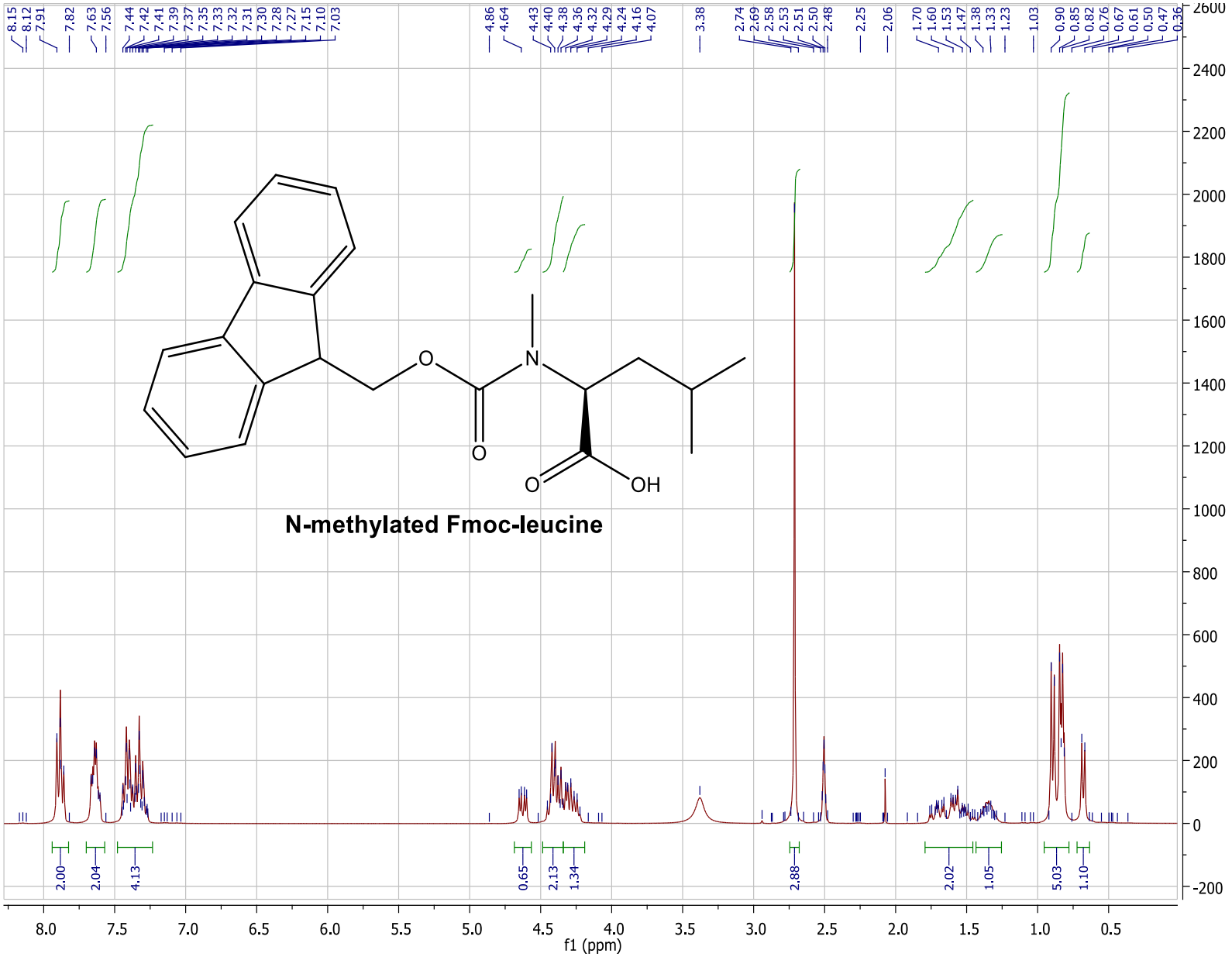


Figure 7.1 5 ^{1}H NMR of N-menthylated F-moc leucine

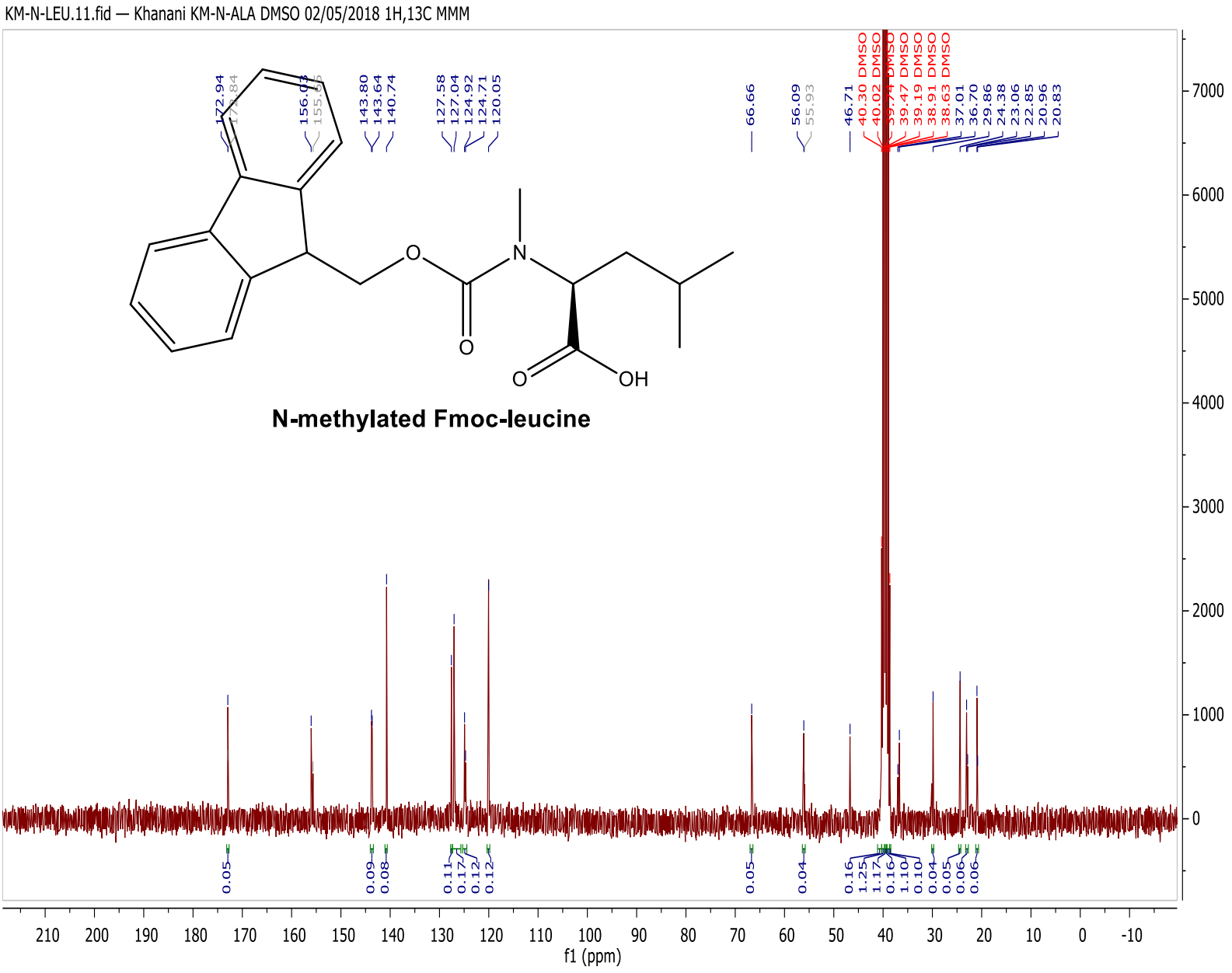


Figure 7.1 6 ^{13}C NMR of N-menthylated F-moc leucine

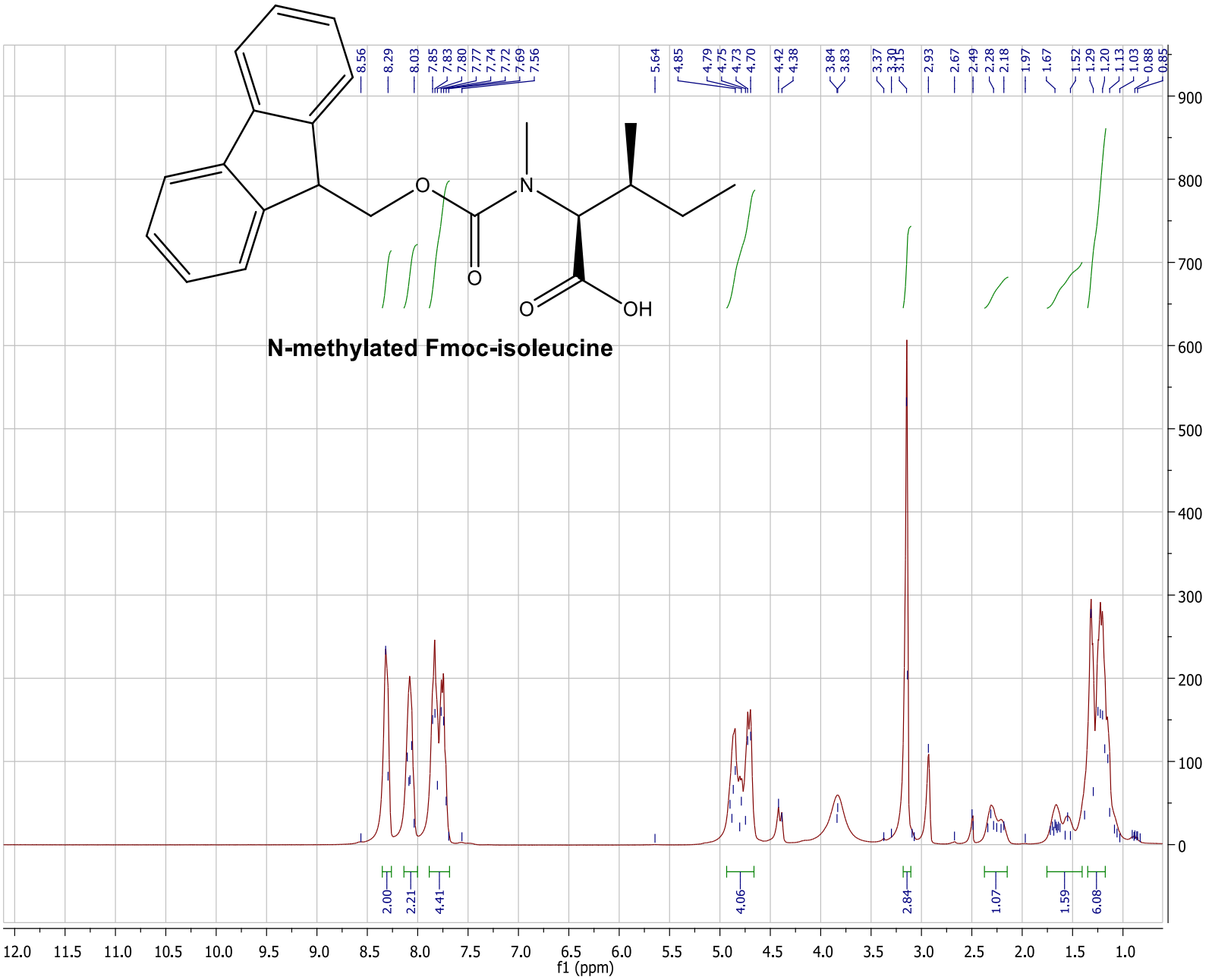


Figure 7.1 7 ^{1}H NMR of N-menthylated F-moc isoleucine

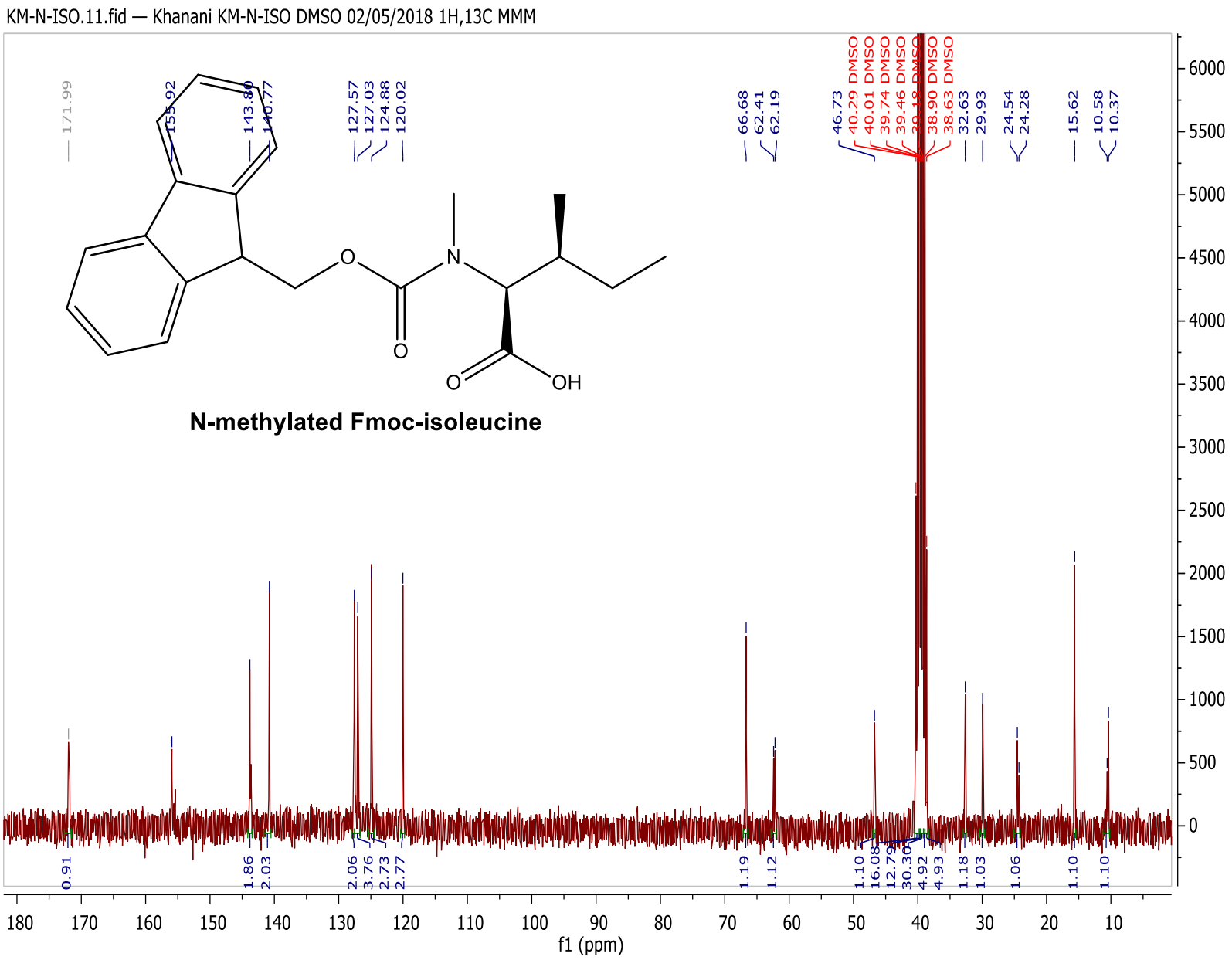


Figure 7.1 8 ^{13}C NMR of N-menthylated F-moc isoleucine

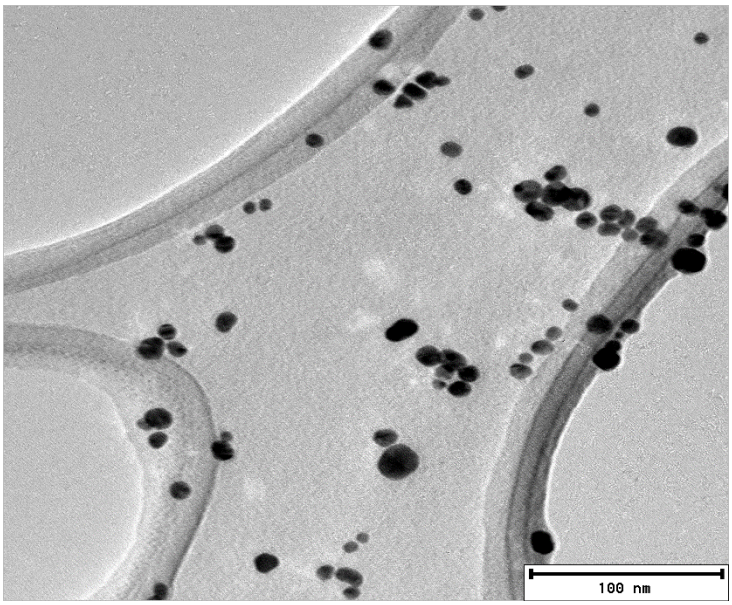


Figure 7.1 9 TEM image of AgNP- $NaBH_4$

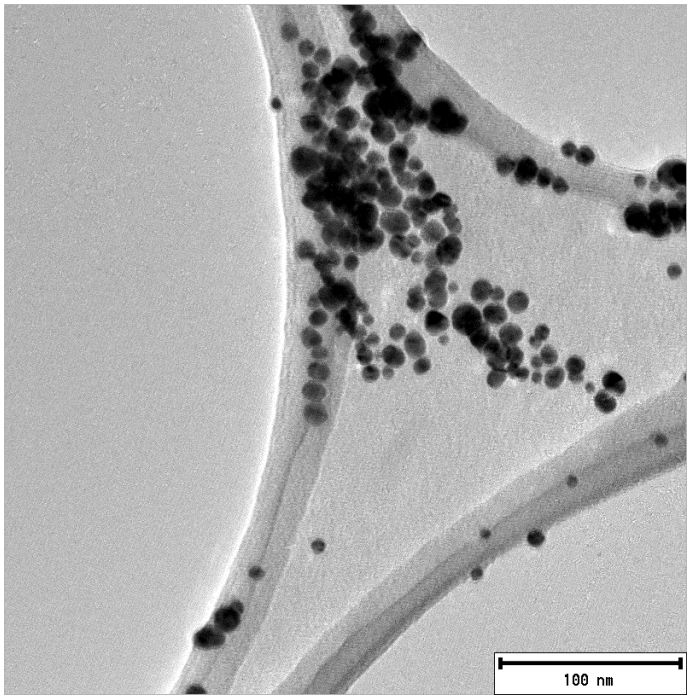


Figure 7.1 10 TEM image of AgNp-PEP-$NaBH_4$

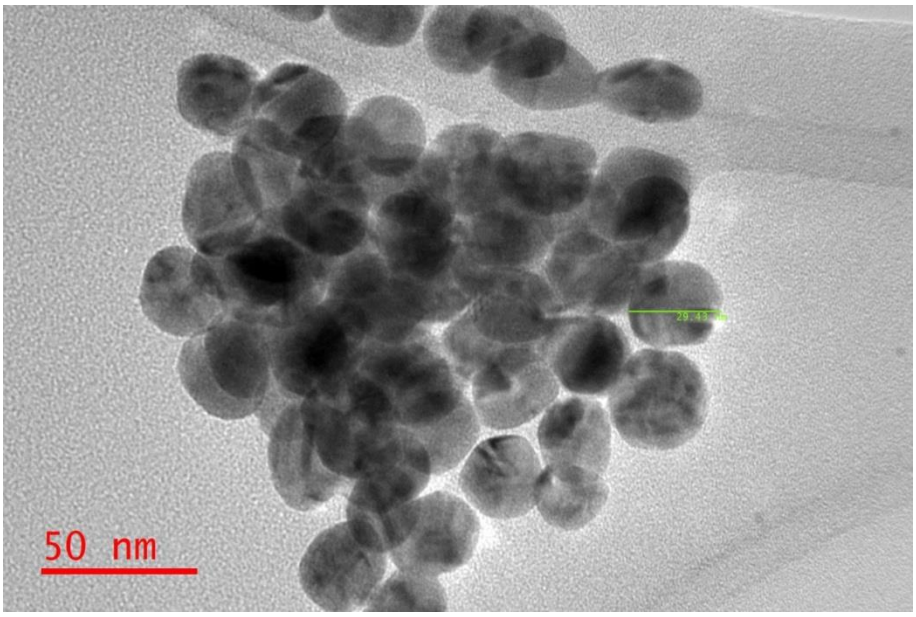


Figure 7.1 11 TEM image of AgNp-1ml

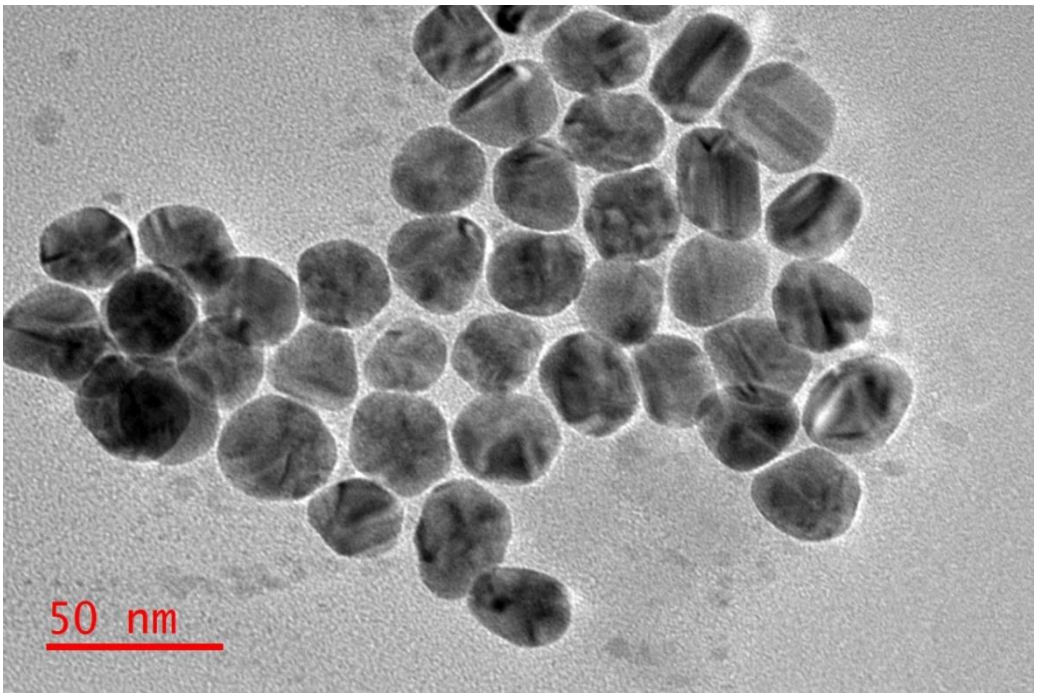


Figure 7.1 12 TEM image of AgNp-PEP-1ml

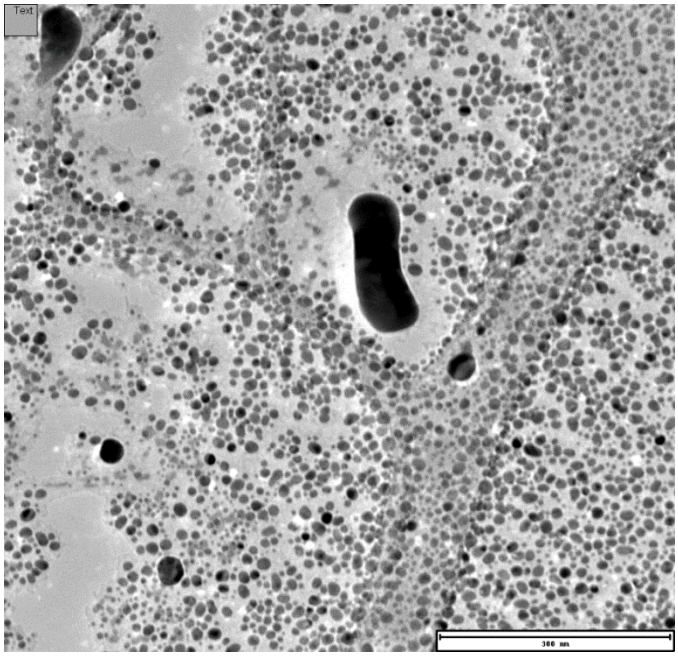


Figure 7.1 13 TEM image of AgNp-PEP-1ml

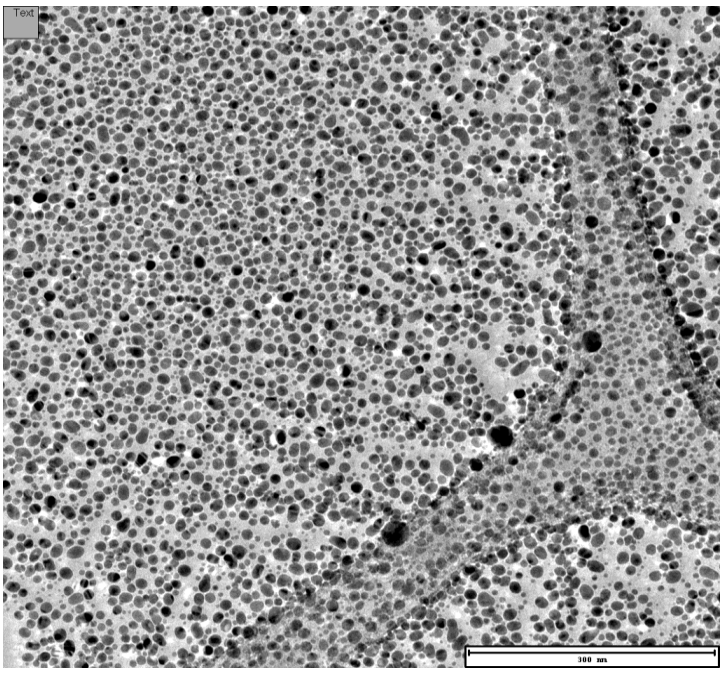


Figure 7.1 14 TEM image of AgNp-PEP-1ml

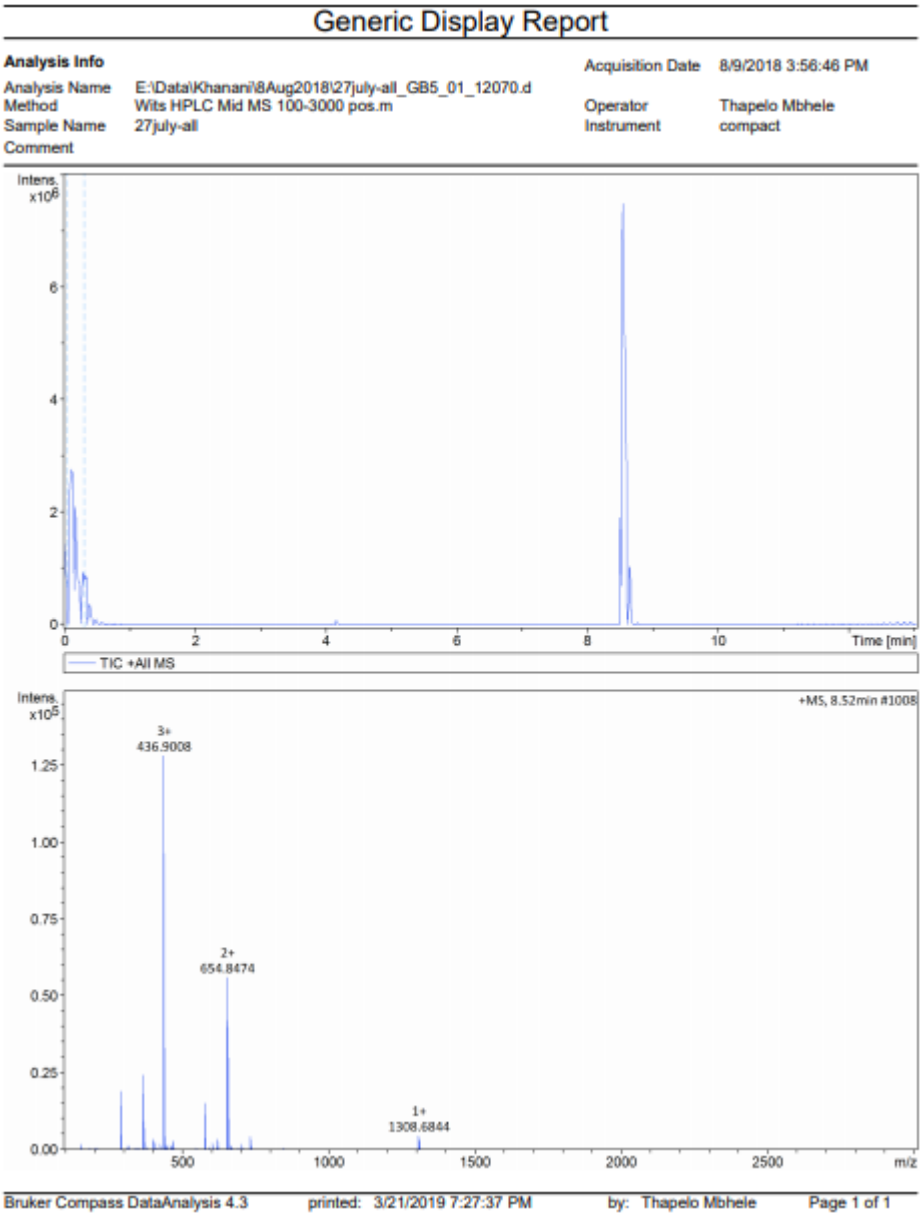


Figure 7.1 15 HRMS of KM-PEP-carb

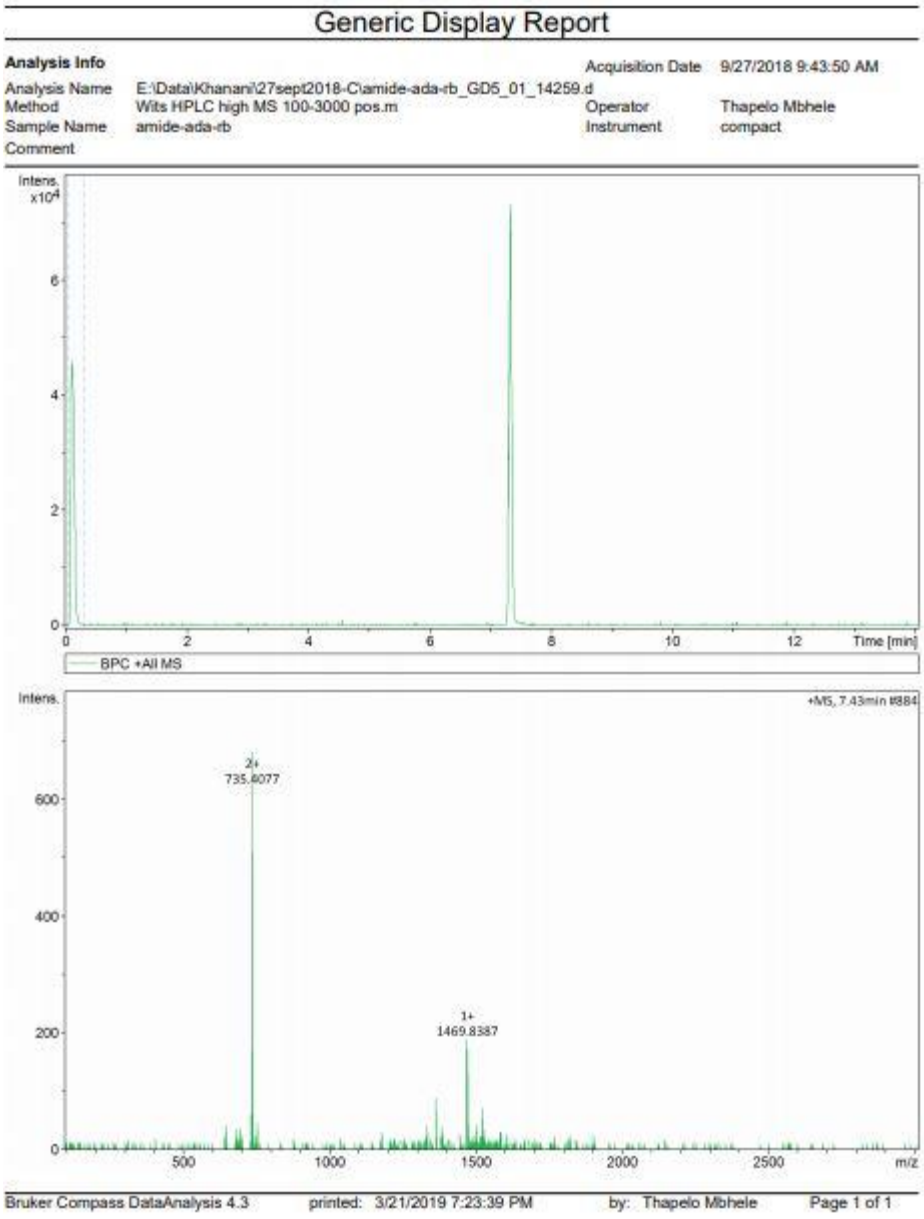


Figure 7.1 16 HRMS of KM-PEP-ada

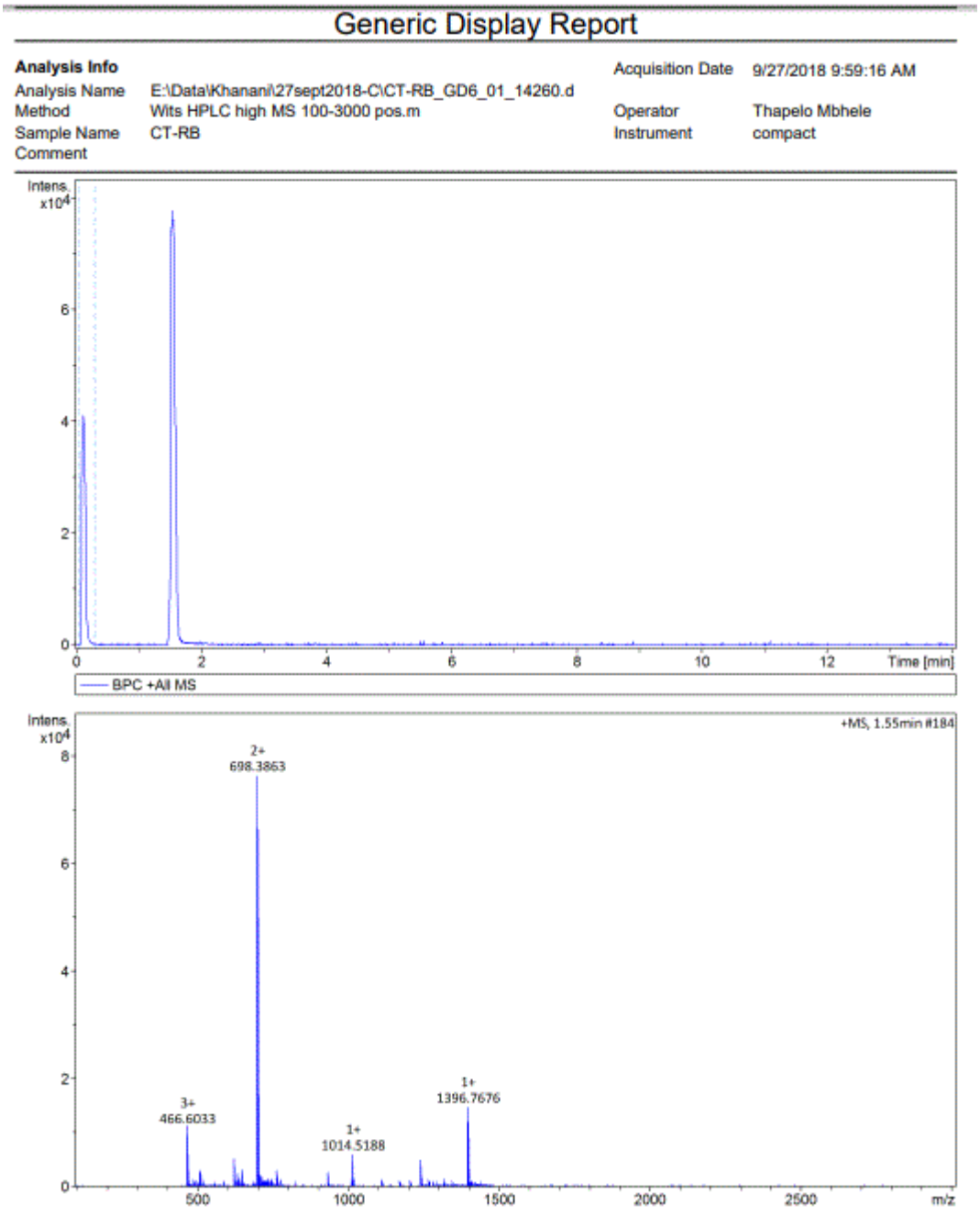


Figure 7.1 17 HRMS of KM-CT

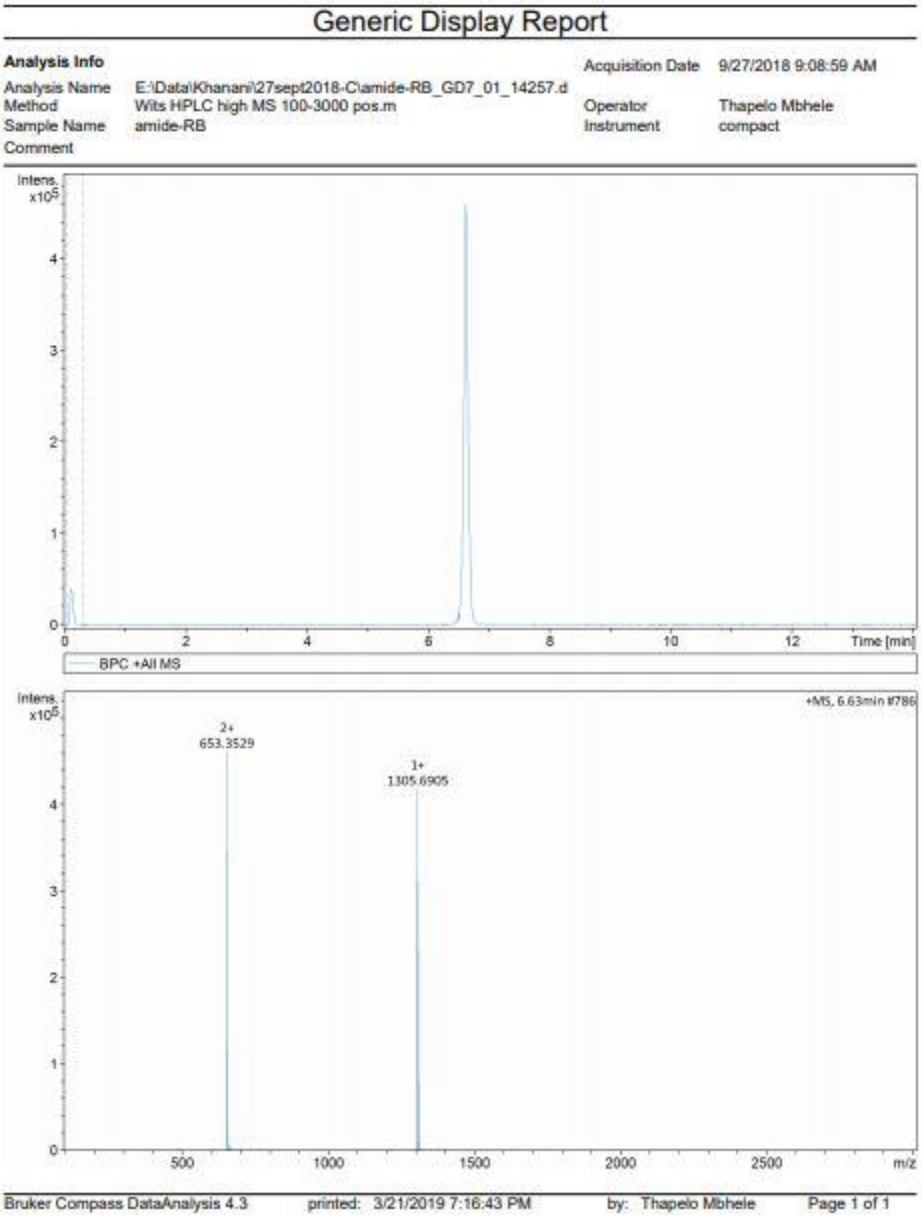


Figure 7.1 18 HRMS of KM-PEP-cyc-amide

MINTEK
A global leader in mineral and metallurgical innovation

Advanced Materials Division

MINTEK
Private Bag X3015, Randburg 2125, South Africa
200 Malibongwe Drive, Randburg, South Africa
Tel: +27 11 709 4111
Fax: +27 11 709 4480
http://www.mintek.co.za

ISO 9001 QUALITY MANAGEMENT SYSTEM
ISO 14001 ENVIRONMENTAL MANAGEMENT SYSTEM
ISO 17025 TESTING AND CALIBRATION LABORATORY
OHSAS 18001 OCCUPATIONAL HEALTH AND SAFETY MANAGEMENT SYSTEM

Materials Evaluation Report

Client: University of the Witwatersrand	**Compact No:** 2018-2.16	**Sheet No:** MER - 2238
Contact Person: Dr Maya Makatini	**Sample Identification:** Peptides in H_2O	
Address: Private Bag 3, Braamfontein, 2050, Republic of South Africa	**Date Received:** 13 March 2018	
Tel: +27 71 383 4420	**Mintek Contact:** Salerwe Mosebi (011 709 4824)	
E-mail: maya.makatini@wits.ac.za	**Project No:** ADC 21809	
Title: Cytotoxicity testing of 10 peptides		

BACKGROUND	University of the Witwatersrand sent 10 samples for testing on the cytotoxic assays developed and optimized in-house. Screening was conducted at 20 µl and 100 µl for the 8 peptides and at dose responses for the two peptides (Pep KM and Pep 2) as requested by the client.

PROCEDURE	**EXPERIMENTS CARRIED OUT ON THE SAMPLES:** **1. Cytotoxicity evaluation in the HIV growth supporting human T cell-line, MT4 (Human T cell leukaemia).** **1.1 Cytotoxicity assay** Number of samples evaluated for single concentration(s): 8 Compound concentration: 20 µl and 100 µl Number of samples for dose response: 2 (Pep KM & Pep 2) Compound concentration (100 µg/ml to 6.25 µg/ml) Control compound: Auranofin (Biomol International, LP) Number of replicates: n = 6 Endpoint method: Absorbance Validation parameters: No compound control: Below 0.3 AU Cell control: Above 1.0 AU

© MINTEK
Subject to any contrary agreement in writing all proprietary rights in and to this report vest in Mintek. This report is confidential and may not be disclosed, quoted, referenced or reproduced without the prior written consent of Mintek. Mintek accepts no liability for any misstatement made by the client or for the interpretation or use by others of this report.

Figure 7.1 9 Cytotoxicity information